DESIGN AND THERMAL MODELING OF A NON-INVASIVE PROBE FOR MEASURING PERFUSION BY THERMODIFFUSION

by

STEVEN KNIGHT CHARLES

B.S. Mechanical Engineering
Brigham Young University, 2001

Submitted to the Department of Mechanical Engineering in Partial Fulfillment of the Requirements for the Degree of

Master of Science in Mechanical Engineering

at the

Massachusetts Institute of Technology

June 2004

Signature of Author: .....
Department of Mechanical Engineering
7 May 2004

Certified by: .....
H. Frederick Bowman
Thesis Supervisor

Accepted by: .....
Ain A. Sonin
Chairman, Department Committee on Graduate Students

DESIGN AND THERMAL MODELING OF A NON-INVASIVE PROBE FOR MEASURING PERFUSION BY THERMODIFFUSION

by

STEVEN KNIGHT CHARLES

Submitted to the Department of Mechanical Engineering on 7 May 2004 in
Partial Fulfillment of the Requirements for the
Degree of Master of Science in Mechanical Engineering

ABSTRACT

This research 1) explores the feasibility of developing a *non-invasive* probe to precisely quantify microcirculatory blood flow (tissue perfusion), in real time and in absolute units, and 2) presents designs and models of such a probe, along with an evaluation of various design-model combinations.

Bowman et al. have developed an *invasive* thermodiffusion probe that measures tissue perfusion accurately, continuously, and in real time. This method employs a self-heated thermistor placed in perfused tissue. From a knowledge of the power required to heat the thermistor probe to a given temperature, perfusion can be calculated using an analytical or numerical model.

Using Bowman's thermodiffusion probe (designed for invasive use) in a non-invasive manner, a perfusion study was performed. The data clearly show the promise of a non-invasive thermodiffusion perfusion probe (designed for non-invasive use), and the design of such a probe was pursued by adapting the invasive technology for a non-invasive probe. Because perfusion is not actually measured but calculated from measured quantities by a model of the probe and perfused tissue, the design of the non-invasive probe occurred hand-in-hand with the development of analytical models.

The results of the clinical study are presented, as well as two designs together with possible one-dimensional analytical models. Using a finite-difference model of the two probe designs and the underlying perfused tissue, the errors that result from approximating these designs as one-dimensional models have been determined. It is shown that modeling a thin, disk-shaped thermistor probe as a hemisphere of appropriate radius can result in an error in calculated perfusion which is small enough for clinical use.

Thesis Supervisor: Dr. H. Frederick Bowman

Title: Senior Academic Administrator for the
Harvard/MIT Division of Health Sciences and Technology

Lecturer in Mechanical Engineering, MIT

Acknowledgments

My experience in the masters program over the last three years has taken me for months at a time to patients' bedsides, to Utah for two summers and Boston for three winters, from friendly BYU to competitive MIT, from traditional mechanical engineering design, dynamics and control through optics and signal and image processing to cardiovascular and renal disease and back to heat transfer. I have been to the depths of the Ph.D. qualifying exams and to the heights of knowing that I have given my best. Through all these experiences I have felt the hand of God guiding and blessing, healing, lifting and loving.

My advisor, Fred Bowman, has taught me the importance of taking a real, personal interest in people. I don't know how many times he has started off a research meeting asking how my family was doing. He has been understanding and supportive despite me changing research preferences and long periods of research drought. Greg Martin has deep engineering insight and a broad range of experience. Always friendly and always available, he has a way of giving feedback and advice in an uplifting way, even after long, after-hours quals practice presentations. I thank Bora Mikic for his kind and undeserved help. His suggestions were important in advancing my research, and his class prepared me wonderfully for the second pass of the qualifying exams.

I am grateful to Brian Whisenant, an interventional cardiologist who was brave enough to share his office and laptop with me for two summers, even after I locked him out of his own computer. John Lund was very helpful in making me feel at home at the University of Utah hospital.

Paul George has been a true friend since we met the week before our MIT experiences began. We feel like brothers even though I'm three years older but three years behind him in school. The fact that my desk has been right next to his has been one of the great blessings of my masters program. When you spend eight or nine hours a day next to a guy with two first names, a so-ugly-he's-cute bulldog and not a clean square inch on his desk, there's bound to be fun in the HST lounge.

I love going home at night because I get to kick off my shoes and roll on the floor with Sam, 3, and Ben, 11 months. Sam and I have gotten along since I comforted him during his neo-natal checkup. I never thought I'd be best friends with a three-year old, but whether it's playing rescue heroes, talking about robots, or philosophizing over a bowl of "Frosted Ninny-Veets" (true quote: "The world is our spaceship."), Sam is my pal.

Ben was a gift during the most difficult period of my masters experience. Part of the gift was his generously laughing personality and fat, cuddly body. The other part of the gift was the fact that dirty diapers, sleepless nights, and an ever-hungry mouth tend to shift the focus away from research and quals to more important things.

My deepest appreciation and love go to my wife Cristie. During 13 months of quals preparations and three years of masters research and classes, she has put her interests on the backburner. She has supported me not knowing what decision I would make, cheered me on, been kind when I needed kindness, and been happy for my success. I know she did it for love. My greatest accomplishment to-date is not turning in this thesis today, but celebrating seven fulfilling years of marriage tomorrow.

Table of Contents

List of Symbols

Symbol	Description	Units
A	area under hyperemia curve	kg/m^3
a	radius of disk-shaped thermistor probe	m
a^*	radius of spherical approximation	m
c	specific heat	J/(kgK)
h	height of disk thermistor probe	m
I	current passing through the thermistor probe	A
k	thermal conductivity	W/(mK)
L	characteristic length used in non-dimensionalization	m
N	sample size (Ch. 3) or intermediate parameter (Ch. 4)	
q	heat	W
q''	heat flux	W/m^2
q'''	volumetric heat generation	W/m^3
r	distance from origin/axis in spherical/cylindrical coordinates	m
R	radius of T_m=T_i boundary condition in FDM	m
t	time	s
T	temperature	°C
t^*	dimensionless time	
v	temperature minus initial temperature	°C
w	tissue perfusion [1 $kg/(m^3*s)$ = 6 ml/(100g*min)]	$kg/(m^3s)$
x	general variable used in non-dimensional analysis	
y	general variable used in non-dimensional analysis	
z	depth in tissue, measured from free probe surface	m
α	thermal diffusivity	m^2/s
γ	dimensionless perfusion	
δ	deviation of adiabat from normal	m
Δh	finite-difference cell height	m
Δr	finite-difference cell width	m
Δt	time interval	s
ΔT_b	volume-averaged probe temperature minus T_i	°C
η	sensitivity	
θ	dimensionless temperature	
ρ	density	kg/m^3
φ	dimensionless thermal conductivity	
ψ	substitution variable in probe-tissue governing equations	W/m^3

List of Subscripts

Subscript	Description
1	relating to the time interval from deflation to maximum in BART
2	relating to the time interval from deflation to baseline in BART
art	arterial
b	thermistor probe (originally from "bead")
base	baseline
bl	blood
calc	calculated
cond	conduction
conv	convection
error	error between true perfusion and calculated perfusion
i	initial, i.e. before heating the thermistor probe
in	inner disk
m	tissue (originally from "medium")
max	maximum
m,n	indices of finite-difference cells
out	outer ring
true	true, actual
ven	venous

List of Values[1]

Symbol	Description	Value	Units
c_{bl}	specific heat of blood	4187	J/(kgK)
k_m	thermal conductivity of tissue	0.485	W/(mK)
k_b	thermal conductivity of thermistor probe material	0.1173	W/(mK)
T_i	initial temperature of probe and tissue	35	°C

[1] These are the values used in calculations throughout this thesis. They are within the range of normal values. For a more complete list of typical ranges of thermal properties of biological substances, see [34].

List of Figures

List of Tables

1 Introduction

1.1 Motivation

The main function of the circulation is to deliver O_2 and nutrients to tissue and remove CO_2 and other waste products; transport substances, such as hormones, platelets, and white blood cells to specific sites in the body; distribute water, solutes and heat throughout the body; and generally maintain homeostasis. Most of these functions involve delivery or removal of gases or solutes or heat. The major site of this exchange is the microcirculation. Figure 1.1 shows a diagram of the circulation. The microcirculation is comprised of arterioles, capillaries, venules, and arteriovenous anastomoses. The blood flowing through this microcirculatory network is defined as tissue perfusion, or simply perfusion. Blood flow through larger vessels is spatially focused and directional. In contrast, tissue perfusion is more of a non-directional, volumetric measure. Perfusion is discussed more formally in Section 4.1.2.

Although there exist many modalities for quantifying blood flow in larger vessels, there currently exist no routine, non-invasive methods for quantifying microcirculatory blood flow (i.e. perfusion) in absolute units in a clinical setting. Given the abundance of exchange that occurs in the microcirculation, however, it is not surprising that an accurate, real-time knowledge of microcirculatory flow would be invaluable in many applications.

1.2 Applications

Potential applications of a non-invasive perfusion probe are many and involve both research and clinical care. Being non-invasive, the probe would be ideally suited for routine check-ups or semi-permanent measurements. In addition to the applications for which the probe *must* be non-invasive, many of the applications that have in the past employed an invasive probe would greatly benefit from switching to a non-invasive probe, thereby reducing the risk of the procedure, patient suffering, expense, and healing time. Examples of applications of a non-invasive probe include:

- Assuring graft patency in reconstructive surgery

- Monitoring ischemia and wound repair in diabetes
- Testing the effect of pharmacological agents on the microcirculation
- Managing shock in a critical care setting
- Investigating vasomotor activity as a potential indicator of cardiovascular status
- Observing the impact of therapy, diet, and life style changes on the microcirculation

In addition, the thermodiffusion method offers the possibility of determining tissue thermal properties such as thermal conductivity and diffusivity [1].

1.3 Other Methods

Methods of measuring perfusion currently used in a clinical setting can be roughly divided into two groups depending on whether the measurement is relative or absolute [2]. Table 1.1 lists the most common techniques. Relative measurement techniques include those which measure tissue perfusion directly, but in relative units, and those techniques which measure another quantity, such as blood flow through large vessels (in absolute or relative units), from which tissue perfusion (in relative units) can then be extrapolated. Table 1.1 also divides the measurement modalities into invasive and non-invasive techniques, showing that there is currently a complete lack of clinical techniques which measure perfusion non-invasively and in absolute units.

Bowman [3], Valvano [2] and Walsh [4] present a more thorough review of current and past techniques for measuring tissue perfusion. Webster's book on medical instrumentation is a good resource for learning about common blood flow measurement techniques (through large vessels) [5].

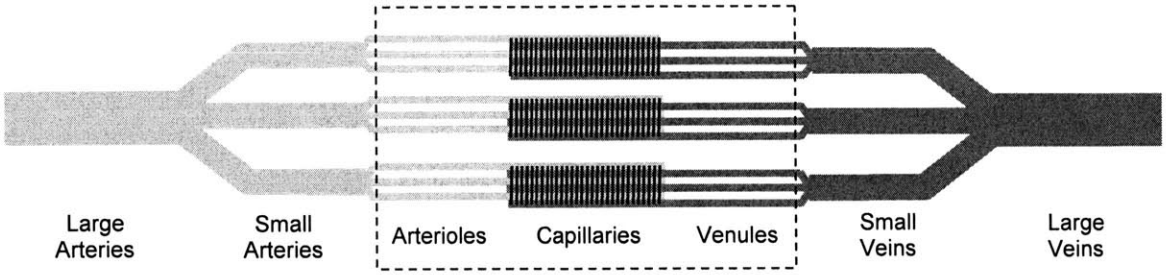

Figure 1.1 The microcirculation in the context of the entire circulation.

	Relative Perfusion	**Absolute Perfusion**
Invasive	Angiography Indicator Dilution	Xenon Washout PET Thermal Clearance Thermodiffusion
Non-invasive	Temperature & Color Blood pressure Plethysmography Laser Doppler MRI Ultrasound Doppler	

Table 1.1 Current methods of measuring perfusion in a clinical setting.

2 Thermodiffusion Probe

2.1 Basic Operation

The thermodiffusion method is a technique by which tissue perfusion can be measured. The method works much like a hot-wire anemometer in that perfusion is determined from the rate at which heat is conducted and convected away from a heated probe. Bowman et al. have developed an invasive thermodiffusion probe [1, 6]. It consists of a spherically-shaped self-heatable thermistor probe perched at the end of a catheter sheath or hypodermic needle, and is meant to be placed in, and completely surrounded by, perfused tissue (see Figure 2.1).

Measuring perfusion by the thermodiffusion method involves the following steps:

1. A thermistor probe is placed in perfused tissue and the baseline or initial tissue temperature, T_i, is established (see Figure 2.2).
2. The thermistor probe is self-heated such that its temperature is raised to and maintained at a fixed value above T_i (see Figure 2.3). The difference between the volume-averaged probe temperature and T_i is defined as ΔT_b. The volume-averaged temperature of the thermistor probe reaches its steady-state value almost instantaneously, while the power, q_b, required to establish and maintain this temperature is initially very large and then drops off to a steady-state value (see Figure 2.4). The power applied to heat the thermistor probe in the form of resistive heating (I^2R) escapes by conduction (q''_{cond}) through the tissue and by convection (q'''_{conv}) due to perfusion. The convection of heat due to perfusion is discussed in more detail in Section 4.1.2.3.
3. From a knowledge of the controlled probe temperature, ΔT_b; the power required to maintain it, q_b; and other, physical parameters of the probe and the surrounding tissue, perfusion is calculated using an analytical or numerical model.

Rather than presenting the governing equations and solutions for the invasive method here, I refer the reader to the work by Bowman, Balasubramaniam and Valvano [1, 6, 7], and instead give a more detailed presentation of the governing equations, assumptions and solutions for the *non*-invasive method in Section 4.1.

2.2 History of the Development of the Invasive Probe

In a nutshell, the development of the invasive thermodiffusion method consisted of laying the intellectual foundation for perfusion extraction and then building and testing prototypes to validate the theory. Once a prototype had been built and the method had been validated, a commercially marketable device was developed and in-depth animal and human studies were performed in order to obtain regulatory approval, and efforts are currently underway to incorporate real-time, absolute perfusion measurement into the clinical setting (see Table 2.1).

The intellectual foundation of the thermodiffusion method consists of the design of the sensor, the formulation of the thermal model of this sensor, and the creation of an algorithm to extract perfusion from the thermal model. The bulk of this work was performed during the 1970's and early 1980's by H. Frederick Bowman and his graduate students and colleagues (mainly T.A. Balasubramaniam and J.W. Valvano), first at Northeastern University in Boston, MA, and then at the Massachusetts Institute of Technology in Cambridge, MA.

Earlier, in 1968, Chato had proposed inserting a small, heated, spherically shaped thermistor probe into biological tissues for the measurement of thermal properties. In his analysis, Chato modeled tissue perfusion as an increase in "effective thermal conductivity", and the probe as a lumped thermal mass [8].

In the early 1970's, Bowman and Balasubramaniam performed a similar analysis, but modeled the probe as a distributed thermal mass. For this model, they found open-form transient solutions to the governing equations for the thermistor probe and the surrounding tissue, which provided an accurate technique for determining thermal properties of tissue [7, 9, 10].

Subsequently, Bowman and Balasubramaniam modeled tissue perfusion by the bioheat equation, an equation proposed in 1948 by Pennes to model the effect of perfusion on heat transfer in tissue [11]. They found the steady-state solution to this model for the probe and surrounding tissue, and proposed a method for calculating tissue

perfusion from a knowledge of the controlled temperature of the probe and the power required to maintain this temperature [6].

In 1979, Jain published the open-form, transient solution to a set of more sophisticated governing equations in which he models the thermistor probe as consisting of an inner, heated core and an outer shell [12]. However, this more complicated model seems to add little to the overall accuracy of the method, and is therefore not used subsequently by Bowman.

Valvano greatly contributed to the intellectual foundation by formulating the closed-form, transient solution for a heated spherical thermistor probe in perfused tissue, which he published in his Ph.D. thesis in 1981 [2] and in the literature in 1984 [1]. The key to finding the close-form solution was to express the Laplace transform of the probe temperature and tissue temperature as a Frobenius series and then perform a term-by-term inverse transform. He also found that, contrary to what was assumed at the time, the power vs. time function required to suddenly heat a thermistor probe in perfused tissue to a fixed temperature is not the same as the function determined by Chato in the 1960's for a thermistor probe in non-perfused tissue, and Valvano determined the correct function. In summary, Valvano's work produced an algorithm for extracting perfusion from both the steady-state and transient models.

On this intellectual foundation, Balasubramaniam, Bowman, Valvano, Woods and others built and tested many prototypes. Hemedex Inc. was created in Cambridge, MA, to develop a commercial thermodiffusion device, and animal studies were performed to validate the thermodiffusion method and refine the device. During the 1990's the use of the device spread to brain surgery, reconstructive surgery, transplantation, and other fields of medicine, in the United States and abroad. Martin and Bowman validated the thermodiffusion probe with the radioactive microsphere technique in 2000 [13]. Regulatory approval was obtained in 2002, and today the Bowman Perfusion Monitor is the only device on the market capable of measuring perfusion in real time and absolute units.

A brief history of the perfusion measurement research performed before 1970 by Von Rein; Hensel, Betz, and Bender; Grayson; and Perl and Hirsch is given by Walsh [4].

2.3 History of the Development of the Non-invasive Probe

Various attempts have been made to develop a truly non-invasive sensor that functions by the thermodiffusion technique, but as far as I know none of the concepts have had the capability of accurately tracking and quantifying quickly fluctuating perfusion in absolute units and in real time.

In 1979 Patera and others proposed a very elegant method for determining perfusion by measuring the phase shift between a sinusoidally applied heat flux at the tissue surface and the temperature response. This method has the strong advantage of not depending on the temperature of the probe or the tissue, but only "on frequency, phase shift, and intrinsic properties of the tissue" [14]. The principal disadvantage of this method is that the magnitude of the dynamic temperature response, and therefore the accuracy of the calculated perfusion, decreases with increasing driver frequency. Since only perfusion fluctuations that are slow compared to the driver frequency can be measured, this technique cannot track perfusion above approximately 0.1 Hz. If the non-invasive probe is to be used to investigate vasomotor tone, which includes fluctuations above 0.1Hz (see section 3.4.1), another method must be used.

In 1984 Walsh showed that a non-invasive probe could be created using two flake thermistors. Upon analytically modeling the probe as an infinite slab and as a sphere (both 1-dimensional models), he found that the slab model is inadequate and that the spherical model is more appropriate. Experimental results showed that the non-invasive probe is sensitive to changes in perfusion [4].

In 2001 and 2002, I used the invasive probe in a non-invasive manner by placing the invasive probe on the backhand of approximately 75 subjects, some healthy and some with heart disease (see Chapter 3). In a nutshell, it was found that while the invasive probe was able to track perfusion very accurately in some cases, in most cases thermal communication between the probe and the tissue was too poor to establish or maintain a sensible signal. In addition, the meaningful signals that were obtained could not be relied on for absolute values of perfusion. It was therefore concluded that the thermodiffusion method had great promise for non-invasive use, but that a truly non-invasive probe should be developed to address the issues of thermal communication and calculation of perfusion in absolute units.

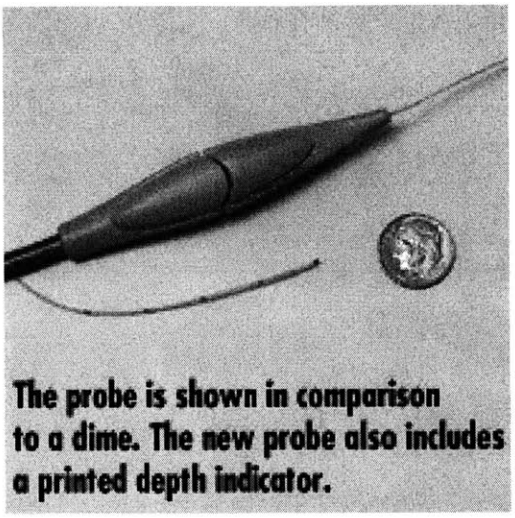

Figure 2.1 The thermodiffusion probe produced by Hemedex, Inc. [15].

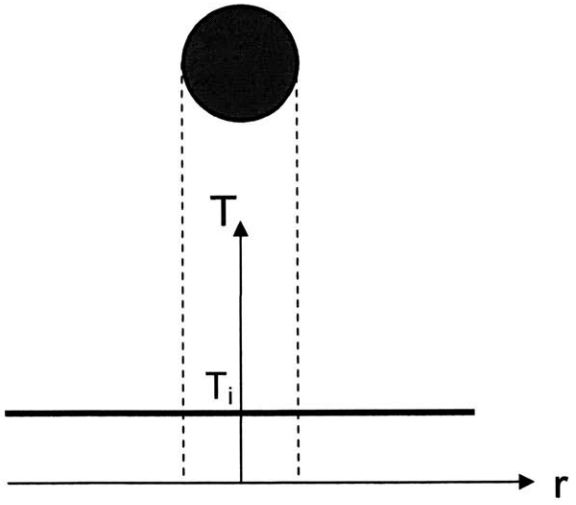

Figure 2.2 Temperature profile of thermistor probe and tissue before heating.

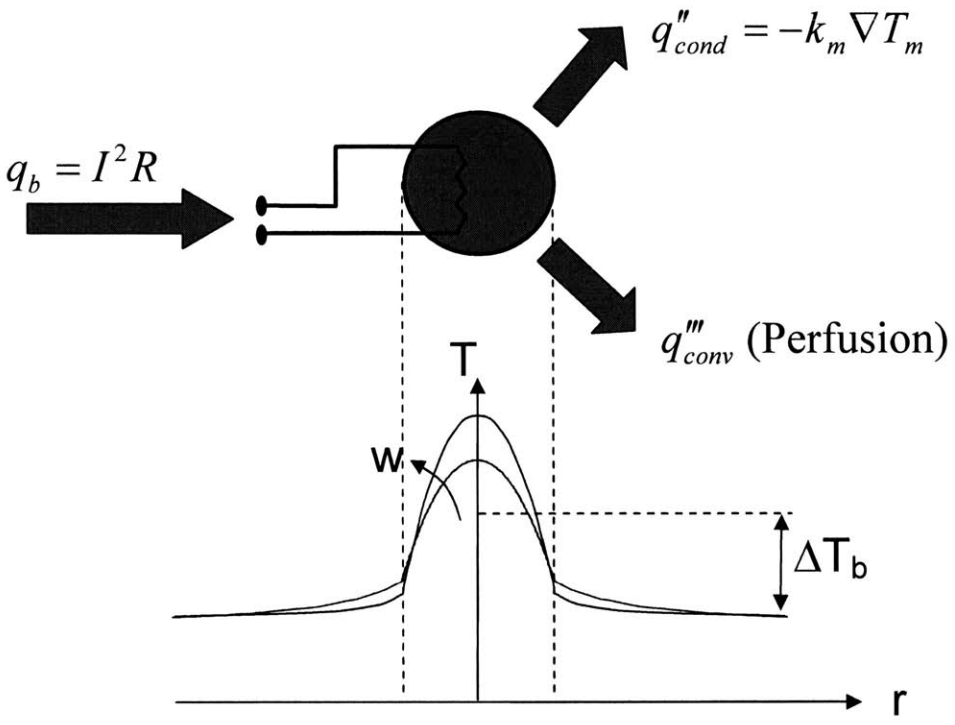

Figure 2.3 Temperature profile of the thermistor probe and tissue after heating, at two different levels of perfusion. k_m=tissue thermal conductivity, I=current, R=probe resistance.

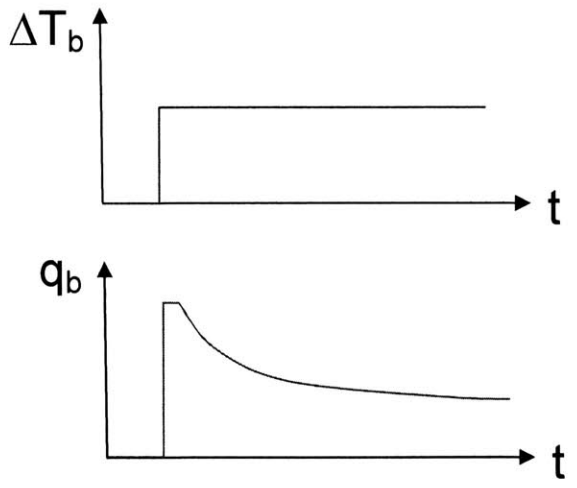

Figure 2.4 Heating the thermistor probe: temperature vs. time and power input vs. time.

Upon heating, ΔT_b reaches a fixed value almost instantaneously. The power required to achieve this step-change in temperature is initially very large, saturates, and then drops off to a steady-state value.

Clinical Studies	**1992-present**
Regulatory Approval	**2002:** Approval by the U.S. Food and Drug Administration
Animal Studies	**1975-present**
Validation Studies	**2000:** Martin and Bowman validate thermodiffusion method against microsphere technique [13]. **2000:** Vajkoczy et al. validate invasive thermodiffusion probe in human against Xe CT [16]. **1999:** Klar et al. validate thermodiffusion probe in pigs against Doppler flowmetry and H-2 clearance [17]. **1984:** Valvano and Bowman validate thermodiffusion method in isolated, perfused rat liver system against multiple radioactive microspheres [18].
Device Development	**2000-present** Hemedex
Prototype	**1970-1999:** Prototype evolution (12 generations). **1989:** Szaijda develops analog subsystem, data acquisition system [19, 20]. **1984:** Valvano et al. measure thermal conductivity, thermal diffusivity, and perfusion in small volumes of tissue [1].
Reduction Algorithm	**1981:** Valvano extracts perfusion from transient and steady-state models [2]. **1977:** Bowman and Balasubramaniam extract perfusion from steady-state model [6].
Sensor Design & Thermal Modeling	**1981:** Valvano solves transient equations for distributed thermistor probe in perfused tissue (closed form) [2]. **1980:** Bowman identifies thermally significant vessels [21]. **1979:** Jain solves transient equations for two-zone distributed thermistor probe in perfused tissue (open form) [12]. **1977:** Bowman, Balasubramaniam, and Woods solve steady-state solutions for distributed thermistor probe in perfused tissue [6]. **1977:** Balasubramaniam and Bowman propose method for measuring thermal properties of biomaterials [7]. **1974:** Balasubramaniam and Bowman solve transient equations for distributed thermistor probe in unperfused tissue [9]. **1968:** Chato solves transient equations for lumped thermistor probe in perfused tissue [8].

Table 2.1 The development of the invasive thermodiffusion probe from the 1960's until present.

3 Clinical Study: Using the Invasive Probe in a Non-invasive Manner

3.1 Introduction

3.1.1 Cardiovascular Disease and Atherosclerosis

As of 1998, cardiovascular disease had been the number one cause of death in the USA since 1918. It accounted for 45% of all deaths, claiming more lives than the next seven leading killers combined. The underlying problem in cardiovascular disease is atherosclerosis {Study, 1998 #25}.

Atherosclerosis is the formation of fibrofatty plaques in the vascular lumen, resulting in calcification and weakening of the vessel wall. Photos of a normal coronary artery as well as one with build-up of atherosclerotic plaque can be found in [23]. Complications of atherosclerosis include hemorrhage, plaque rupture, and thrombosis. Common clinical manifestations include heart attack, stroke and aneurysm [24]. The initiating event in atherosclerosis is endothelial dysfunction [25].

3.1.2 Endothelial Dysfunction

The endothelium is a monolayer of cells that lines the entire vascular system. As a semi-permeable membrane, the endothelium is critical to vessel wall homeostasis and blood flow. Its functions are many and include [24]:

- Modulating vascular tone and blood flow
- Maintaining the non-thrombogenic blood-tissue interface
- Metabolizing hormones
- Regulating immune and inflammatory reactions
- Modifying lipoproteins in the vessel wall
- Regulating growth of other cell types, particularly smooth muscle cells

Endothelial dysfunction, which describes "changes in the functional state of endothelial cells," is the initiating event in atherosclerosis and plays a role in the disease

process as well [24]. The endothelium becomes damaged decades before the development of atherosclerosis and following cardiac events.

3.1.3 Assessment of Endothelial Dysfunction

Many techniques have been developed for evaluating the health of the endothelium and thereby assessing the onset or progression of atherosclerosis. Anderson presents a review of the assessment and treatment techniques of endothelium dysfunction in humans [25]. "Local vascular control depends on a balance between dilators and constrictors, with endothelium-dependent nitric oxide (NO) being the best characterized and probably the most important. Nitric oxide is stimulated by a variety of stimuli that serve as the basis for the assessment of endothelium–dependent vasodilation" [25].

Two vasodilator stimuli used in the assessment of endothelial function are administration of acetylcholine and flow-mediated vasodilation. The intracoronary administration of acetylcholine has been the gold standard in testing for endothelial dysfunction. Acetylcholine triggers the healthy endothelium to release nitric, causing the blood vessel to vasodilate. In contrast, acetylcholine vasoconstricts the diseased vessel.

Flow-mediated vasodilation (FMD) involves temporary occlusion of a vessel using a blood pressure cuff. Cuff deflation results in reactive hyperemia, which is a temporary increase in blood flow beyond the baseline level. Most often, the occluded artery is the brachial artery, and the technique is called Brachial Artery Reactivity Test (BART). The magnitude of the reactive hyperemia has been shown to correlate with coronary endothelial dysfunction [26]. Table 3.1 presents these two techniques (administration of acetylcholine and FMD).

A variety of sense techniques are available for each of these two methods. Some are listed in Table 3.2, along with their advantages and disadvantages. It is clear that a non-invasive, cheap, easy-to-use technique that gives perfusion in real time and absolute units would be highly desirable. The thermodiffusion method has this potential.

3.2 Data Gathering

During Summer 2001 and January 2002, I used the invasive thermodiffusion probe in a non-invasive manner in order to measure tissue perfusion in the backhands of approximately 80 subjects. The goal of the study was three-fold:

1. Establish a protocol.
2. Determine the feasibility of using the invasive thermodiffusion probe non-invasively
3. Perform BART on subjects with and without heart disease in order to study the impact of heart disease on endothelial function and vasomotor activity of peripheral tissue

3.2.1 Protocol

3.2.1.1 Probe Placement

Location

It makes sense to place the probe on tissue with a high capillary density. This suggests placing the probe in or close to the digital district as opposed to the forearm. Informal studies have shown that it is much easier to pick up a sensible signal on the hand/fingers than on the forearm.

Complete Enclosure

Since the perfusion extraction algorithm assumes a 4π-geometry (spherical probe completely and symmetrically surrounded by tissue), it is critical that the probe have as much contact as possible with the surrounding tissue. Most importantly, this will decrease the likelihood that a slight disturbance in probe position or orientation would disrupt the measurement.

As shown in Figure 3.1, probes (object shown is not actually the probe) were placed on the backhand, between the thumb and the index finger, and the thumb and the index finger were brought together, enclosing the probe (as well as approximately 10-15mm of wire). The thumb was then taped to the rest of the hand in such a manner that

the subject could relax his/her hand but the probe would not move. It is important that the "squeezing pressure" be below the capillary collapse pressure.

"Squeezing Pressure" vs. Capillary Collapse Pressure

It is important that the pressure with which the probe pushes against the tissue not substantially diminish perfusion, let alone occlude the capillaries. Martin has shown that a pressure of approximately 5mmHg should not be exceeded [27].

3.2.1.2 Contact Gels

Standard ultrasound gel was used for some of the measurements. It is difficult to say whether its use improved the measurements. No negative effects were observed.

3.2.1.3 Insulation of the Hand

Wrapping the hand in a towel or blanket insulates it from air currents and temporary changes in room temperature. Also, it is assumed that the amount of heat lost along the probe wire is decreased. However, insulating the hand does drive the hand temperature up.

3.2.1.4 Manual Mode vs. Automatic Mode

The Bowman Perfusion Monitor produced by Hemedex allows for manual or automatic operation. In automatic operation, the software will recalibrate if limits in certain parameters have been exceeded. During the occlusion phase of BART, perfusion drops to zero, and the software will often command a recalibration, frustrating the measurement (and the measurer). Manual operation sidesteps this problem. However, it is possible that a recalibration really is necessary, and the measurement in manual mode would continue despite the need for recalibration.

3.2.1.5 Patient at Rest

Because the probe is not actually completely surrounded by malleable tissue but is instead in contact with tissue on some areas of its surface and with air/liquid on other areas, slight perturbation in the probe's position and/or angular orientation can cause huge, non-physiological spikes or drops in measured perfusion. It is therefore critical than

the subject's arm, hand and fingers be at complete rest. Interaction with doctors, nurses or family must be avoided. Even using his/her other hand, e.g. to change the TV channel, can disturb the measurement.

3.2.1.6 Measurement Duration

Various protocols have been used by different groups. Except for the sense site and method, the protocol used in this study is representative of many other BART studies found in the literature.

Ideally, after the calibration period, a 5-minute baseline measurement is recorded. Subsequently, the cuff is quickly inflated to approximately 50mmHg above systolic blood pressure (some groups set a safe, fixed pressure for all subjects, e.g. 200mmHg) and left inflated for 5 minutes, then deflated. After deflation, the measurement should be continued until perfusion has returned to its baseline value. This typically takes between 5 and 15 minutes. If studies of post-occlusion baseline are planned, the measurement should be continued for some time after perfusion has returned to baseline values. If pre- or post-occlusion baseline perfusion is to be analyzed in the frequency domain, measurement duration and sampling frequency must be chosen such that the desired bandwidth and resolution are obtained (see section 3.4.5).

3.2.2 Measurement Issues

Many difficulties arose in making perfusion measurements. The most typical measurement challenges are shown in the middle row of Figure 3.2. They include:

1. Failure to detect physiological baseline perfusion
2. Failure to detect zero perfusion during occlusion despite high occlusion pressure
3. Non-physiological spikes and drops in perfusion

There may exist simple explanations for some of these challenges. For example, consider the middle row of Figure 3.2. Bowman [28] has suggested that both of these plots may show normal measurements that are shifted downward or upward due to an offset caused by a deviation from assumed model conditions (e.g. the 4π-geometry assumption).

Perfusion measurements were performed on 80 subjects. A stable baseline measurement was obtained for approximately 65% of subjects. Of those measurements it was possible to perform and record BART on 45%, resulting in 21 good BART measurements (13 of those measurements were recorded from patients with heart disease, and 8 without heart disease).

Despite this rather low success rate, the measurements clearly prove the feasibility of a non-invasive thermodiffusion probe. For example, in many cases, the probe was able to very nicely track drops and rises in perfusion due to BART. Also, as shown in the bottom row of Figure 3.2, the probe is capable of picking up high- and low-frequency signals undetectable by most other routine techniques. This frequency information can be used in analyzing vasomotor activity, as discussed in section 3.4.5. It appears possible that these capabilities could be harnessed and the difficulties discussed above overcome if a truly non-invasive thermodiffusion probe were designed and developed—hence the efforts presented in chapter 4 of this thesis to design a truly non-invasive thermodiffusion probe.

3.2.3 Non-collocation of Event, Stimulus, and Sense Sites

In this study, the site where

1. the events, such as myocardial infarction and stroke, occur (i.e. the heart),
2. the test stimulus (i.e. occlusion) is administered (i.e. the brachial artery, upper arm), and
3. the response to the stimulus is sensed using the thermodiffusion method (i.e. the backhand)

are all non-collocated, as depicted in Figure 3.3. Unfortunately, the three-way relationship between these sites is not obvious. Vita and Keaney discuss this issue in particular in their 2002 editorial [29].

In hindsight it is clear that collocating these sites and/or posing a more tractable and straightforward research question would have led to more useful data. The usefulness of this study rests mainly in the evidence that the invasive thermodiffusion probe, even when applied non-invasively, tracks perfusion and temperature very closely, with a high

temporal resolution, and in real time, and that the development of a truly non-invasive probe should be pursued.

3.2.3.1 Event Site to Test Site

The reason why the event and test sites were separated is that "although assessment of coronary endothelial function is clearly germane for coronary artery disease events, this methodology is limited by the risk and expense of coronary angiography and selective intracoronary agonist infusion. As a consequence, there has been considerable interest in the study of endothelial vasomotor function in more accessible vascular beds, such as brachial circulation... The relevance of the brachial circulation to coronary and carotid artery events is not obvious. However, the systemic nature of many risk factors makes it plausible that they might affect central and peripheral arteries in a parallel manner. Indeed, studies suggest that endothelial dysfunction detected noninvasively in the arm correlates with coronary endothelial dysfunction [26]. Despite these findings, it is well recognized that physiological mechanisms differ importantly according to vascular bed" [29].

3.2.3.2 Test Site to Sense Site

In many published studies, test and sense sites are collocated. In other words, the response of the brachial artery to BART is measured in the brachial artery, using methods such as ultrasound and laser doppler flowmetry. Non-invasive thermodiffusion seems to work best in tissue with a high capillary density such as the skin of the hand and fingers.

For this reason the test and sense sites were non-collocated. Cuff inflation and deflation on the upper arm are immediately detectable and traceable in the measurement of perfusion on the backhand, showing clearly that there exists a strong relationship with very little time lag. No doubt the signal received at the backhand is a filtered version of what originates in the upper arm, though the exact filter is unknown.
Also, the non-collocation of test and sense site in flow-mediated vasodilation is not without precedent [30].

3.3 Database of Measurement Data and Subject Information

The measurement data and subject information for each patient were compiled in a database, as outlined below.

3.3.1 Measurement Data

The measurement data, automatically collected by the thermodiffusion monitor, include (all vs. time):

- probe temperature
- skin temperature (measured by the passive thermistor probe)
- power
- perfusion calculated by the transient model
- perfusion calculated by the steady-state model

as well as six other parameters. Measurements were made at 10 Hz and typically lasted about 25 minutes, adding up to approximately 15,000 measurements of each of 11 parameters for each of approximately 80 subjects. These data were converted and stored in matrix format in MATLAB for easy manipulation and analysis.

3.3.2 Subject Information

The following information was recorded for each subject:

- gender
- age
- weight
- current medication

The following yes/no information was recorded for each subject:

- coronary artery disease (any history of coronary intervention automatically qualified)
- diabetes mellitus
- hyperlipidemia (normally evaluated by looking at prescribed medications)
- hypertension
- smoking

- family history of heart disease

3.4 Analysis

3.4.1 Physiological Issues

Blood flow is a complex, dynamic phenomenon in space and time. It is influenced by numerous factors both locally and systemically. For purposes of this clinical study, the following understanding is important:

- "THE PRIMARY FUNCTION OF THE CUTANEOUS CIRCULATION IS MAINTENANCE OF A CONSTANT BODY TEMPERATURE. Consequently, blood flow to the skin fluctuates widely depending on the need for loss or conservation of body heat" [31]. This severely complicates the analysis of baseline or steady-state perfusion. Local perfusion can change suddenly in a step-like manner, making it difficult to determine a baseline value in the first place, and making it clear that any comparison between baseline values over time is suspect.
- Cutaneous circulation contains oscillations, and "there are indications that these oscillations may represent the influence of the heart beat, the respiration, the intrinsic myogenic activity of vascular smooth muscle, and the neurogenic activity on the vessel wall, with frequency around 1, 0.3, 0.1, and 0.04 Hz, respectively... In addition, periodic oscillations with a period of 1 min (0.01Hz) have been demonstrated..." [32].

3.4.2 Filtering

Like much of biological data, the collected perfusion and temperature data contained much noise, artifact, and human variability. Therefore, it was necessary to filter the data prior to statistical analysis. As shown in Figure 3.4, the measurements were first manually segmented using the following information:

- a record of unusual events during the measurement
- an understanding of normal physiological baseline values and responses
- temperature data (especially useful in establishing occlusion starts and stops)

- known characteristics of the thermodiffusion device

The data were then analyzed in the frequency domain, where non-physiological oscillations (presumably stemming from instrument artifacts) were filtered out. In hindsight, there is some concern that the manual segmentation and filtering could have subjectively corrupted or biased the data by removing what were thought to be abnormal (assumed to be artifactual) features.

The perfusion and temperature data were both split into baseline and BART segments and statistically correlated with whether or not the subject had heart disease. Perfusion and temperature analysis are each discussed in turn.

3.4.3 Perfusion

In the past, the analysis of BART studies has focused on the way vessel diameter (and therefore perfusion) reacts to reopening of the artery upon cuff deflation, but useful information may be gleaned from investigating baseline perfusion as well. The high-sampling rate and high accuracy of the thermodiffusion method makes baseline examination feasible.

3.4.3.1 BART

The analysis of flow-mediated vasodilation data has generally been limited to observing how simple BART characteristics vary between subjects. Typical characteristics include [33]:

- maximum increase in the post-stimulus vessel diameter as a percentage of baseline diameter (this is the most commonly used characteristic)
- time from cuff deflation to maximum response
- duration of the vasodilator response
- area under the dilation curve

By the thermodiffusion method, perfusion is measured instead of vessel diameter. Analogous characteristics can be defined as (see Figure 3.5):

- maximum hyperemic increase in perfusion (w_{max}-w_{base}) as a percentage of baseline perfusion:

$$100 \times \frac{w_{\max} - w_{base}}{w_{base}}$$

- time from cuff deflation to maximum response, Δt_1
- duration of the vasodilator response, Δt_2
- area under the dilation curve, A

The last two characteristics, Δt_2 and A, require that perfusion return to baseline, and that the measurement be continued to that point. In many cases, post-maximum perfusion was non-physiological, or the measurement was terminated pre-maturely for other reasons. The result was that the final sample size was too small to compare subject populations on the last two characteristics.

Figure 3.6 shows the change in post-stimulus perfusion and time to maximum response for healthy and heart-diseased subjects. The bars indicate one standard deviation.

3.4.3.2 Baseline

As discussed in 3.4.1, comparing baseline perfusion values at different times or between subjects is highly problematic. However, it is reasonable to suggest that some aspect of baseline perfusion may be affected by endothelial dysfunction and atherosclerosis. As seen in Figure 3.2, perfusion can be highly variable over a large frequency range. In other words, perfusion contains relatively large fluctuations of a variety of frequencies. Some component of this variation may correlate with endothelial dysfunction. Because most methods are not suited to long, high-sampling rate perfusion measurements, no standard procedure for analyzing baseline perfusion exists. One candidate is to look at how often the perfusion vs. time curve changes from increasing to decreasing or vice versa, or, alternatively, how often it crosses over an average value. This is close to, but distinct from, a simple spectral analysis because the magnitude of the oscillation at a specific frequency bears no weight.

As shown in Figure 3.7, determination of the frequency with which a data set changes from increasing to decreasing or vice versa is dependent on the frequency range under consideration. In other words, one can count high-frequency, low-magnitude jitter, or low-frequency, high-magnitude changes, or anything in-between. Thus it is possible to

create a continuum of 'frequency at which a data set changes from increasing to decreasing or vice versa' vs. 'frequency range under examination'.

In practice, one can low-pass or band-pass filter the data set with filters of various cut-off frequencies, and count the number of times the data set changes from increasing to decreasing or vice versa. Dividing the number of changes by the time interval of the data set gives the frequency of change.

Figure 3.8 shows the frequency of change at low frequencies (band-pass filtered with cut-off frequencies of 0.025 and 0.06 Hz) for healthy and heart-diseased subjects. The lack of statistically significant differences is typical of the results obtained from this frequency continuum.

3.4.4 Temperature

Since the main function of the cutaneous circulation is thermal regulation, which is achieved by orchestrating the flow of perfusion through the complex microcirculatory network, it is conceivable that some aspect of a subject's temperature vs. time profile, whether baseline or in BART, might correlate with endothelial dysfunction and atherosclerosis. However, exactly what aspect would provide such a correlation is unclear, and it seems probable that such a correlation would be a step removed from a more direct correlation between endothelial dysfunction and perfusion.

Nevertheless, various characteristics of the temperature vs. time profile were examined. Following are most of the examined characteristics, divided into BART and baseline.

3.4.4.1 BART

The slope of the temperature vs. time profile during occlusion, as well as the total temperature drop during occlusion, were investigated.

3.4.4.2 Baseline

In the time domain, the mean and standard deviation of the temperature vs. time profile were examined. The signal was also investigated in the frequency domain. Several profiles showed a very large spike around 2 Hz, which is thought to be an artifact of the

thermodiffusion device. Also, the "frequency of change" analysis introduced in section 3.4.3.2 was applied to the temperature profile.

Unfortunately, the correlations between these temperature characteristics (in BART and baseline) and the subject's disease state proved either statistically insignificant or physiologically meaningless, and are therefore not reproduced in this thesis.

3.4.5 Frequency-domain Analysis

As stated above, it is reasonable to think that differences might exist in the frequency spectrum of the perfusion vs. time profile (and possibly of temperature as well) between subjects with and without endothelial dysfunction. In the past, low sampling rates and short measurement durations have precluded thorough investigation of the frequency spectrum. However, some methods, such as the thermodiffusion method, are capable of providing high sampling rates, and could therefore be used to gather data for examination in the frequency domain. For example, the data for this study were gathered at 10 Hz, and the average duration of recorded stable baseline perfusion was approximately 2 minutes (120 seconds). The highest non-aliased frequency is given by the Nyquist theorem as 5 Hz, and the lowest frequency is given by the frequency resolution as 1/120s=0.0083 Hz.

Though no statistically significant correlations were obtained from the data of this study, it is reasonable to think that frequency domain analysis of perfusion may provide a valuable view of the differences between subjects with and without endothelial dysfunction. Kvernmo et al. present some of the promises and challenges associated with the frequency domain analysis of perfusion [32].

3.4.6 Conclusions

The goal of this study was three-fold: to establish a protocol, to investigate the feasibility of a non-invasive thermodiffusion probe, and to study correlations between cutaneous circulation (in baseline and BART) and endothelial dysfunction. Several conclusions can be drawn:

3.4.6.1 Feasibility of a Non-invasive Thermodiffusion Probe

- The thermodiffusion method, applied non-invasively, is sometimes capable of tracking (relative) perfusion very closely.
- The thermodiffusion probe offers advantages over other perfusion measuring devices, such as high sampling frequency, which could be very useful in analysis.
- However, most of the time, poor thermal communication between the probe and the skin caused unstable and non-physiological signals. In addition, when stable signals were obtained, the absolute magnitude had no meaning since the model assumption of isotropic 4π-geometry was not valid.
- Therefore, the development of a truly non-invasive should be pursued.

3.4.6.2 Cutaneous Circulation and Endothelial Dysfunction

- Although the initial sample population was large, much of the data were non-physiological and therefore discarded. The resulting final data set was quite small (only 21 good BART tests).
- BART studies in the literature show a correlation between endothelial dysfunction and characteristics of vessel diameter vs. time, as discussed in section 3.4.3. The data in this study were not found to be statistically significant with regard to analogous perfusion characteristics. This lack of statistically significant results was likely caused by a combination of two of the major difficulties of this study: measurement noise caused by poor thermal communication and poor thermal stability at the probe-tissue interface; and non-collocation of event, stimulus, and sense sites.
- The non-collocation of event site, test site, and sense site made interpretation of results difficult.
- With a high sampling rate and the possibility of long-duration measurements, a reliable non-invasive thermodiffusion method/probe would allow for new analysis techniques, especially frequency domain analysis of baseline perfusion.

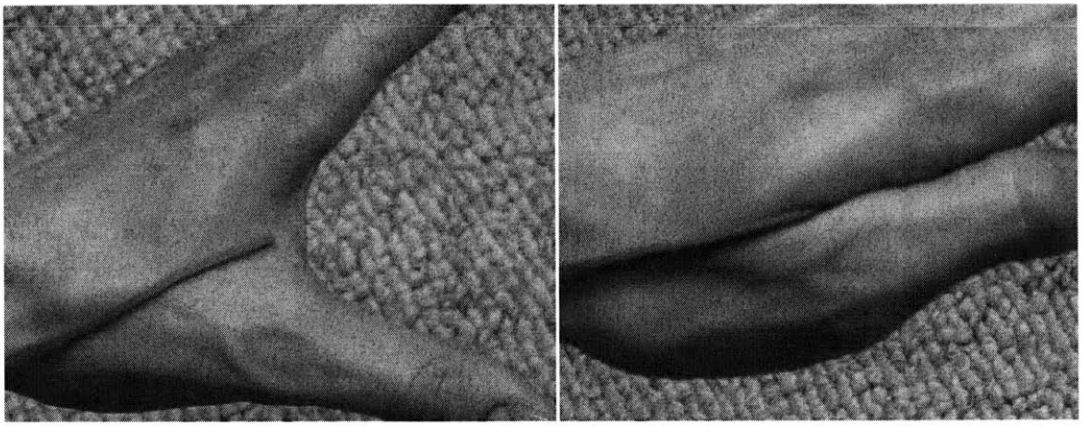

Figure 3.1 Non-invasive placement of the thermodiffusion probe (originally designed for invasive use) for non-invasive clinical study (the object shown is not the actual probe).

Stimulus	Normal function	Dysfunction
Acetylcholine (Gold Standard)	vasodilation	vasoconstriction
Temporary occlusion (Brachial Artery Reactivity Test)	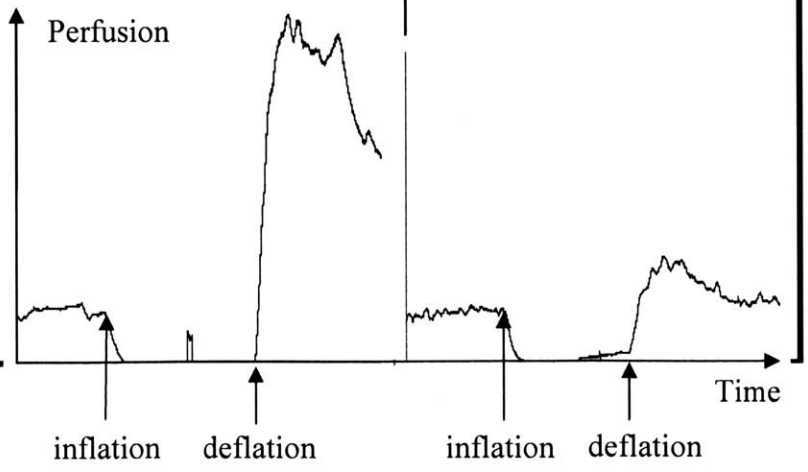	

Table 3.1 Two tests for endothelial dysfunction.

Upon intracoronary administration of acetylcholine, the healthy vessel vasodilates while the diseased vessel vasoconstricts; following temporary occlusion, the healthy brachial artery shows more pronounced reactive hyperemia compared to the diseased artery.

Sense method	Coronary angiography	Ultrasound	Laser doppler flowmetry
Vascular bed	Coronary circulation	Brachial artery	Forearm microvasculature
Stimulus	Acetylcholine (by intracoronary infusion)	Acetylcholine or temporary occlusion (FMD)	Acetylcholine or temporary occlusion (FMD)
Measurement variable	Vessel diameter	Vessel diameter	Net erythrocyte velocity (doppler shift)
Test variable	Vasoconstriction vs. vasodilation	Vasoconstriction vs. vasodilation Change in diameter	Perfusion
Advantages	Looks at coronary circ. (where events occur)	Non-invasive	Minimally/non-invasive Continuous, real time
Disadvantages	Invasive Risk, cost of cardiac catheterization die injection	Ultrasound technician Expensive equipment	Not in absolute units Depends on optical tissue properties

Table 3.2 Comparison of three of the most popular sense methods used in tests of endothelial dysfunction.

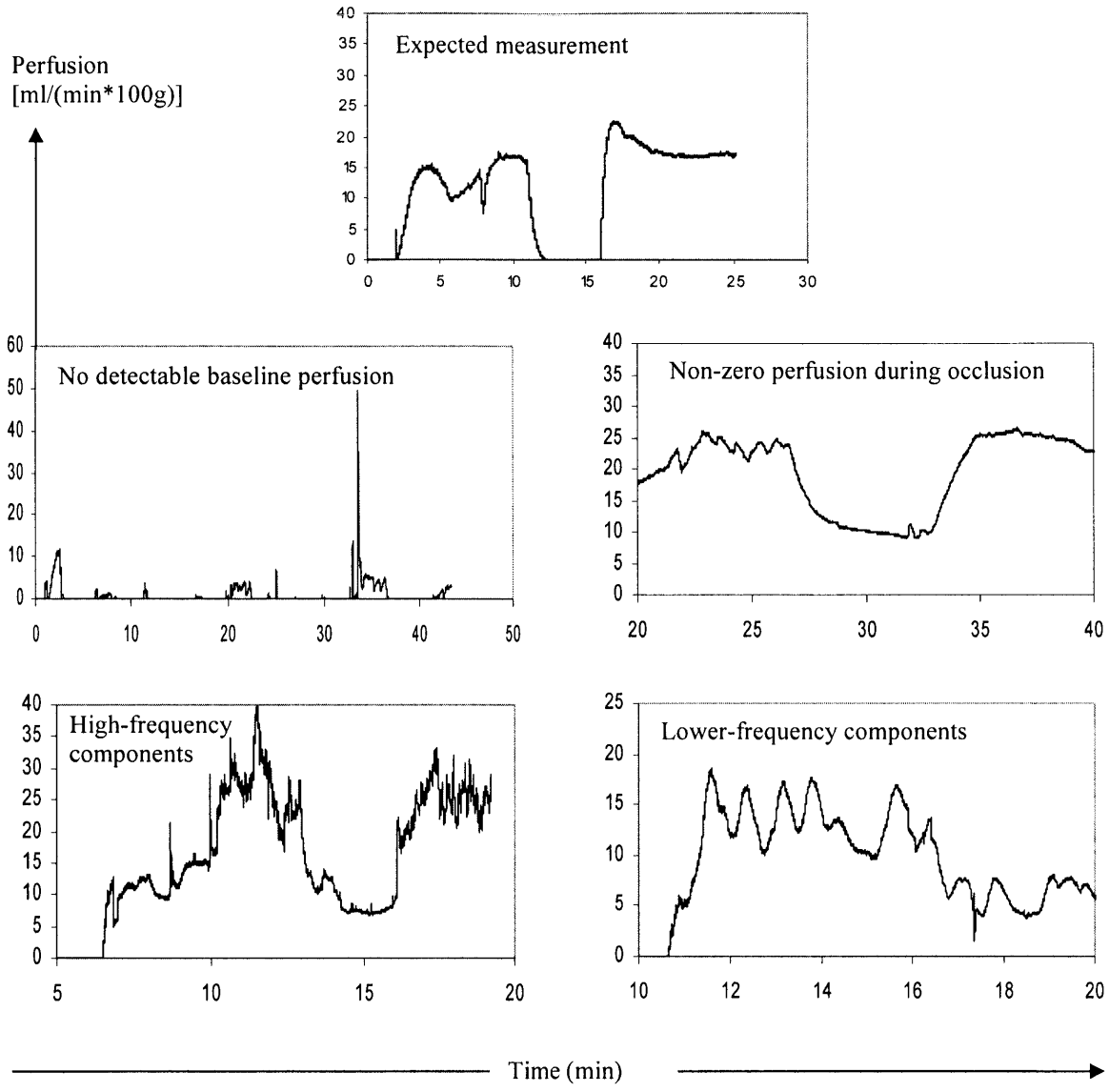

Figure 3.2 Challenges and strengths of the thermodiffusion method.

A clear signal is shown in the top row; failure to pick up baseline perfusion and failure to measure zero perfusion during occlusion are shown in the middle row; the unique ability of the thermodiffusion method to clearly pick up a large range of frequencies is shown in the bottom row.

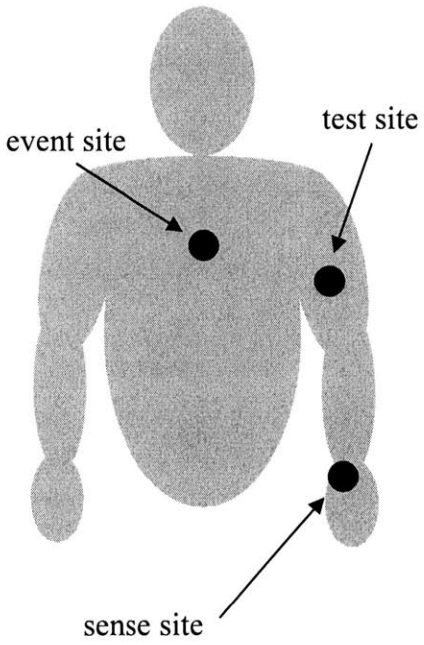

Figure 3.3 Non-collocation of event, test, and sense sites.

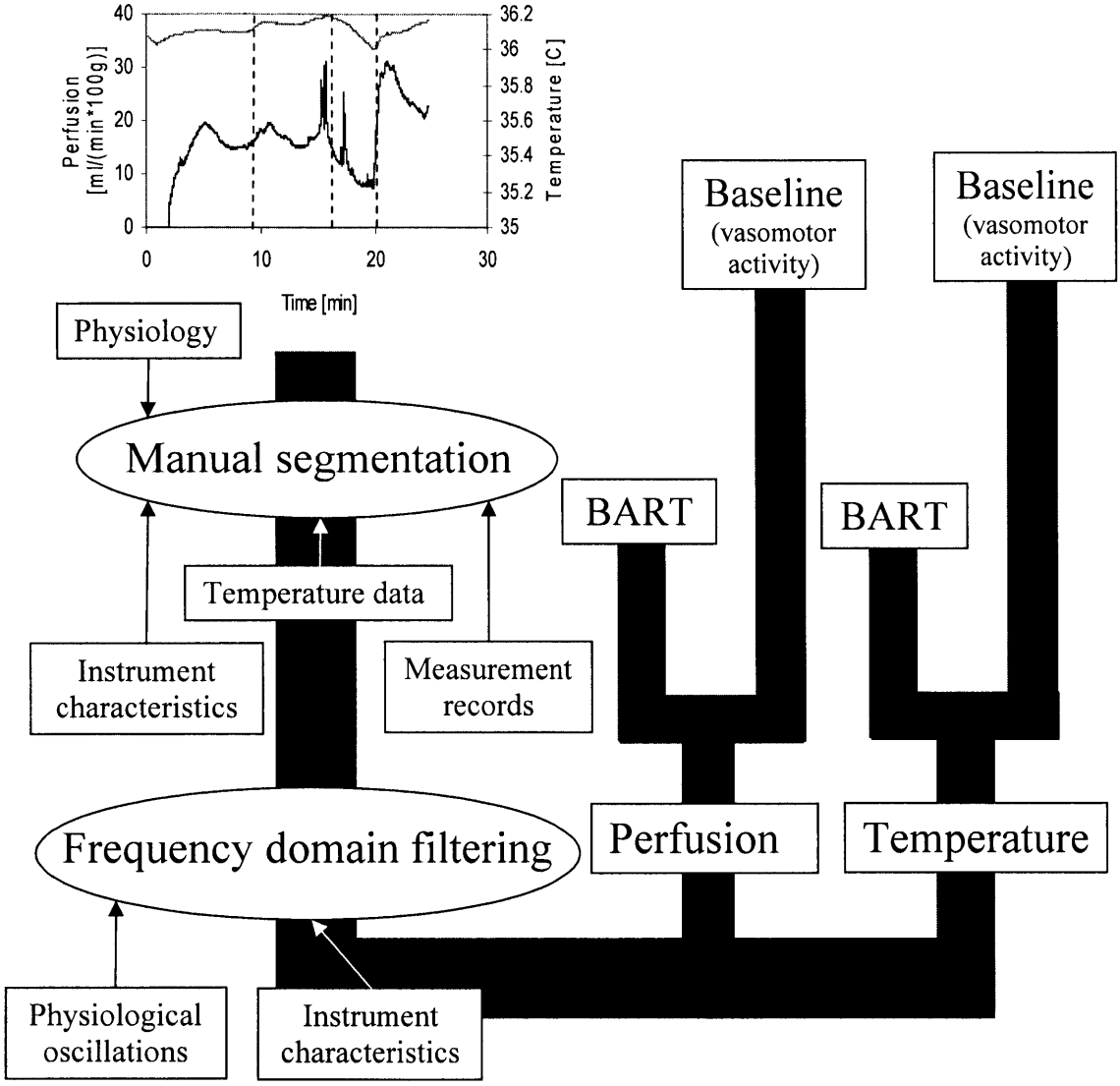

Figure 3.4 Flow chart of segmentation, filtering, and analysis process.

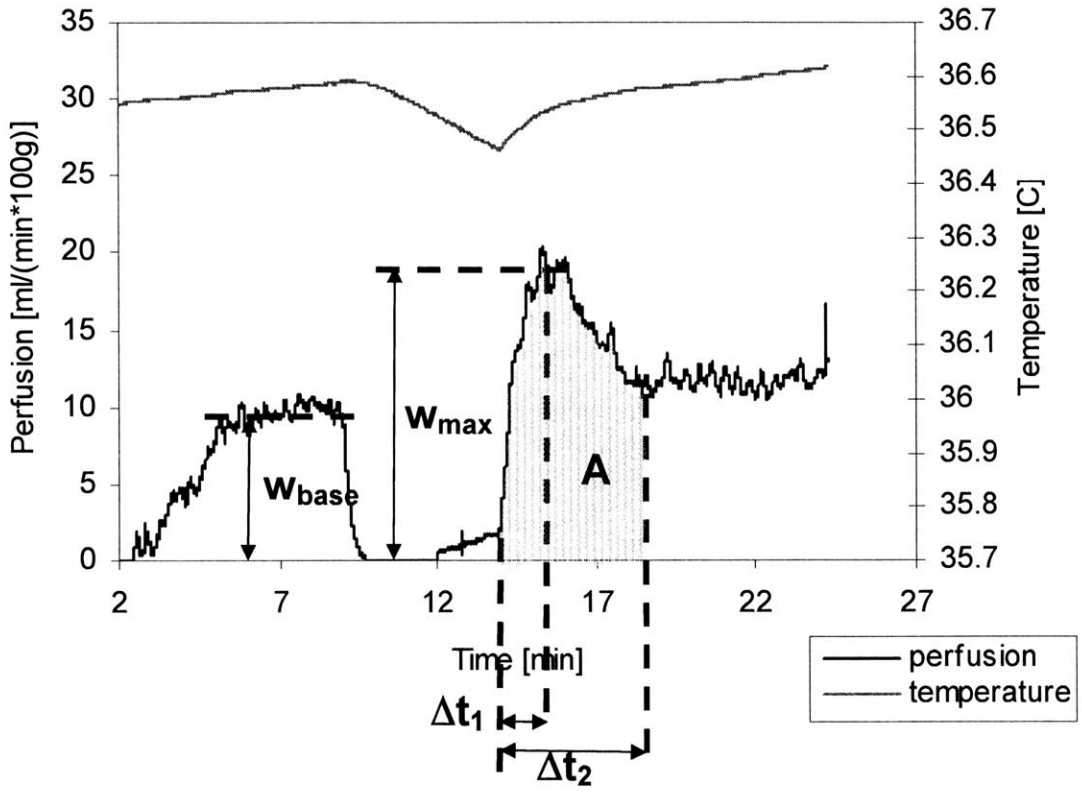

Figure 3.5 Commonly used metrics in the Brachial Artery Reactivity Test (BART) (top curve is temperature, bottom curve is perfusion).

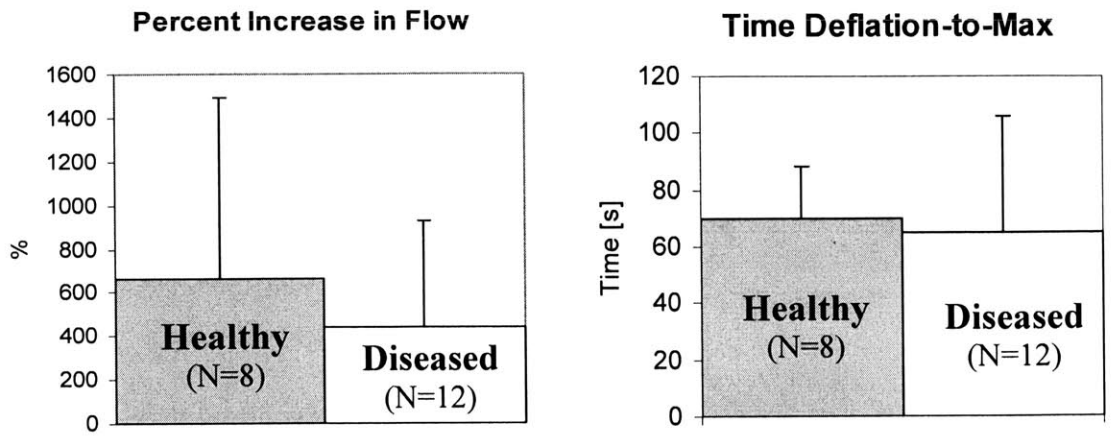

Figure 3.6 Results from the BART study: percent increase in flow (left) and time from deflation to maximum perfusion (right). Bars show one standard deviation. *N*=sample size.

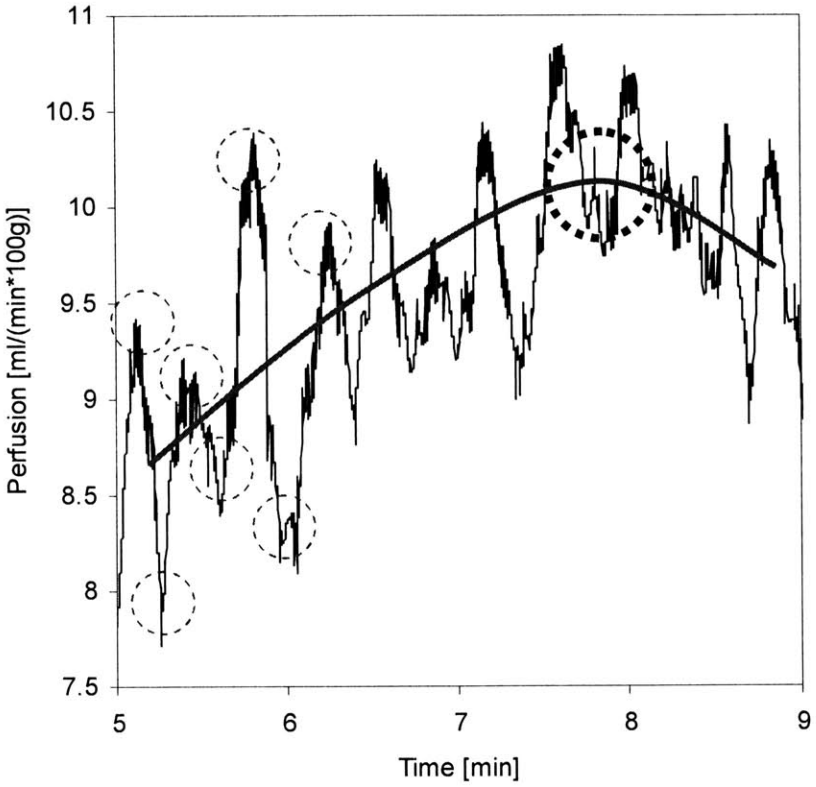

Figure 3.7 Rate at which perfusion changes from increasing to decreasing or vice versa, at two different frequencies.

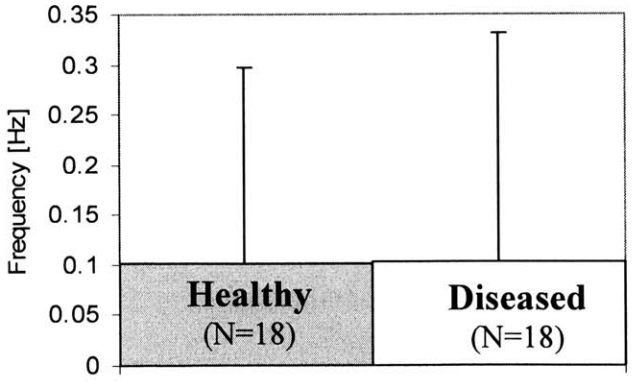

Figure 3.8 Result from the study of the frequency at which baseline perfusion changes from increasing to decreasing or vice versa, analyzed at low frequency (band-pass filtered with cut-off frequencies at 0.025 and 0.06 Hz). *N*=sample size.

4 Theoretical Study: Design and Thermal Modeling of a Non-invasive Probe

4.1 Governing Equations

As explained in Section 2.1, from a knowledge of the controlled temperature of the thermistor probe and the steady-state power required to maintain that temperature, tissue perfusion can be obtained from an analytical or numerical model of the probe and tissue. Indeed, an analytical or numerical model is necessary to obtain perfusion (unless a calibration curve of perfusion vs. power is experimentally produced for each probe). This section explores the analytical models available for modeling the thermistor probe and the adjacent perfused tissue.

The thermistor probe and adjacent tissue can be thermally modeled in a variety of ways. In 1985, Eberhart and Shitzer compiled two volumes on various subjects in heat transfer in medicine and biology, including ten chapters on the thermal modeling of tissues [34]. The model presented here is discussed in great detail in those chapters, but originates from Pennes [11] and is essentially the same as the model used by Bowman, Balasubramaniam, Valvano, Walsh, and others.

As stated in earlier chapters, the thermodiffusion method involves a self-heated thermistor probe in thermal communication with tissue. The *non*-invasive thermodiffusion probe would presumably rest on the tissue surface. In order to maximize the signal and simplify the analysis, the probe is insulated on all sides except the probe-tissue interface. Likewise, the tissue surface is assumed insulated everywhere except the probe-tissue interface.

4.1.1 Thermistor Probe

In this analysis, the thermistor probe is assumed to be uniform in terms of thermal transport properties and volumetric heat generation. Jain modeled the probe as a two-zone sphere consisting of an internal core, in which heat is uniformly generated, and an outer, non-heated layer [12]. However, validation studies of the invasive perfusion device developed by Bowman et al. show that a simple 1-zone spherical model is sufficient [13].

The thermistor probe can be modeled by the standard heat diffusion equation:

$$\nabla^2(k_b T_b) + q_b''' = \rho_b c_b \frac{\partial T_b}{\partial t},$$

where T_b=probe temperature, k_b=probe thermal conductivity, q_b'''=volumetric heat generation in the probe (by resistive heating), ρ_b=probe density, c_b=probe specific heat, and t=time. A detailed report on self-heated thermistors is given by Sapoff and Oppenheim [35].

4.1.2 Tissue

Biological tissue is far more complex and challenging to model than the thermistor probe. Tissue heterogeneity and microcirculatory heat transport are two of the main challenges.

4.1.2.1 Microscopic Tissue Heterogeneity

Tissue is terribly heterogeneous, made up of microscopic components such as cells (~10μm) and microvasculature (~10-150μm). "It is clear that an exact accounting of these microscopic features, including the effect of blood flow through each vessel, would be highly impractical. A more tenable approach would be to seek a formulation which accounts only for the collective behavior of the microscopic features. This is analogous to the "continuum" formulation of non-biological tissues: ignoring the presence of molecules, and sometimes crystal grains and grain boundaries" [36].

In order to justify a continuum formulation, it must be shown that the thermally interrogated volume is large compared to microscopic thermal heterogeneities. First, it is clear that tissue far removed from the heated probe does not experience an increase in temperature, i.e. $T_m(\infty)=T_i$ for all t, where T_m is the tissue temperature, T_i is the initial tissue temperature (before heating), and t is time. The thermally interrogated volume can be defined as the volume of tissue within the boundary at which the tissue temperature has dropped to a certain fraction of the temperature at the tissue-probe interface, all with reference to the tissue temperature at infinity. In this thesis, this fraction is arbitrarily taken to be 10%. Thus the interrogated volume is the volume within the boundary at r for which

$$\frac{T_m(r)-T_i}{T_m(\text{interface})-T_i} \geq 0.1.$$

Using the finite-difference analysis presented later in this chapter it was shown that for a disk-shaped thermistor probe of radius 1mm and typical thermal properties (see List of Values), placed on tissue of typical thermal properties and zero perfusion (perfusion, w, will be formally introduced in Section 4.1.2.3), and heated to ΔT_b=3.3°C (ΔT_b=2.9°C for w=20 kg/m^{3}s), the interrogated volume is roughly a hemisphere of radius 3.6mm (2.2mm for w=20 kg/m^{3}s). In both cases the probe was heated by 7.5MW/m^3. Thus, the interrogated volume for average perfusion levels is roughly a hemisphere of radius 3mm, with volume≈50mm^3 and interface area≈30mm^2.

Approximately, 1mm^2 of skin is supplied by 15 capillary loops and 300 anastomoses in fingers/feet (through which 60% of blood passes). Also, 1cm^3 of muscle tissue contains approximately 400 arterioles and 10'000 capillaries [6].

Thus, roughly speaking, the tissue volume thermally interrogated by a probe of radius 1mm and typical thermal properties (see List of Values) contains approximately 10^6 cells, 120 to 750 capillary loops, 3000 to 15,000 anastomoses (in fingers/feet), and, in the case of muscle tissue, 20 arterioles. Therefore, a continuum formulation is justified, meaning that thermal transport properties such as thermal conductivity and diffusivity represent average tissue values.

4.1.2.2 Macroscopic Tissue Heterogeneity

Various tissues display heterogeneities in tissue composition on a macroscopic scale as well as on a microscopic scale. Human skin is composed of the top, thin (sub-millimeter) layer, the epidermis, followed by a thicker, perfused layer, the dermis. The combined thickness of the epidermis and dermis ranges from 1.4mm on the backhand to 3.9mm on the soles of the feet [37]. For a histological stain of the epidermis and dermis of skin tissue, see [38]. The dermis is perfused by a network of arterioles, capillary networks, venules, and anastomoses. From a horizontal plexus of arterioles running deep in the dermis, vessels run upward to a superficial horizontal plexus, which feeds the capillary loops that climb to the interface of the epidermis and dermis. For a diagram of

the vasculature of the dermis and epidermis, see [39]. Detailed information on human skin can be found in [40].

4.1.2.3 Transport of Heat by the Circulatory System

"The detailed description of the local contribution of blood perfusion to energy exchange is an intricate task. Blood vessels are organized in a nonregular manner in most tissues. Blood flow rates vary considerably with both time and position. Alternate flow routes may be opened and closed (collateral circulation) in response to need, on a dynamic basis" [41].

Chen explains that "there are at least three potential mechanisms for the microcirculation to contribute to heat transfer. Firstly, the vector average blood velocity in the microvasculature may have a mean convective contribution, much like that in nonbiological porous fluids. Secondly, the multidirectional aspect of blood flow in a tortuous microvascular network may provide a contribution similar to that of random molecular motion or turbulent eddies, resulting in an effective diffusivity and thus a conductive contribution. Finally, the microvasculature distributes essentially fresh (arterial) blood to ever cubic millimeter of tissue. It is natural to expect that there would be a heat transfer contribution directly proportional to this distributed perfusion term" [36]. Chen proceeds to formulate the heat transfer contribution of each term, but admits in the end that such rigorous mathematical formulations are of limited use since, at least as of the time of publication of Chen's formulation (1985), data on the vascular architecture were neither detailed enough nor comprehensive enough to determine all the parameters of the formulation.

Probably the most commonly used approach to modeling the heat transfer contribution of the microvascular stems from the experimental work of Pennes [11], and is based on Fick's principle, which can be stated as follows: the time rate at which an organ or control volume stores a substance is equal to the blood flow rate times the arterial level of the substance minus the venous level of that substance:

$$q'''_{conv} = wc_{bl}(T_{art} - T_{ven}),$$

where q'''_{conv}=volumetric heat removed by convection due to perfusion, w=perfusion, c_{bl}=specific heat of blood, T_{art}=temperature of arterial blood, and T_{ven}=temperature of venous blood.

In this formulation, perfusion is modeled as a volumetric phenomenon—a heat sink or source, depending on the relative temperature magnitudes of blood its surroundings. The units of perfusion can be thought of as a mass or volume of blood flowing through a mass or volume of tissue per unit time. In this thesis, the SI units $\frac{kg_{blood}}{m^3_{tissue} \cdot s}$ are used. Physiologists generally prefer the units of $\frac{ml_{blood}}{100g_{tissue} \cdot \min}$. Assuming that the density of blood and tissue are equal, 1 kg/(m^{3}s) = 6 ml/(100g*min). Very roughly, perfusion ranges in the body from about 1 or 2 kg/m^{3}s to 15 kg/m^{3}s.

Pennes went on to assume that by the time the blood has passed through the capillaries and into the venules, the blood has thermally equilibrated with the surrounding tissue, so that $T_{ven}=T_m$. Later, Chen and Holmes found that most of the thermal equilibration actually occurs between the terminal arterial branches and arterioles [36]. It should be mentioned that some controversy has surrounded Pennes' model of microcirculatory heat transfer. Nevertheless, the fact that it has been used successfully by many researchers over the last fifty years justifies its future use.

With $T_{ven}=T_m$,

$$q'''_{conv} = wc_{bl}(T_{art} - T_m).$$

Combining the microcirculatory heat transfer term with the standard heat diffusion equation, the governing equation of perfused tissue becomes

$$\nabla^2(k_m T_m) + q'''_m + wc_{bl}(T_{art} - T_m) = \rho_m c_m \frac{\partial T_m}{\partial t},$$

where k_m=tissue thermal conductivity, q'''_m = metabolic heat generation in the tissue, ρ_m=tissue density, c_m=tissue specific heat, and t=time.

4.1.3 Probe-Tissue System

Combining the governing equations for the thermistor probe and perfused tissue,

$$\nabla^2(k_b T_b) + q_b''' = \rho_b c_b \frac{\partial T_b}{\partial t} \quad \text{in probe}$$

$$\nabla^2(k_m T_m) + q_m''' + wc_{bl}(T_{art} - T_m) = \rho_m c_m \frac{\partial T_m}{\partial t} \quad \text{in tissue}$$

These partial differential equations are subject to the initial condition of uniform temperature throughout the thermistor probe and tissue before the probe is heated,

$$T_b = T_i \quad t \le 0$$
$$T_m = T_i \quad t \le 0$$

and subject to the boundary conditions of continuity of temperature and flux at the probe-tissue interface; zero flux at the probe-insulation interface; and zero temperature rise in the tissue at infinity:

$$T_b = T_m \quad \text{at probe - tissue interface}$$
$$k_b \nabla T_b = k_m \nabla T_m \quad \text{at probe - tissue interface}$$
$$k_b \nabla T_b = 0 \quad \text{at center (sphere, cylinder) or insulated back (slab)}$$
$$T_m = T_i \quad \text{at infinity}$$

4.1.4 Non-dimensionalized Equations

Patera presents three dimensionless groups which characterize the steady-state problem for various one-dimensional geometries (e.g. sphere, infinite slab, infinite cylinder) [42]:

$$\theta = \frac{\Delta T_b k_m}{q_b''' L^2}$$

$$\gamma = \sqrt{\frac{wc_{bl}}{k_m}} L,$$

$$\varphi = \frac{k_b}{k_m}$$

where θ=dimensionless probe temperature, γ=dimensionless perfusion, φ=dimensionless thermal conductivity, and L=characteristic length ($L=a$ for the sphere and infinite cylinder (a is the radius of the spherically-shaped or disk-shaped probe), and $L=h$ for the infinite slab, where h is the height of the slab).

Plugging these dimensionless variables into the governing equations above, dimensionless time becomes

$$t^* = \frac{\alpha t}{L^2},$$

where α=thermal diffusivity.

4.2 Solutions

Sections 4.2 and 4.3 do not discern between invasive and non-invasive geometries. This distinction is discussed in Section 4.5.

4.2.1 One-dimensional solutions

Steady-state and transient solutions exist for at least three one-dimensional geometries: the sphere, infinite slab, and infinite cylinder.

A practical way of solving the governing equations is given by Bowman et al. [6] and involves substituting the following three variables into the governing equations:

$$\begin{aligned} v_b &= T_b(r) - T_i \\ v_m &= T_m(r) - T_i \\ \psi &= q_m''' + wc_{bl}(T_{art} - T) \end{aligned} \quad .$$

The steady-state solutions presented in 4.2.1.1 must hold true when the probe is unheated, in which case T_b=T_m=T_i. It follows that

$$\psi = 0 \quad or$$

$$T_i = T_{art} + \frac{q_m'''}{wc_{bl}}$$

Thus it is seen that metabolic heat generation establishes the initial or baseline temperature. This is a fortunate by-product of modeling by the bioheat equation because knowledge of T_{art} and q_m''' are no longer needed to solve for the temperature profile.

The thermal contact resistance between the thermistor probe and the skin can be assumed negligible because high-conductivity materials such as gels could be added at the interface [43]. In a similar vein, it can easily be shown that if an electrode must be placed at the interface between thermistor probe and skin (in order to ensure uniform heat generation in the probe), the temperature drop across the electrode is on the order of 1000 times smaller than ΔT_b and is thus negligible (assuming disk radius of 0.5mm and a Palladium electrode with thermal conductivity 70W/mK).

4.2.1.1 Heated Sphere in Infinite, Perfused Tissue

The steady-state solution for a spherically-shaped thermistor probe of radius a embedded in perfused, infinite tissue can be found by integrating the governing probe equation. The solution for the tissue can be found by plugging the ansatz

$$v_m(r) = \frac{C_1}{r} e^{C_2 r}$$

into the governing tissue equation, where r is the distance from the origin and C_1 and C_2 are unknown constants. The solutions are [6]:

$$v_b(r) = \frac{q_b'''}{6k_b}\left(a^2 - r^2\right) + \frac{q_b'''a}{3k_m} \cdot \frac{1}{\sqrt{\frac{wc_{bl}}{k_m}} + \frac{1}{a}}$$

$$v_m(r) = \frac{q_b'''a^2}{3k_m} \cdot \frac{1}{r} \cdot \frac{\exp\left[\sqrt{\frac{wc_{bl}}{k_m}}(a-r)\right]}{\sqrt{\frac{wc_{bl}}{k_m}} + \frac{1}{a}}$$

The temperature profiles of probe and tissue are shown in Figure 4.1 for various levels of perfusion.

Due to symmetry, this solution also holds for a hemispherical probe embedded in a semi-infinite solid, where the free surfaces of the probe and tissue are insulated. Open-form and closed-form transient solutions are given by Jain [12] and Valvano [1], respectively. It must be mentioned that the closed-form transient solution by Valvano was derived using a term-by-term inverse transform in which terms of negligible contribution were dropped. It appears that the final solution can be used with accuracy to calculate the power required to reach and maintain a controlled volume-averaged probe temperature. However, the solution of probe temperature as a function of space and time is itself not reliable. As far as I know, there exists no closed-form transient solution of the temperature distribution in a heated sphere and the surrounding perfused tissue.

4.2.1.2 Heated, Infinite Slab on Semi-Infinite, Perfused Tissue

The steady-state solution for a thermistor probe in the shape of an infinite slab of height h, insulated on one side and abutting on the other side a semi-infinite, perfused

tissue, can be found by integration of the governing probe equation. The solution for the tissue can be found by plugging the ansatz

$$v_m(z) = C_1 e^{C_2 z}$$

into the governing tissue equation, where z is the tissue depth, measured from the side of the slab *not* in contact with the tissue (i.e. the probe-tissue interface is at $z=h$), and C_1 and C_2 are unknown constants. The solutions are:

$$v_b(z) = \frac{q_b'''}{2k_b}\left(h^2 - z^2\right) + \frac{q_b'''h}{k_m} \cdot \frac{1}{\sqrt{\frac{wc_{bl}}{k_m}}}$$

$$v_m(z) = \frac{q_b'''h}{k_m} \cdot \frac{\exp\left[\sqrt{\frac{wc_{bl}}{k_m}}(h-z)\right]}{\sqrt{\frac{wc_{bl}}{k_m}}}$$

The temperature profiles of probe and tissue are shown in Figure 4.2 for various levels of perfusion.

It is very informative to compare the solutions for the sphere and infinite slab. Many similarities are apparent. However, one critical difference between the sphere and the slab for both probe and tissue solutions is found in the denominator:

$$sphere: \quad \sqrt{\frac{wc_{bl}}{k_m}} + \frac{1}{a}$$

$$slab: \quad \sqrt{\frac{wc_{bl}}{k_m}}$$

While a solution exists for the sphere for zero perfusion, the solution for the infinite slab (and for the infinite cylinder) blows up for zero perfusion! This trend can be observed in Figure 4.2. The geometry of a sphere is able to dissipate heat by conduction alone, while for the infinite slab (and the infinite cylinder), heat transfer by convection due to tissue perfusion is very important—to the point of determining the form of the solution (i.e. for zero perfusion the solution takes on an entirely different form).

Transient solutions of the governing equations for the slab-shaped thermistor probe and adjacent tissue are given by Walsh [4]. However, accuracy is suspect [44].

4.2.1.3 Heated, Infinite Cylinder in Infinite, Perfused Tissue

The solution for a thermistor probe in the shape of an infinite cylinder, placed in infinite, perfused tissue involves modified Bessel functions, and is given by Patera [42]. Patera also looked at the effect of probe geometry on the accuracy of tissue perfusion calculations, and compared the sphere vs. infinite and finite cylinders (see Section 4.3).

4.2.2 Higher-dimensional Solutions

As far as I know, no *n*-dimensional closed-form solutions are available for $n \geq 2$, be they steady-state or transient. One of the closest available solutions is given by Carslaw and Jaeger for the temperature profile in semi-infinite, *unperfused* tissue heated with uniform flux over a circular region on its surface [45].

4.3 Error Analysis

Patera presents an error analysis of perfusion vs. measured quantities (such as temperature, characteristic probe length, power, specific heat of blood, and thermal conductivity of tissue) for spherically and cylindrically shaped probes [42]. He shows that a cylindrically shaped probe is superior to a spherically shaped probe because perfusion is far less sensitive to errors in the measured quantities for the cylinder than for the sphere. The goal of this present section is to extend Patera's work to thermistor probes in the shape of an infinite slab. Infinite slabs are obviously impractical, but provide helpful benchmark values for the designs presented in 4.5.

Following Patera's derivation, the sensitivity η of a parameter y on the measurement of parameter x is given by

$$\eta_{x,y} = \left| \frac{\frac{\partial y}{y}}{\frac{\partial x}{x}} \right| = \left| \frac{x}{y} \frac{\partial y}{\partial x} \right|.$$

According to Patera, "Given the accuracy $\partial x/x$ to which x can be found, a change in the measurement system which decreases the $\eta_{x,y}$ will result in a more accurate determination of y" [42]. Patera determined that, for the sphere and the infinite cylinder,

$$\begin{aligned}
\eta_{\Delta T_b,w} &= N \\
\eta_{q_b'',w} &= N \\
\eta_{c_{bl},w} &= 1 \\
\eta_{k_m,w} &= |1-N| \\
\eta_{a,w} &= 2|1-N|
\end{aligned} \quad ,$$

where

$$N(\gamma) = \frac{-2}{\frac{\gamma}{\theta}\frac{\partial\theta}{\partial\gamma}}$$

and γ and θ are introduced in 4.1.4. I have shown that this derivation is true for the infinite slab as well. Evaluating N for the sphere and infinite slab,

$$\begin{aligned}
N_{sphere}(\gamma) &= 2\left(\frac{\gamma+1}{\gamma}\right)\left(\frac{\gamma+1}{5\varphi}+1\right) \\
N_{slab}(\gamma) &= 2\left(\frac{\gamma}{3\varphi}+1\right)
\end{aligned} \quad ,$$

where φ is likewise introduced in Section 4.1.4.

Figure 4.3 shows the sensitivity of w on the measurement of ΔT_b, $\eta_{\Delta T_b,w}$, for a sphere, an infinite cylinder, and an infinite slab (the data for the infinite cylinder are taken from Patera [42]). As noted previously by Patera, w is far less sensitive on errors in ΔT_b for an infinite cylinder than for the sphere. Here I have expanded Patera's work to include the sensitivity for an infinite slab. As shown, w is even less sensitive for an infinite slab than for an infinite cylinder. A two-dimensional, non-invasive probe will presumably have a sensitivity of w on ΔT_b that is intermediate between that of a sphere and an infinite slab. In other words, the non-invasive probe represents an improvement over the spherically-shaped invasive probe in terms of error sensitivity.

It is informative to take a look at the sensitivity of w on other measured quantities as shown in Figure 4.4. In particular, note that w is most sensitive to errors in the measured value of the slab height, h.

4.4 Simultaneous Selection of Designs and Models

As explained in Section 2.1, from a knowledge of the controlled temperature of the thermistor probe and the steady-state power required to maintain that temperature, tissue perfusion can be obtained from an analytical or numerical model of the probe and tissue. Indeed, an analytical or numerical model is necessary to obtain perfusion unless a calibration curve of perfusion vs. power is experimentally established for each probe. Therefore, it is critical to design the thermistor probe hand-in-hand with analytical and/or numerical modeling to ensure that an accurate model of the design is available for perfusion extraction.

4.5 Design-Model Combinations

The two most promising designs are shown in Figure 4.5.

4.5.1 Disk Design

4.5.1.1 Description

The first design is a simple disk of radius a and height h resting on tissue. The exposed surfaces of the probe and tissue are insulated. This design is called "Disk".

4.5.1.2 Dimensions

The dimensions of the disk are constrained by a variety of limits:

- Typical thermistors such as those fabricated by *Thermometrics* have dimensions between 0.5mm and 2mm in diameter/width.
- The (presumably flat) thermistor probe must lie flush against the tissue surface to ensure good thermal communication. Anatomical topography constrains the disk diameter to less than approximately 10mm.
- It is important to keep the thermal mass of the probe as low as possible in order to ensure good dynamic tracking. Low thermal mass necessitates a small value of h, perhaps on the order of 0.5mm.

No doubt, a non-dimensional analysis would be helpful in evaluating designs of various dimensions. However, its usefulness is limited by the fact that the range of allowable dimensions is quite small.

4.5.2 Disk and Ring Design

4.5.2.1 Description

The second design was suggested by Mikic and represents an effort to approximate the one-dimensional temperature distribution in an infinite slab in order to facilitate analytical modeling [43]. It consists of an inner disk of radius a_{in} and an outer ring of outer radius a_{out}, both of height h. The disk and ring are both heated, though not necessarily by the same amount. A thin insulating ring separates the disk and ring in order to prevent heat transfer from the inside to the outside. It is the disk (not the ring) for which the temperature is controlled, and the power required to maintain this temperature is used in the calculation of perfusion. This design is called "Disk and Ring."

4.5.2.2 Dimensions

Although the size constraints for the Disk design apply to the overall body of the Disk and Ring design as well, the situation is complicated by extra choices such as the ratio of a_{out} to a_{in}. One criterion for determining these extra variables is that the heat transfer from the inner disk to the tissue resemble as closely as possible the heat transfer from an infinite slab to tissue. Adiabats show the direction of heat flow. Considering that the adiabats in tissue under an infinite slab are straight lines, the straightness of the adiabats in tissue under a disk can be used as a measure of how well a disk resembles an infinite slab (with regard to heat transfer, of course).

Using a coarse version of the finite-difference model (FDM) described below, the heat transfer from the disk was simulated numerically, and the deviation, δ, of the adiabat from a straight line (at a given tissue depth) was determined for various probe dimensions and heat fluxes.

The following trends were observed:

1. Increasing the ratio a_{out}/a_{in} decreases δ (see Figure 4.6). This makes sense since the infinite slab, for which δ=0, has a ratio a_{out}/a_{in} of infinity.

2. Increasing the ratio q_{out}/q_{in} decreases δ, mainly by strongly reducing δ at small tissue depths.
3. Increasing q_{out} and q_{in} simultaneously has negligible effect on δ.
4. Varying perfusion has negligible effect on δ.
5. Increasing h has negligible effect on δ.

Thus the disk and ring should be designed to maximize the ratio a_{out}/a_{in}, possibly with $q_{out}>q_{in}$ (though $q_{out}\neq q_{in}$ may introduce considerable complexity).

4.5.3 Models

As stated above, no solutions exist for the two-dimensional temperature profiles that would exist for the two designs suggested above. The main contribution of this thesis is the examination of whether the two-dimensional designs could possibly be approximated by one-dimensional models, and what the ensuing errors in calculated perfusion would be. It is immediately evident that both the Disk design and the Disk and Ring design could possibly be modeled by a (one-dimensional) infinite slab. It is also possible to approximate the Disk design by another 1-dimensional model: when one considers that, due to symmetry, the solution of the sphere in infinite tissue is identical to the solution of a hemisphere in a semi-infinite tissue (with all exposed surfaces insulated), and that the isotherms in tissue heated by a disk approach at a large distance those of the hemispherical solution (which are perfectly spherical), one might suspect that the Disk design could be modeled as a hemisphere in a semi-infinite tissue (which is the same as a sphere in an infinite tissue). The designs and their proposed one-dimensional models are shown in Figure 4.7.

4.6 Method for Obtaining the Error in Calculated Perfusion due to 1-D Approximation

4.6.1 Method

It is necessary to determine the errors in calculated perfusion that result from approximating the 2-dimensional designs as one-dimensional models. Steady-state finite-difference models (FDM) of both designs were created for this purpose.

Figure 4.8 shows diagrams of the information flow involved in thermodiffusion. According to the traditional thermodiffusion method (Figure 4.8a), a probe is placed on perfused tissue (perfusion level unknown) and heated to, and controlled at, a predetermined temperature, ΔT_b. The power q_b''' required to maintain ΔT_b is recorded. Subsequently, ΔT_b and q_b''' are inserted into an analytical or numerical model of the probe, from which perfusion is calculated. This calculated perfusion is denoted by w_{calc}, and it is understood that this calculated perfusion differs from the true tissue perfusion, w_{true}, by an error, w_{error}.

It is equally feasible (Figure 4.8b) to heat the thermodiffusion probe at a predetermined rate q_b''' and record the steady-state temperature increment of the probe, ΔT_b. ΔT_b and q_b''' are then inserted into an analytical or numerical model of the probe from which perfusion, w_{calc}, is calculated.

In order to analytically determine the error in calculated perfusion resulting from the approximation of two-dimensional probes by one-dimensional models, the following procedure was applied (see Figure 4.8c). As in Figure 4.8b, the thermodiffusion probe is heated at a predetermined rate q_b''', but now the perfusion level in the tissue of the FDM, w_{true}, is also an input. The steady-state temperature ΔT_b of the probe is obtained from the iterations of the FDM, and ΔT_b and q_b''' are inserted into the one-dimensional model, from which perfusion, w_{calc}, is calculated as before. The error between calculated perfusion and true perfusion, w_{error}, can then be determined as

$$w_{error} = w_{true} - w_{calc}\,.$$

4.6.1.1 Extra Degree of Freedom for the Spherical Approximation

Approximating the Disk design as a sphere adds an extra degree of freedom, as shown in Figure 4.9. The radius, a, and height, h, of the probe can be specified, but the choice of the radius of the spherical model, a^*, is not clear. Some possibilities include choosing:

1. $a^*=a$
2. a^* such that the total amount of heat exiting the disk and sphere are equal. Then
$$a^* = \left(\frac{3}{2}a^2 h\right)^{\frac{1}{3}}.$$
3. a^* such that the heat fluxes exiting the disk and sphere are equal. Then
$$a^* = 3h.$$
4. a^* such that $w_{calc}=0$ when $w_{true}=0$. In the laboratory this would involve a simple no-flow calibration in a high-viscosity liquid (such as glycerol), which is common practice for invasive probes.

It is not clear by which criterion a^* should be determined.

4.6.2 Finite-Difference Model

4.6.2.1 Setup

Finite-difference models (FDM) of the probe and tissue were created for both designs. As shown in Figure 4.10, symmetry allowed the FDM to be limited to half of the probe-tissue system in order to save computing power. Since both designs are disk-shaped, the FDMs were created in cylindrical coordinates. The exposed surfaces and the symmetry line of the probe and tissue were modeled as being insulated. The boundary condition for the lower boundary of the tissue was stated in Section 4.1.3 as $T_m \rightarrow T_i$ approaching the boundary at infinity. In the FDM this lower bound was implemented by specifying $T_m=T_i$ on a semi-hemisphere of "very large radius", R. The error associated with approximating infinity by R is discussed in Section 4.6.2.2. Tissue perfusion was implemented in the FDM as stated in the bioheat equation, i.e. as a heat sink. Appendix A presents the FDM layout and equations for both designs. For a more formal discussion of FDM and finite-element analysis for tissue, see [46].

The FDMs were created in Microsoft Excel and solved using Excel's built-in iteration solver. The advantage of using Excel is two-fold: simple models with few nodes can be set up and solved very quickly, and Excel's cells can be used as FDM cells, providing a very helpful graphical representation of the model. The main disadvantage of Excel is that the number of cells in the horizontal direction (i.e. columns in Excel) is limited to 256. Thus R is severely limited. In addition, computation time quickly becomes very large in Excel: when the maximum width of the spreadsheet is used (R=256 cells), the tissue and probe contain on the order of 50'000 cells, which can take up to 60'000 iterations to solve (up to 6 or 8 hours on a 2 GHz processor).

Since w_{calc} is extremely sensitive to ΔT_b (see Section 4.3), it is important to understand that the value of ΔT_b determined by the FDM is not exactly equal to the true value of ΔT_b, but differs by an error from three sources:

1. the discretization inherent in finite-difference modeling assumes each cell to have uniform temperature
2. the iterative solution method ends when the desired level of accuracy is reached, not when the exact solution is found
3. the boundary at infinity is approximated by a boundary at a very large distance, R

The error between ΔT_b calculated in the FDM and the true temperature increment of the probe is therefore reduced by:

1. refining the mesh
2. increasing the number of iterations
3. increasing R

A quantitative measure of these approximation errors was obtained by varying each of these three parameters in turn and observing the resulting change in w_{calc}.

4.6.2.2 Validation

Since no exact solutions exist for the proposed designs, it is necessary to validate the FDM against existing exact solutions for situations that are as similar as possible.

Unperfused Tissue

In order to validate the implementation in cylindrical coordinates of the FDM, the tissue temperature profile obtained from the FDM of a semi-infinite, *unperfused* tissue heated with uniform flux over a circular region on its surface was compared to Carslaw and Jaeger's exact solution [45].

Figure 4.11 shows the tissue temperature profiles obtained from the exact solution and from the FDM. It is seen that the FDM tracks the exact solution very nicely except for an offset. This offset is due to the fact that the lower tissue boundary was not actually placed at infinity, but at R. T_m is therefore constrained to equal T_i at R, pulling the entire curve down. Appendix B shows that the error in w_{calc} caused by this finite value of R is on the order of 3 kg/m^{3}s. The effect of this error is discussed in the subsection Approximation Error below.

Perfused Tissue

In order to validate the implementation of perfusion, a FDM in spherical coordinates of a sphere in perfused tissue was created. According to the method outlined in 4.6.1, w_{calc} was obtained and compared to w_{true}. Figure 4.12 shows that the calculated perfusion tracks true perfusion very nicely.

Approximation Error

More quantitatively, the errors in calculated perfusion resulting from the three sources of FDM error—discretization, finite number of iterations, and finite R, as explained above—were estimated by varying each of the sources in turn and observing the resulting change in w_{error}. Roughly,

1. refining the probe mesh from 1000 to 2000 cells produced a change in calculated perfusion on the order of 0.02 kg/m^{3}s.
2. decreasing the 'maximum change between iterations required to terminate the iterations' from 10^{-7} to 10^{-8} (i.e. increasing the number of iterations) produced a change in calculated perfusion on the order of 0.06 kg/m^{3}s.
3. increasing R from 12.7mm to 21.3mm produced a change in calculated perfusion on the order of 3 kg/m^{3}s (see Appendix B).

This analysis demonstrates that the mesh size and number of iterations are adequate, but that the finite value of R produces a large error (3 kg/m^{3}s is approximately equal to the typical level of perfusion in skin and other tissues). As explained above, the FDM was solved in Microsoft Excel which sets a limit on R. The results are meaningful despite this large FDM error because the magnitude of w_{error} caused by approximating two-dimensional probes as one-dimensional (which is the purpose for creating the FDM in the first place) is huge compared to the FDM error for the infinite slab, and on the order of the FDM error for the sphere. However, further, more detailed studies definitely call for FDM in software that can allow for larger R and less computation time.

4.7 Temperature Distributions

4.7.1 Probe and Tissue Temperature Profiles

The output of the finite-difference models (FDM) is the two-dimensional temperature profile of the probe and adjoining tissue. A number of isotherm plots for the probe and tissue are shown in Appendix C for the Disk design and the Disk and Ring design at various levels of perfusion. It can be seen on those plots that increasing perfusion has the effect of lowering the temperature in the probe as well as tightening the temperature profile of the tissue closer to the probe (which is the same as decreasing the interrogated tissue volume).

4.7.2 Volume-averaged Temperature Increment of the Probe, ΔT_b

In practice, the directly measurable probe quantities are voltage, current, and resistance. The resistance measured represents the thermistor resistance averaged over its volume. From this measured, volume-averaged resistance and the probe's resistance-vs.-temperature calibration curve, the volume-averaged temperature of the probe, ΔT_b, can be obtained.

Figure 4.13 shows ΔT_b vs. w for disks of radius a=1mm (q_b''' =7.5MW/m^3) and a=0.5mm (q_b''' =10MW/m^3). It doesn't make any sense to compare the magnitudes of the two curves because they are proportional to q_b'''. However, it can be seen that the

sensitivity of w on ΔT_b is larger for larger radii. This phenomenon is discussed in more detail in Section 4.3.

Figure 4.14 shows ΔT_b vs. w for the Disk and Ring design of outer radius a_{out}=2mm for two values of a_{in} (0.4mm and 0.8mm). It is surprising that the relatively large reduction in the deviation, δ, caused by increasing a_{out}/a_{in} from 2.5 to 5 has a very small effect on ΔT_b and, as is shown in 4.8.2, on w_{calc}.

4.8 Results: Error in Calculated Perfusion due to 1-D Approximation

4.8.1 Disk Design

As discussed in more detail in Section 4.6.1.1, approximating the Disk design as a sphere adds an extra degree of freedom (see Figure 4.9). The radius, a, and height, h, of the probe can be specified, but the choice of the radius of the spherical model, a^*, is not clear. Some possibilities include choosing:

1. $a^*=a$.
2. a^* such that the total amounts of heat exiting the disk and sphere are equal.
3. a^* such that the heat fluxes exiting the disk and sphere are equal.
4. a^* such that $w_{calc}=0$ when $w_{true}=0$.

Table 4.1 shows w_{calc} vs. w_{true} for a disk of radius a=1mm, where w_{calc} is calculated with a^* determined by each of the four criteria above. Table 4.2 is analogous to Table 4.1 for a disk of radius a=0.5mm. The fifth column shows w_{calc} when the thermistor probe is modeled as an infinite slab, and the last column gives ΔT_b.

It is evident from the tables that $|w_{error}|=|w_{true}-w_{calc}|$ is extremely large for several values of a^*, meaning that w_{calc} is extremely sensitive to a^*, as discussed in Section 4.3. It is also evident that even the smallest values of w_{error} are still very significant over the physiological range of w_{true} from 0 to 15 kg/m^{3}s.

Also, the best criterion for a disk of radius 1mm in some cases does not work for a disk of radius 0.5mm. In other words, it is not clear by which criterion a^* should be determined. It is important to realize that *no* choice of a^* will cause $w_{calc}=w_{true}$ for all values of w_{true}. There may be a more sophisticated way to match w_{calc} and w_{true}, but the

purpose of this research is to determine whether one can "get away with" simply approximating the two-dimensional probe design by a one-dimensional model.

The left plot in Figure 4.15 shows the best matches of w_{calc} vs. w_{true} for a=1mm and a^* determined by criteria 3 and 4 above. The graph also shows w_{calc} for the infinite slab model. It makes sense that w_{calc} for the infinite slab would be much larger than w_{true}: heat escaping the disk-shaped thermistor probe flows downward and sideward, while heat escaping from an infinite slab flows only downward. The power required to maintain ΔT_b is therefore larger for the disk than for the slab. When the slab is used as a model of the disk, the high power input for the same ΔT_b can only be explained by a higher level of perfusion.

The right plot in Figure 4.15 is analogous to left one, but for a probe radius of 0.5mm. The best matches of w_{calc} vs. w_{true} are for criteria 1 and 4. The values of w_{calc} for the infinite slab are not shown because they are in the 700-800 kg/m^{3}s range.

4.8.2 Disk and Ring

The slab model of the Disk and Ring design does not offer the same degree-of-freedom phenomenon exhibited by the spherical model of the Disk design. However, there are more choices in dimensions, as discussed in 4.5.2.2.

Figure 4.16 shows w_{calc} vs. w_{true} for a_{out}=2mm and a a_{out}/a_{in} ratio of 2.5 and 5. It is surprising that increasing a_{out}/a_{in} from 2.5 to 5, which drastically decreases the adiabat deviation δ, has negligible effect on w_{calc}.

When the Disk design modeled as an infinite slab (see circle markers in the left plot of Figure 4.15) is compared to the Disk and Ring design modeled as an infinite slab (both square and triangle markers in Figure 4.16), it is evident that the ring does provide substantial improvement, as was the idea, decreasing w_{error} from approximately 200 kg/m^{3}s for the Disk design to 40 kg/m^{3}s for the Disk and Ring design. Also, notice the fairly linear relationship between w_{calc} and w_{true}, at least at higher values of w_{true}.

4.9 Discussion

The feasibility of thermally modeling two probe designs by various one-dimensional analytical models has been studied. In general, the errors between true perfusion and calculated perfusion are very large. However, for the Disk design and hemispherical model, it is possible to reduce the error to a clinically acceptable level by proper choice of probe and model dimensions. For example, for a disk radius a=1mm, height h=0.2mm, and power $q_b''' = 7.5\text{MW/m}^3$, and a model radius a^* based on criterion 4, the average error over a physiologic perfusion range of 0 to 15 $\text{kg/m}^3\text{s}$ is approximately 20%. It may be possible to determine an optimal combination of probe dimensions, i.e. the combination that produces the smallest error.

In some cases where the error in calculated perfusion is prohibitively large, such as the Disk and Ring design with the slab model, relative measurements are possible thanks to a fairly linear relationship between w_{calc} and w_{true}.

In terms of manufacturability and cost, the Disk design, being simpler than the Disk and Ring design, is clearly easier and cheaper to fabricate.

4.10 Suggestions for Further Work

A more thorough investigation of design-model combinations is necessary to explore various design and model dimensions and find an optimal combination. Perhaps a non-dimensional analysis would be appropriate. Also, there may exist completely different design-model combinations that result in smaller errors.

The details of the physical probe design must be finalized, paying special attention to designing a probe with low thermal mass and high thermal communication for good dynamic tracking and signal stability. Upon developing an exact perfusion extraction algorithm, prototypes can be fabricated and validated *in vitro* at zero perfusion and then *in vivo* in an animal model.

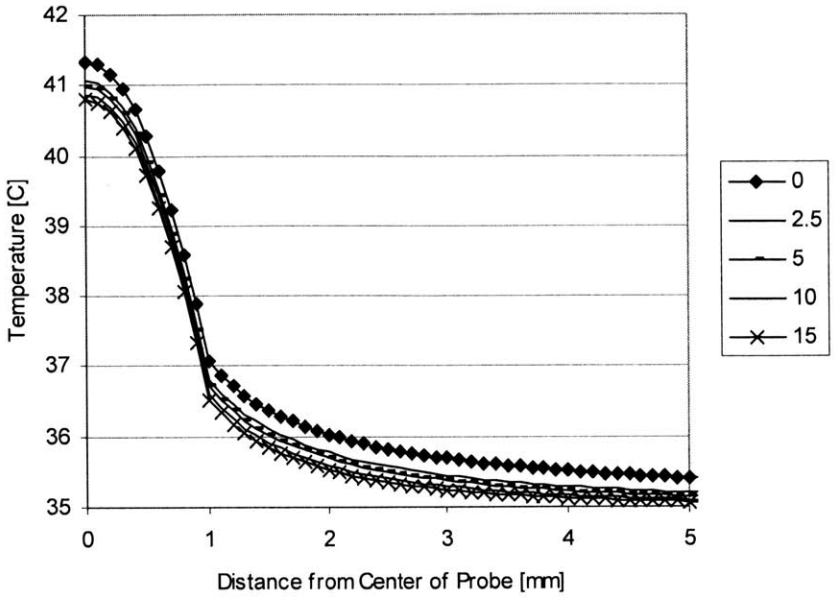

Figure 4.1 Temperature profile in a spherical probe and surrounding tissue for various levels of perfusion. Perfusion units are kg/m^{3}s. a=1mm and q_b'''=3MW/m^3.

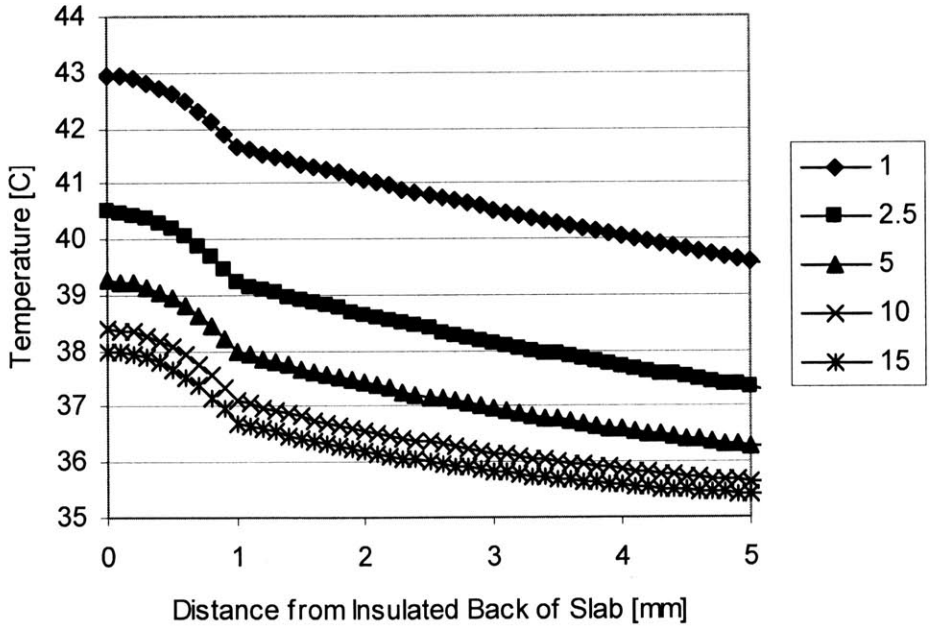

Figure 4.2 Temperature profile in an infinite slab and abutting tissue for various levels of perfusion. Perfusion units are kg/m^{3}s. h=1mm and q_b'''=0.3MW/m^3.

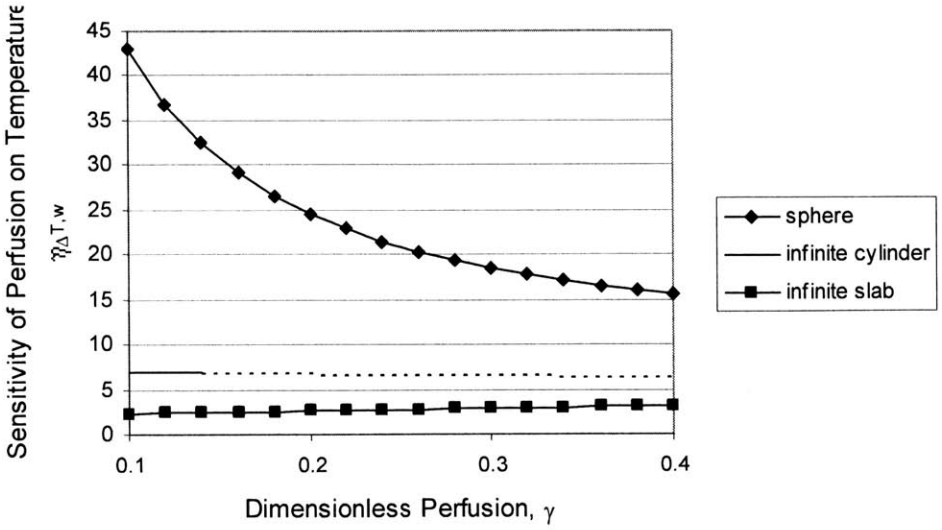

Figure 4.3 Sensitivity of w_{calc} on errors in the measurement of ΔT_b for a sphere, infinite cylinder and infinite slab.

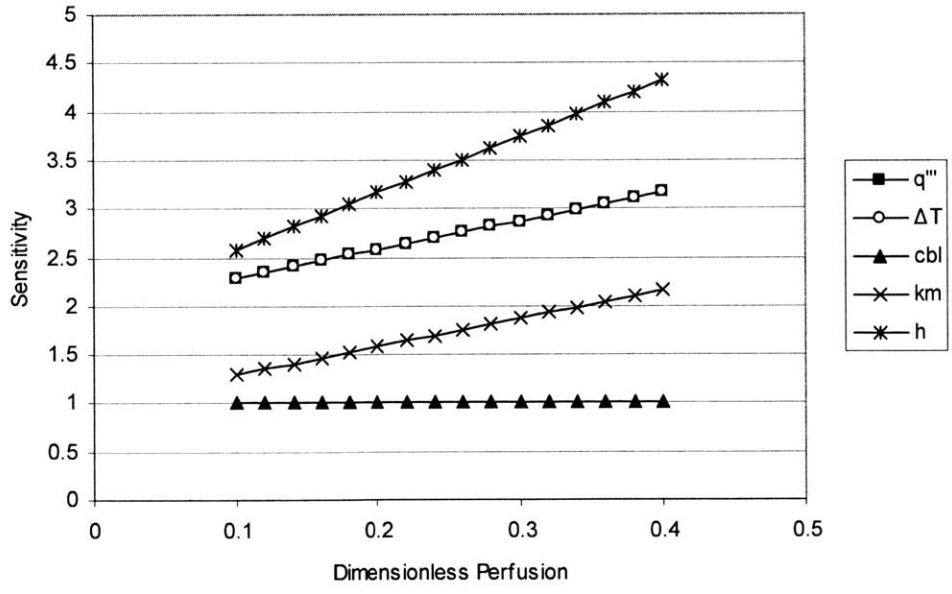

Figure 4.4 Sensitivity of calculated perfusion on errors in the measurement of h, ΔT_b, q_b''', k_m, and c_{bl}.

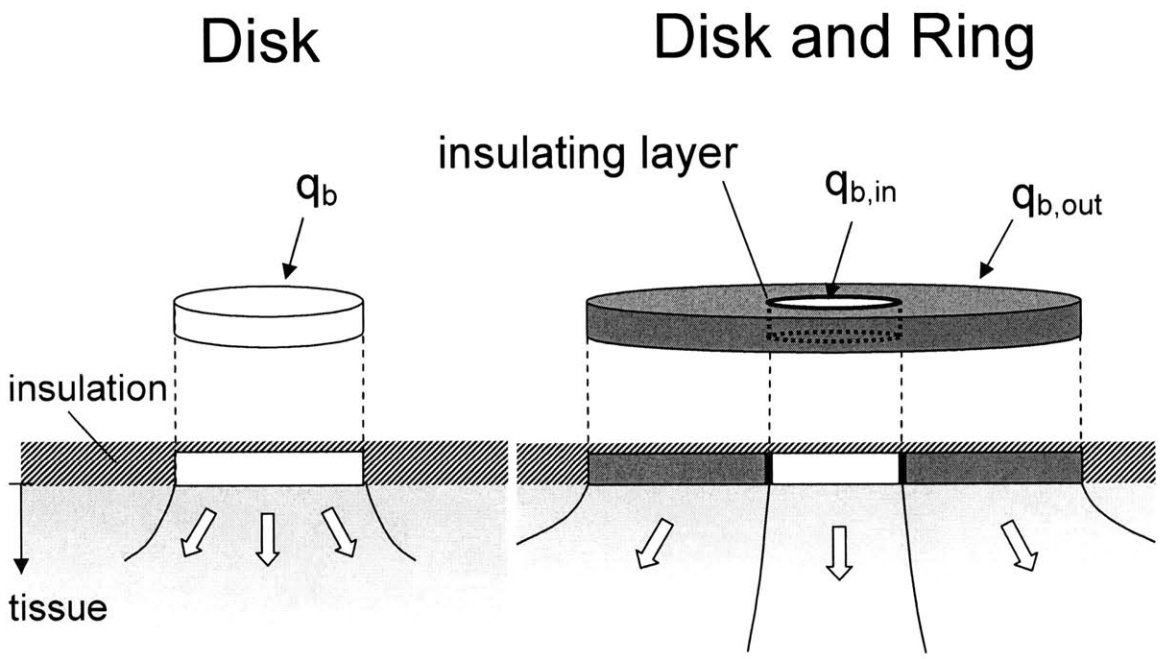

Figure 4.5 Two probe designs.

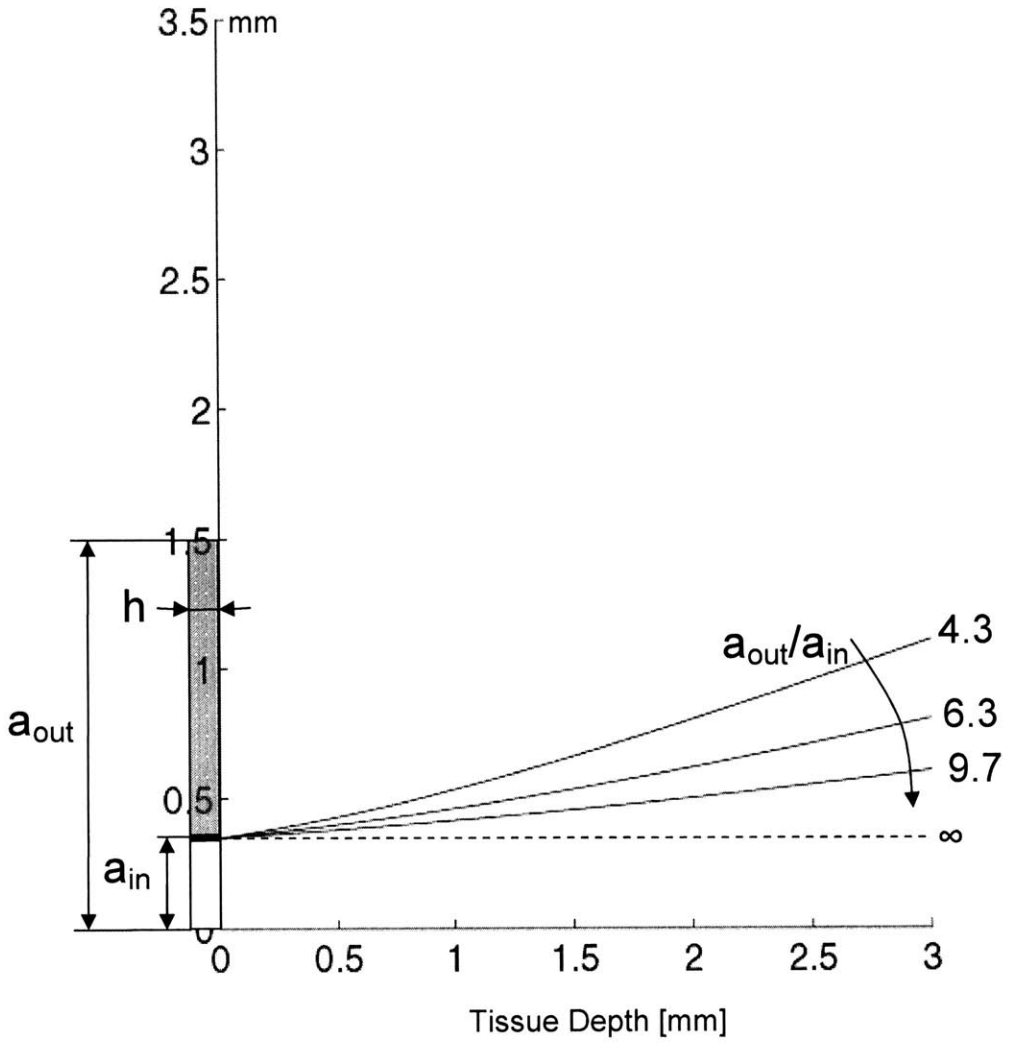

Figure 4.6 Increasing the ratio of a_{out} to a_{in} causes the heat transfer pattern in the tissue abutting a disk to approach the pattern in tissue abutting an infinite slab, as evidenced by the fact that the adiabat approaches a straight line. The size of the outer ring shown here is for a_{out}/a_{in}=4.3. In all cases, a_{in}=0.35mm.

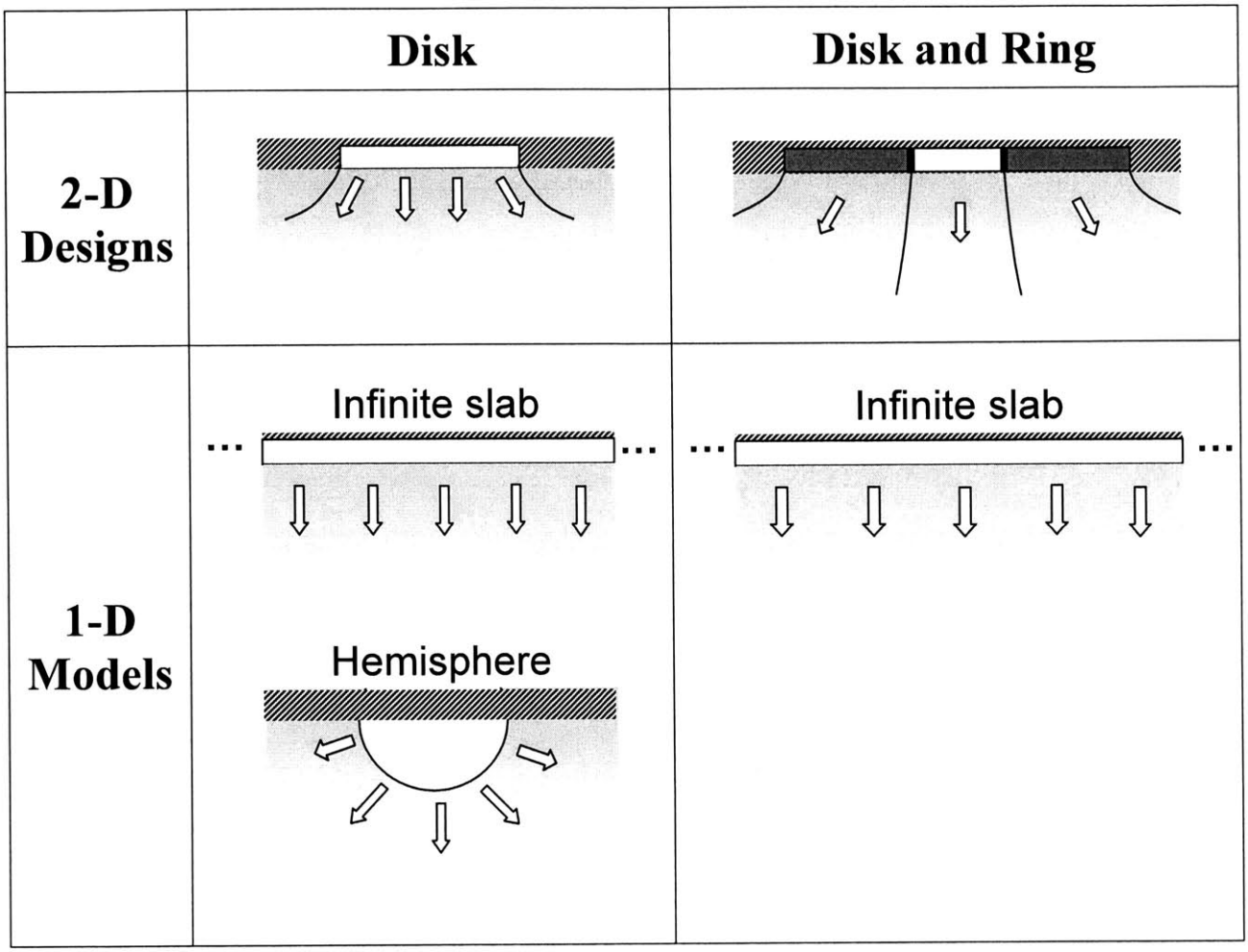

Figure 4.7 Two-dimensional designs and their proposed one-dimensional models.

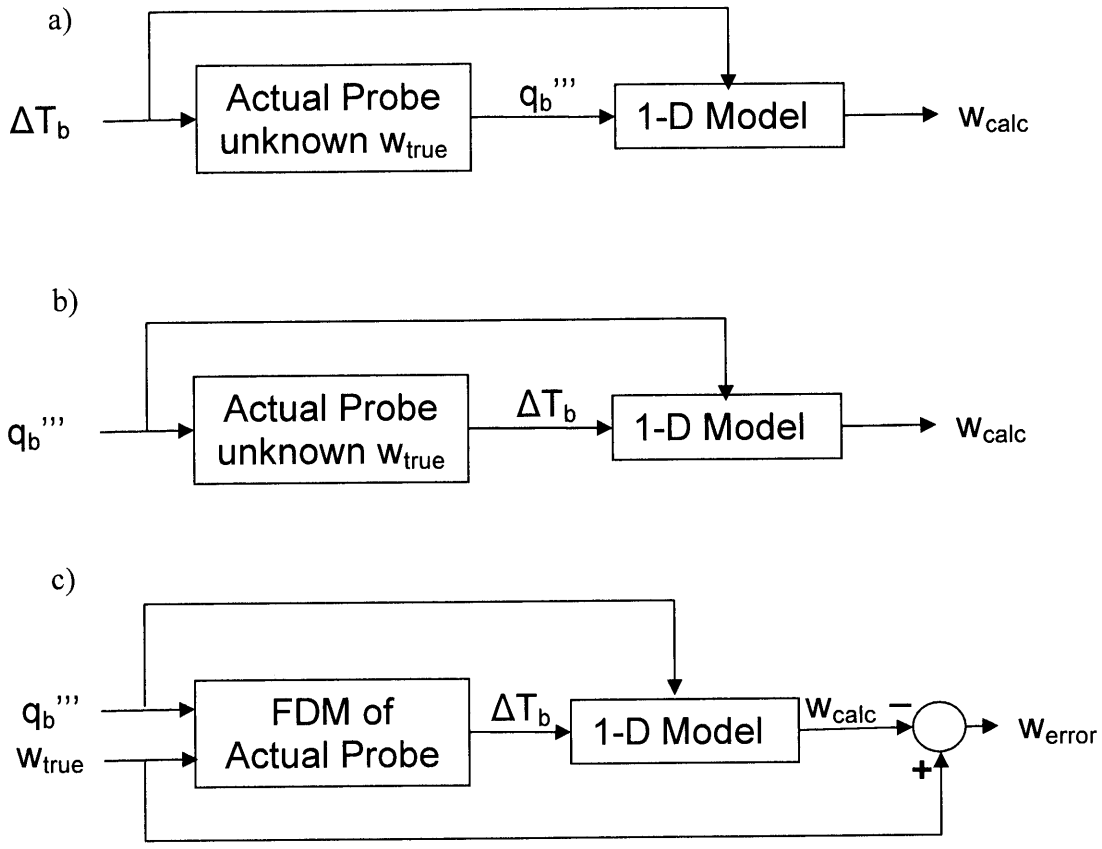

Figure 4.8 Flow of information in the thermodiffusion method.

a) the thermodiffusion method initially proposed by Bowman et al.
b) an equivalent thermodiffusion method
c) the set-up used to determine the error created by modeling a two-dimensional probe as one-dimensional.

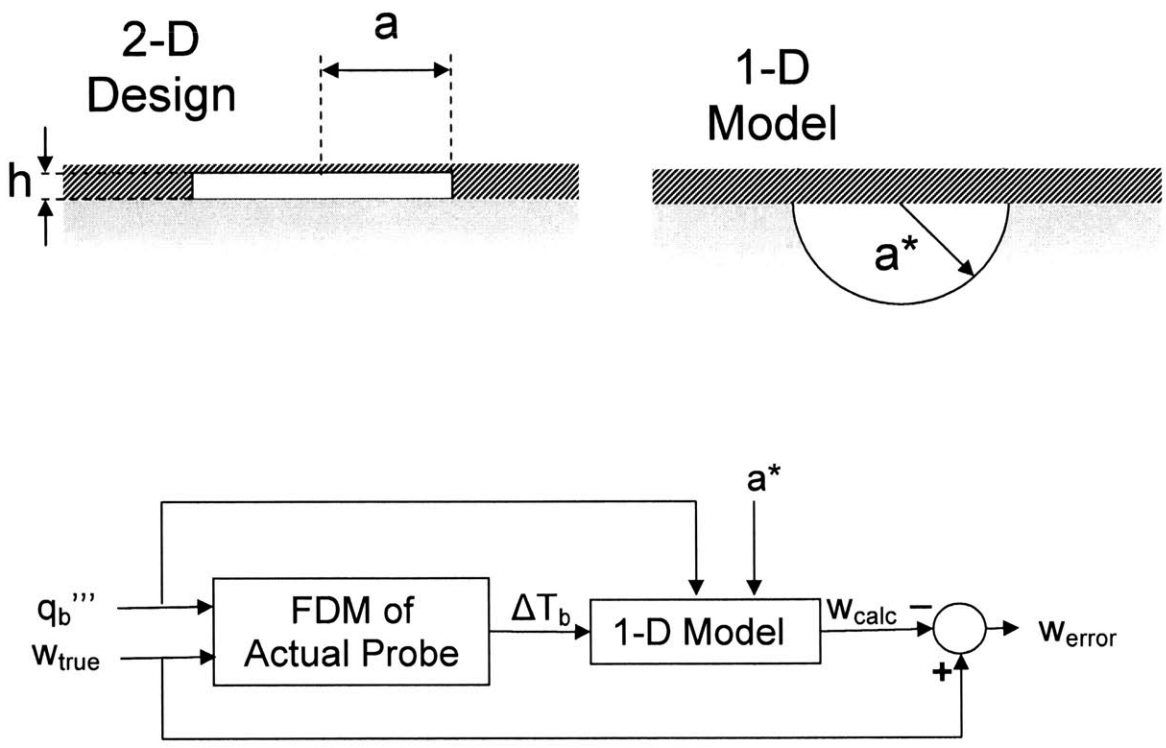

Figure 4.9 In modeling the disk-shaped probe as a hemisphere, the radius of the hemisphere, *a, is a free variable.**

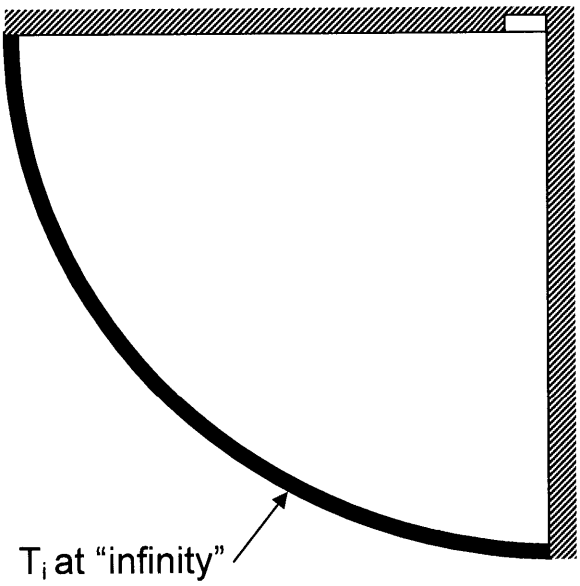

Figure 4.10 FDM model.

A diagram of the finite-difference model of half of the probe and tissue, with external boundary conditions of insulation at the top and the symmetry line, and T_i at a "very large distance," R (approximating infinity).

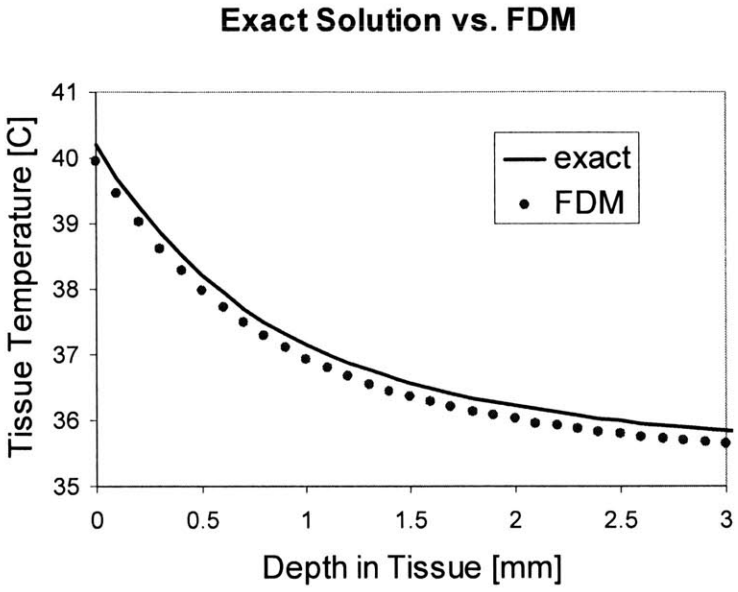

Figure 4.11 Validation of the finite-difference model with Carslaw & Jaeger's exact solution of the temperature profile in a semi-infinite, unperfused medium heated with uniform flux over a spherical region on its surface [45].

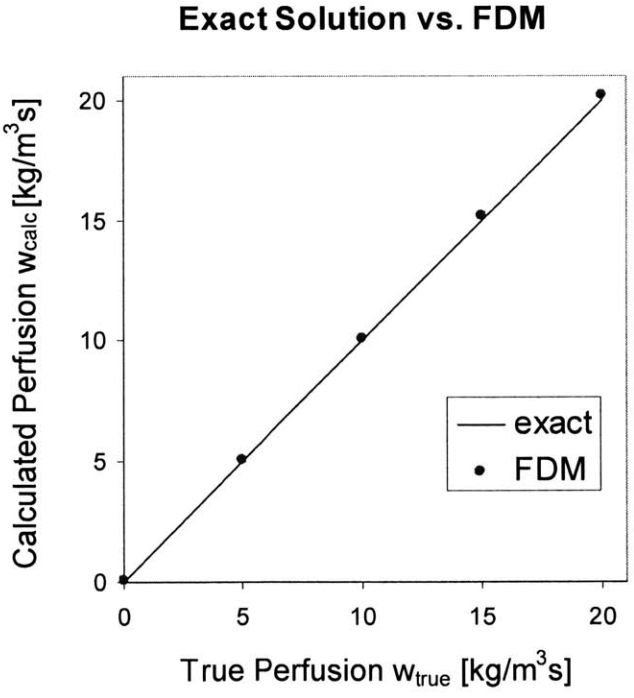

Figure 4.12 Validation of the finite-difference model of a heated sphere in perfused tissue. w_{true} and w_{calc} are compared according to the method presented in Section 4.6.1.

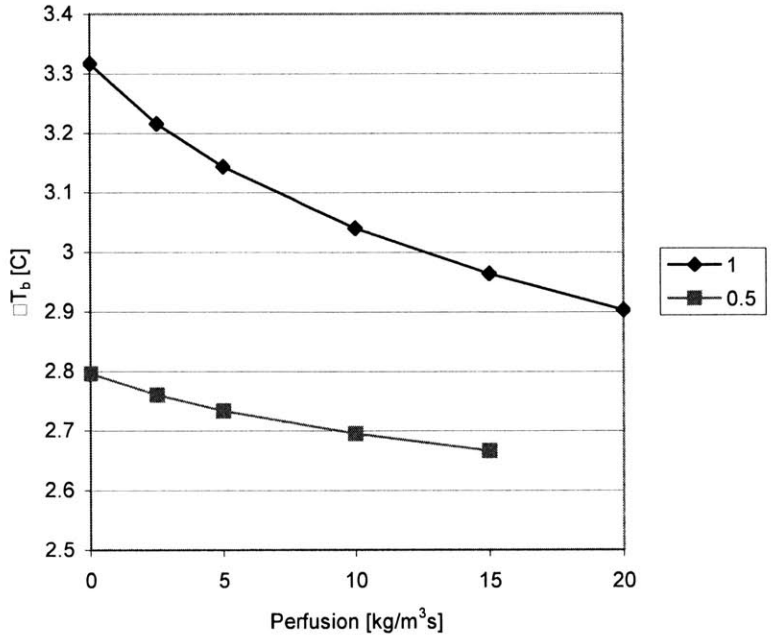

Figure 4.13 Output from the finite-difference model of the Disk design: ΔT_b vs. w, for two probe radii (in mm). h=0.2mm. q_b'''=7.5MW/m^3 for a=1mm and q_b'''=10MW/m^3 for a=0.5mm.

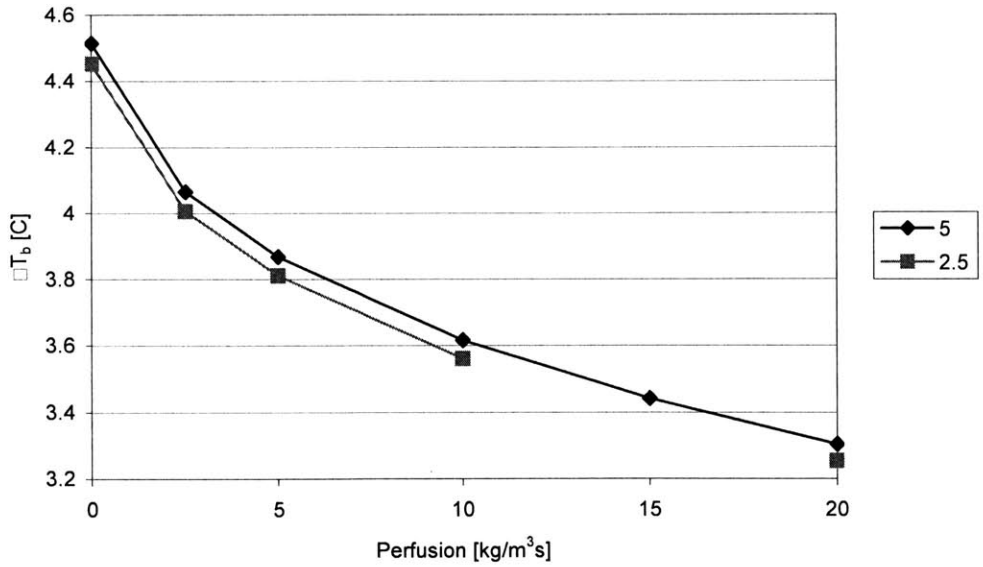

Figure 4.14 Output from the finite-difference model of the Disk and Ring design: ΔT_b vs. w, for two values of a_{out}/a_{in} (a_{out}=2mm in both cases). h=0.2mm. $q_{out}'''=q_{in}'''$=5MW/m^3.

w_{true}	Crit. 1	Crit. 2	Crit. 3	Crit. 4	Planar Heater	ΔT_b
N/A	1.000	0.669	0.600	0.593	N/A	N/A
0	4729.88	108.40	0.60	0.00	182.72	3.32 °C
2.5	3997.41	155.53	3.63	1.15	198.71	3.22 °C
5	3584.00	200.27	7.83	3.68	211.47	3.14 °C
10	3107.46	286.74	17.88	10.69	231.98	3.04 °C
15	2823.35	373.39	29.25	19.22	248.98	2.96 °C
20	2626.40	462.66	41.64	28.79	264.04	2.90 °C

Table 4.1 w_{calc} vs. w_{true} for a=1mm.

The 1st column contains the input to the FDM, w_{true}. The 6th column contains the output of the FDM, ΔT_b. Columns 2 through 6 contain w_{calc}. Columns 2 through 5 contain w_{calc} calculated by the hemispherical model using various criteria (top row) to calculate a^* (2nd row, in mm). The criteria are outlined in Section 4.8.1. The 6th column contains w_{calc} calculated by the planar model. Perfusion values are in kg/m^{3}s.

w_{true}	Crit. 1	Crit. 2	Crit. 3	Crit. 4	Planar Heater	ΔT_b
N/A	0.500	0.422	0.600	0.472	N/A	N/A
0	29.64	64.34	1736.17	0.00	718.04	2.80 °C
2.5	37.98	58.74	1994.58	0.30	749.93	2.76 °C
5	45.25	54.58	2219.02	0.94	775.23	2.73 °C
10	57.32	48.69	2595.07	2.57	813.55	2.70 °C
15	68.16	44.22	2939.27	4.46	845.00	2.67 °C

Table 4.2 w_{calc} vs. w_{true} for a=0.5mm.

The 1st column contains the input to the FDM, w_{true}. The 6th column contains the output of the FDM, ΔT_b. Columns 2 through 6 contain w_{calc}. Columns 2 through 5 contain w_{calc} calculated by the hemispherical model using various criteria (top row) to calculate a^* (2nd row, in mm). The criteria are outlined in Section 4.8.1. The 6th column contains w_{calc} calculated by the planar model. Perfusion values are in kg/m^{3}s.

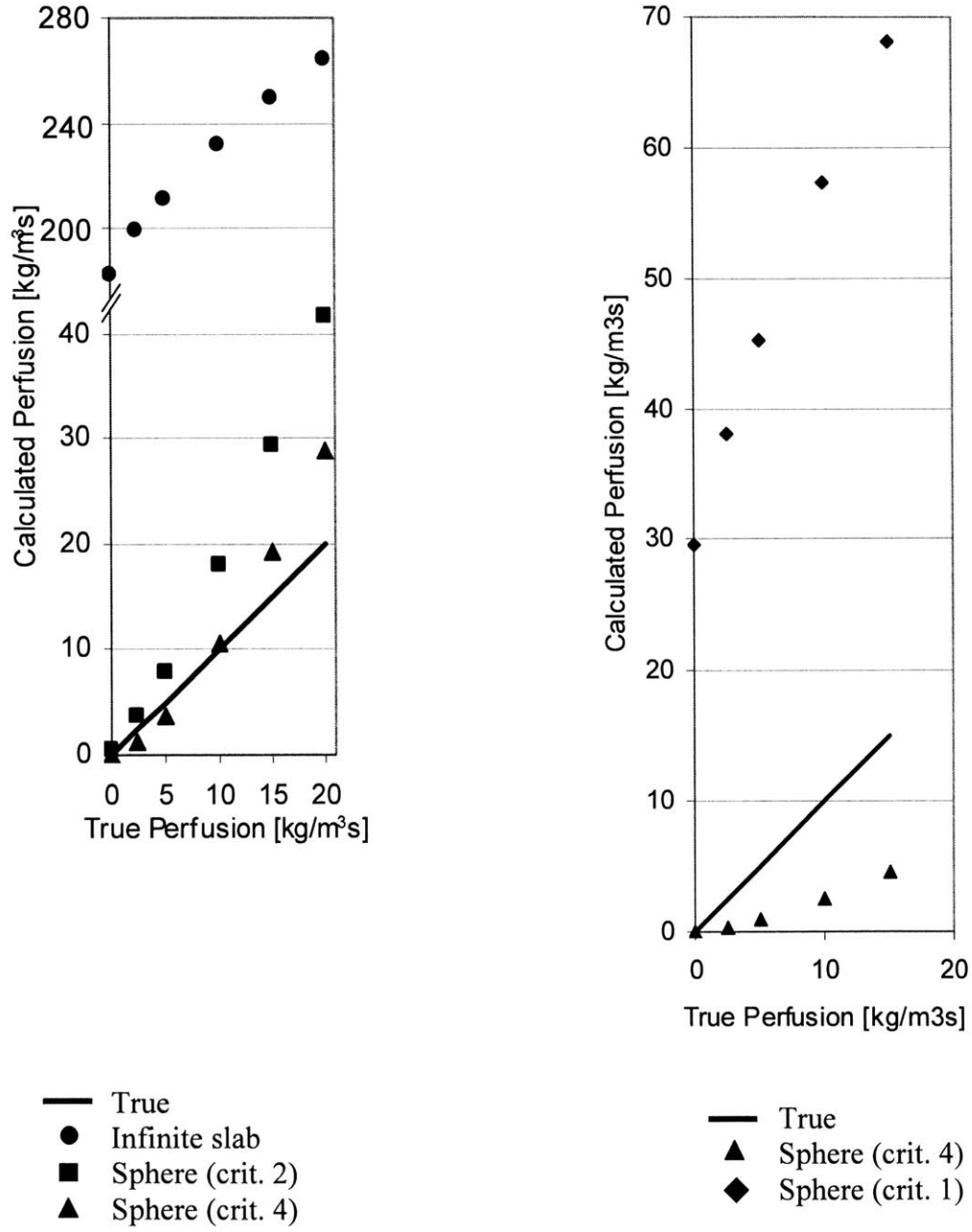

Figure 4.15 Disk design: w_{calc} vs. w_{true} for the hemi-spherical model for various choices of a^* (see 4.8.1 for criteria) and the planar model. Left: a=1mm; Right: a=0.5mm.

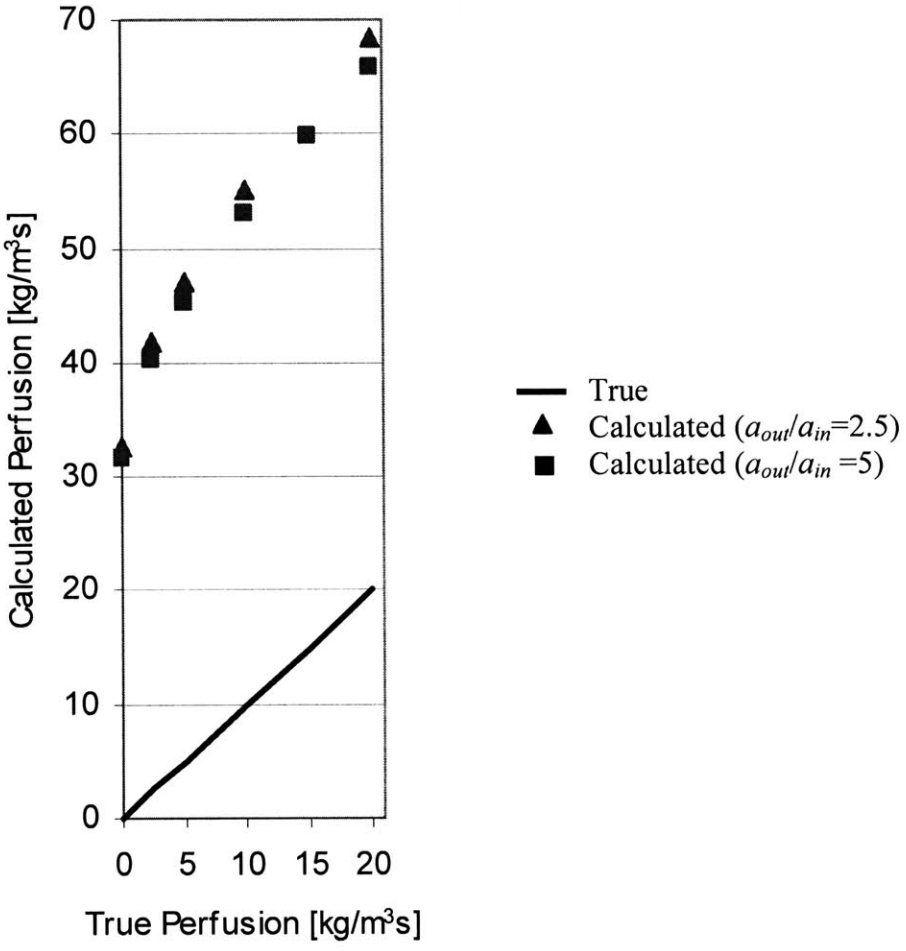

Figure 4.16 Disk and Ring design: w_{calc} vs. w_{true} for the planar model for two values of the ratio a_{out}/a_{in} (a_{out}=2mm in both cases).

5 Conclusion

This thesis explores the feasibility and subsequent design of a non-invasive thermodiffusion probe. The clinical study evidenced the promise of a non-invasive probe by showing that the invasive thermodiffusion probe, applied non-invasively, is capable of tracking perfusion, with clear advantages over other methods. However, using an invasive probe in a non-invasive manner caused a number of challenges, necessitating the development of a truly non-invasive probe. Two designs for a non-invasive probe are presented.

Because perfusion is not actually measured but estimated from measured quantities by an analytical or numerical model of the probe, the design of the probe must occur hand-in-hand with the development of the analytical or numerical model. While no two-dimensional analytical models exist of a finite, heated object placed on a perfused medium, one-dimensional analytical models have been developed for an infinite, heated object placed on a perfused medium and for a spherical, heated object *in* a perfused medium. It is natural to begin the design process by proposing a design and trying to "get away with" approximating the design by one of the existing one-dimensional models.

The main theoretical contribution of this thesis is the development and execution of a technique to determine the error that results from approximating the two proposed designs as existing one-dimensional analytical models.

It is shown that, in general, the error between true and calculated perfusion caused by approximating a two-dimensional geometry by a one-dimensional model is prohibitively large. Nevertheless, by proper choice of model and of probe and model dimensions, it appears possible to limit the error to a clinically acceptable range.

6 Bibliography

[1] J. W. Valvano, J. T. Allen, and H. F. Bowman, "The Simultaneous Measurement of Thermal-Conductivity, Thermal-Diffusivity, and Perfusion in Small Volumes of Tissue," *Journal of Biomechanical Engineering-Transactions of the Asme*, vol. 106, pp. 192-197, 1984.

[2] J. W. Valvano, "The Use of Thermal Diffusivity to Quantify Tissue Perfusion." Ph.D. Thesis, Cambridge, MA: Massachusetts Institute of Technology, 1981.

[3] H. F. Bowman, "Estimation of Tissue Blood Flow," in *Heat Transfer in Medicine and Biology*, vol. 1, A. Shitzer and R. C. Eberhart, Eds. New York: Plenum Press, 1985.

[4] J. T. Walsh, "A Noninvasive Thermal Method for the Quantification of Tissue Perfusion." M.S. Thesis, Cambridge, MA: Massachusetts Institute of Technology, 1984.

[5] J. G. Webster, "Medical Instrumentation, Application and Design," 3 ed. New York City, NY: John Wiley & Sons, 1998.

[6] H. F. Bowman, T. A. Balasubramaniam, and M. Woods, "Determination of Tissue Perfusion from "in vivo" Thermal Conductivity Measurements," *Heat Transfer in Biotechnology - ASME*, 1977.

[7] T. A. Balasubramaniam and H. F. Bowman, "Thermal Conductivity and Thermal Diffusivity of Biomaterials: A Simultaneous Measurement Technique," *Journal of Biomechanical Engineering*, vol. 99, pp. 148-154, 1977.

[8] J. C. Chato, "A Method for the Measurement of Thermal Properties of Biologic Materials," presented at Thermal Problems in Biotechnology, ASME, LCN068-58741, NY, 1968.

[9] T. A. Balasubramaniam and H. F. Bowman, "Temperature Field Due to a Time-Dependent Heat Source of Spherical Geometry in an Infinite Medium," *Journal of Heat Transfer-Transactions of the Asme*, vol. 96, pp. 296-299, 1974.

[10] T. A. Balasubramaniam, "Thermal Conductivity and Thermal Diffusivity of Biomaterials: A Simultaneous Measurement Technique." Ph.D. Thesis, Boston, MA: Northeastern University, 1975.

[11] H. H. Pennes, "Analysis of Tissue and Arterial Blood Temperature in the Resting Human Forearm," *Journal of Applied Physiology*, vol. 1, pp. 93-122, 1948.

[12] R. K. Jain, "Transient Temperature Distributions in an Infinite, Perfused Medium Due to a Time-Dependent, Spherical Heat-Source," *Journal of Biomechanical Engineering-Transactions of the Asme*, vol. 101, pp. 82-86, 1979.

[13] G. T. Martin and H. F. Bowman, "Validation of real-time continuous perfusion measurement," *Medical & Biological Engineering & Computing*, vol. 38, pp. 319-325, 2000.

[14] A. T. Patera, G. Eden, B. B. Mikic, and H. F. Bowman, "Prediction of Tissue Perfusion from Measurement of Phase Shift between Heat Flux and Temperature," presented at Winter Annual Meeting, ASME, # 79-WA/HT-71, 1979.

[15] Hemedex Inc., "Product Info," [online] www.hemedex.com (accessed 2004), 2002.

[16] P. Vajkoczy, H. Roth, P. Horn, T. Lucke, C. Thome, U. Hubner, G. T. Martin, C. Zappletal, E. Klar, L. Schilling, and P. Schmiedek, "Continuous monitoring of regional cerebral blood flow: experimental and clinical validation of a novel thermal diffusion microprobe," *Journal of Neurosurgery*, vol. 93, pp. 265-274, 2000.

[17] E. Klar, T. Kraus, J. Bleyl, W. H. Newman, H. F. Bowman, W. J. Hofmann, R. Von Kummer, M. Bredt, and C. Herfarth, "Thermodiffusion for continuous quantification of hepatic microcirculation - Validation and potential in liver transplantation," *Microvascular Research*, vol. 58, pp. 156-166, 1999.

[18] J. W. Valvano, J. T. Allen, J. T. Walsh, D. J. Hnatowich, J. F. Tomera, H. Brunengraber, and H. F. Bowman, "An Isolated Rat-Liver Model for the Evaluation of Thermal Techniques to Quantify Perfusion," *Journal of Biomechanical Engineering-Transactions of the Asme*, vol. 106, pp. 187-191, 1984.

[19] K. S. Szaijda, "A digitally controlled analog subsystem for perfusion measurement." B.S. Thesis, Cambridge, MA: Massachusetts Institute of Technology, 1987.

[20] K. S. Szaijda, "A digitally data acquisition system for temperature and perfusion measurement." M.S. Thesis, Cambridge, MA: Massachusetts Institute of Technology, 1989.

[21] H. F. Bowman, "The bio-heat transfer equation and discriminiation of thermally significant vessels," *Annals of the New York Academy of Sciences*, vol. 335, pp. 155-160, 1980.

[22] Department of Independent Study, "Cardiovascular Health," in *Life Style Management Health Education/Physical Education 129*. Provo, UT: Division of Continuing Education, Brigham Young University, 1998, pp. 13-15.

[23] E. C. Klatt, "Cardiovascular Pathology Index," in *Organ System Pathology Index, The Internet Pathology Laboratory for Medical Education*, Florida State University College of Medicine, [online] http://medlib.med.utah.edu/WebPath/CVHTML/CV004.html and http://medlib.med.utah.edu/WebPath/CVHTML/CV005.html (accessed 2003), 1994.

[24] F. J. Schoen, "Blood Vessels," in *Pathologic Basis of Disease*, R. S. Cotran, Ed., 6 ed. Philadelphia, PA: Saunders, 1999.

[25] T. J. Anderson, "Assessment and treatment of endothelial dysfunction in humans," *Journal of the American College of Cardiology*, vol. 34, pp. 631-638, 1999.

[26] T. J. Anderson, A. Uehata, M. D. Gerhard, I. T. Meredith, S. Knab, D. Delagrange, E. H. Lieberman, P. Ganz, M. A. Creager, A. C. Yeung, and A. P. Selwyn, "Close Relation of Endothelial Function in the Human Coronary and Peripheral Circulations," *Journal of the American College of Cardiology*, vol. 26, pp. 1235-1241, 1995.

[27] G. T. Martin, personal communication with author, 2001.

[28] H. F. Bowman, personal communication with author, 2003.

[29] J. A. Vita and J. F. Keaney, "Endothelial function - A barometer for cardiovascular risk?," *Circulation*, vol. 106, pp. 640-642, 2002.

[30] A. K. Andreassen, L. Gullestad, T. Holm, S. Simonsen, and K. Kvernebo, "Endothelium-dependent vasodilation of the skin microcirculation in heart transplant recipients," *Clinical Transplantation*, vol. 12, pp. 324-332, 1998.

[31] R. M. Berne and M. N. Levy, "Principles of Physiology," 3 ed. St. Louis, MO: Mosby Inc., 2000.

[32] H. D. Kvernmo, A. Stefanovska, K. A. Kirlteboen, and K. Kvernebo, "Oscillations in the human cutaneous blood perfusion signal modified by endothelium-dependent and endothelium-independent vasodilators," *Microvascular Research*, vol. 57, pp. 298-309, 1999.

[33] M. C. Corretti, T. J. Anderson, E. J. Benjamin, D. Celermajer, F. Charbonneau, M. A. Creager, J. Deanfield, H. Drexler, M. Gerhard-Herman, D. Herrington, P. Vallance, J. Vita, and R. Vogel, "Guidelines for the ultrasound assessment of endothelial-dependent flow-mediated vasodilation of the brachial artery - A report of the International Brachial Artery Reactivity Task Force," *Journal of the American College of Cardiology*, vol. 39, pp. 257-265, 2002.

[34] A. Shitzer and R. C. Eberhart, "Heat Transfer in Medicine and Biology." New York: Plenum Press, 1985.

[35] M. Sapoff and R. M. Oppenheim, "Theory and Application of Self-heated Thermistors," *IEEE Proceedings*, vol. 51, pp. 1292-1305, 1963.

[36] M. M. Chen, "The Tissue Energy Balance Equation," in *Heat Transfer in Medicine and Biology*, A. Shitzer and R. C. Eberhart, Eds. New York: Plenum Press, 1985.

[37] B. D. Fornage and J. L. Deshayes, "Ultrasound of Normal Skin," *Journal of Clinical Ultrasound*, vol. 14, pp. 619-622, 1986.

[38] G. T. Overney, "Human Histology for Amateur Histologists," Microscopy-UK, [online] www.microscopy-uk.org.uk/mag/artaug02/gohisto.html (accessed 2004), 1995.

[39] S. Singh and R. Swerlick, "Dermal Blood Vessels," in *For Health Care Professionals*, American Academy of Dermatology, [online] www.aad.org/education/dermbloodvessels.htm (accessed 2004), 2003.

[40] C. Livingstone, "Skin," in *Gray's Anatomy*, 38 ed. Great Britain: Pearson Professional Limited, 1995.

[41] A. Shitzer and R. C. Eberhart, "Heat Generation, Storage, and Transport Processes," in *Heat Transfer in Medicine and Biology*, A. Shitzer and R. C. Eberhart, Eds. New York: Plenum Press, 1985.

[42] A. T. Patera, "The Effect of Cylindrical Probe Geometry on the Accuracy of Tissue Perfusion Measurements made with a Thermal Diffusion Probe," B.S. Thesis, Cambridge, MA: Massachusetts Institute of Technology, 1978.

[43] B. B. Mikic, personal communication with author, 2003-2004.

[44] G. T. Martin, personal communication with author, 2004.

[45] H. S. Carslaw and J. C. Jaeger, *Conduction of Heat in Solids*, 2 ed. New York: Oxford University Press, 1946.

[46] A. Shitzer, L. J. Hayes, R. W. Olsen, and R. C. Eberhart, "Finite-difference and Finite-element Methods of Solution," in *Heat Transfer in Medicine and Biology*, A. Shitzer and R. C. Eberhart, Eds. New York: Plenum Press, 1985.

7 Appendix A: Finite-Difference Model

As outlined in Section 4.6.2, I created a finite-difference model (FDM) for the Disk design and the Disk and Ring design. The FDM for the Disk design is actually just a degenerate version of the FDM for the Disk and Ring design.

I created the FDM in Microsoft Excel and solved it using Excel's built-in iteration solver. The advantage of using Excel is two-fold: simple models with few nodes can be set up and solved very quickly, and Excel's cells can be used as FDM cells, providing a very helpful graphical representation of the model. The main disadvantage of Excel is that the number of cells in the horizontal direction (i.e. columns in Excel) is limited to 256. Thus R is severely limited. In addition, computation time quickly becomes very large in Excel: when the maximum width of the spreadsheet is used (R=256 cells), the tissue and probe contain on the order of 50'000 cells, which can take up to 60'000 iterations to solve (up to 6 or 8 hours on a 2 GHz processor).

Figure 7.1 shows the entire layout of the FDM, where dots represent temperature nodes and cells represent areas approximated as having uniform temperature. The layout is not to scale. Also, only a small number of nodes, in disproportion, are shown for illustration purposes. As shown, symmetry allowed the FDM to be limited to half of the probe-tissue system in order to save computing power. Since both designs are disk-shaped, the FDMs were created in cylindrical coordinates. There is also angular symmetry about the r=0 axis, so the FDM is a two-dimensional model in r and z (see Figure 7.1). The origin of the z-axis is immaterial. The exposed surfaces and the symmetry line of the probe and tissue were modeled as being insulated (shown as hatched lines). The boundary condition for the lower boundary of the tissue was stated in the Section 4.1.3 as $T_m \rightarrow T_i$ approaching the boundary at infinity. In the FDM this lower bound was implemented by specifying $T_m = T_i$ on a semi-hemisphere of "very large radius," R. These boundary nodes (for which the temperature is specified as T_i) are shown as white dots. The error associated with this approximation, as well as the other approximations inherent in finite-difference modeling, are presented in Section 4.6.2. Tissue perfusion was implemented in the FDM as stated in the bioheat equation, i.e. as a

heat sink. For a more formal discussion of FDM and finite-element analysis for tissue, see [35].

Because w_{calc} is extremely sensitive on measurement errors in ΔT_b, the probe was modeled with a finer mesh than the tissue. This was achieved, as shown in Figure 7.1, by choosing $\Delta r_b < \Delta r_m$ and $\Delta h_b < \Delta h_m$, where Δr is the cell width, Δh the cell height, and b and m refer to probe and tissue, respectively. Implementation in Excel necessitated splitting the tissue into a coarse-mesh area covering the vast majority of the modeled tissue volume, and an intermediate-mesh area (Δh_m but Δr_b) located directly below the probe. These three areas (one for probe and two for tissue) are separated in Figure 7.1 by the thick line running through nodes 11 and 15, and the thick line running through nodes 15 and 16. Nodes located on the boundaries between these three areas have asymmetric cells and require special attention.

The thick triple line dividing the probe vertically represents the boundary between the inner disk and outer ring of the Disk and Ring design. The FDM for the Disk design can be obtained by simply ignoring this line and treating nodes 5-8, 12, and 13 as node 1.

Following the standard method of formulating finite-difference equations from an energy balance on a given cell, I developed the equations for the node temperature of each cell, $T_{m,n}$. The cells can be divided into groups of nodes having the same node equation:

- Probe and tissue center-nodes (1, 17, 19)
- Boundary nodes (2-6, 9-10, 18, 20)
- Probe-tissue interface nodes (12-14)
- Probe-tissue interface and boundary nodes (11, 15)
- Nodes on boundary between intermediate- and coarse-mesh tissue areas (16)
- Only for Disk and Ring design: nodes on the interface of inner disk and outer ring (5-8, 12, 13)

The equations for the temperatures of these nodes are given on the following pages.

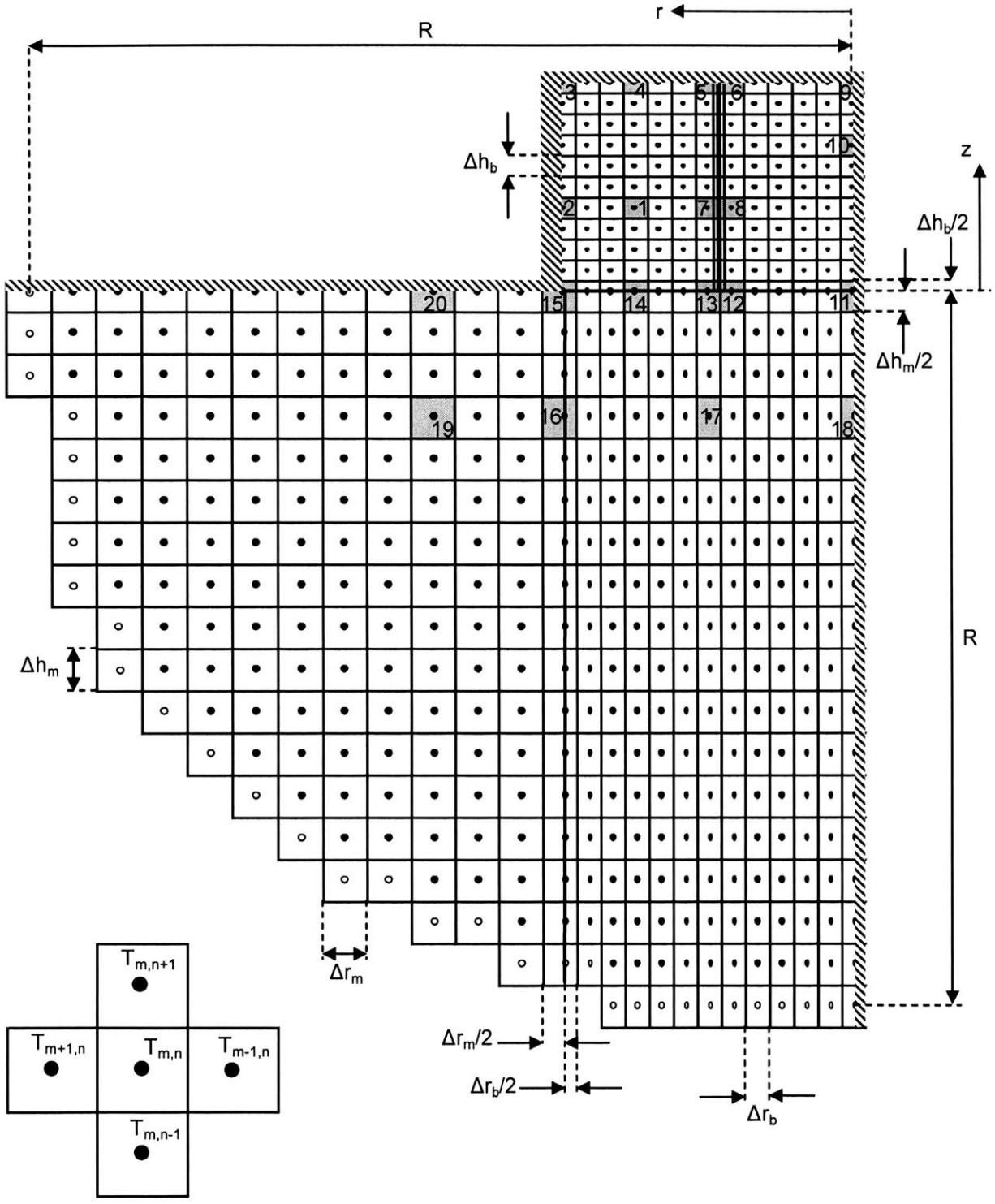

Figure 7.1 Layout of the FDM, including cell nomenclature (lower left).

$$T_{m,n}{}^{1} = \frac{1}{\frac{2}{\Delta r_b{}^2} + \frac{2}{\Delta h_b{}^2}} \left[\begin{array}{l} T_{m+1,n}\left(\frac{1}{2r\Delta r_b} + \frac{1}{\Delta r_b{}^2} \right) + T_{m-1,n}\left(\frac{-1}{2r\Delta r_b} + \frac{1}{\Delta r_b{}^2} \right) \\ + T_{m,n+1}\left(\frac{1}{\Delta h_b{}^2} \right) + T_{m,n-1}\left(\frac{1}{\Delta h_b{}^2} \right) + \frac{q_b'''}{k_b} \end{array} \right]$$

$$T_{m,n}{}^{2} = \frac{1}{\frac{r - \frac{\Delta r_b}{2}}{r - \frac{\Delta r_b}{4}} \cdot \frac{2}{\Delta r_b{}^2} + \frac{2}{\Delta h_b{}^2}} \left[T_{m-1,n}\left(\frac{r - \frac{\Delta r_b}{2}}{r - \frac{\Delta r_b}{4}} \cdot \frac{2}{\Delta r_b{}^2} \right) + T_{m,n+1}\left(\frac{1}{\Delta h_b{}^2} \right) + T_{m,n-1}\left(\frac{1}{\Delta h_b{}^2} \right) + \frac{q_b'''}{k_b} \right]$$

$$T_{m,n}{}^{3} = \frac{1}{\frac{r - \frac{\Delta r_b}{2}}{r - \frac{\Delta r_b}{4}} \cdot \frac{2}{\Delta r_b{}^2} + \frac{2}{\Delta h_b{}^2}} \left[T_{m-1,n}\left(\frac{r - \frac{\Delta r_b}{2}}{r - \frac{\Delta r_b}{4}} \cdot \frac{2}{\Delta r_b{}^2} \right) + T_{m,n-1}\left(\frac{2}{\Delta h_b{}^2} \right) + \frac{q_b'''}{k_b} \right]$$

$$T_{m,n}{}^{4} = \frac{1}{\frac{2}{\Delta r_b{}^2} + \frac{2}{\Delta h_b{}^2}} \left[T_{m+1,n}\left(\frac{1}{2r\Delta r_b} + \frac{1}{\Delta r_b{}^2} \right) + T_{m-1,n}\left(\frac{-1}{2r\Delta r_b} + \frac{1}{\Delta r_b{}^2} \right) + T_{m,n-1}\left(\frac{2}{\Delta h_b{}^2} \right) + \frac{q_b'''}{k_b} \right]$$

$$T_{m,n}{}^{5} = \frac{1}{\frac{1}{\Delta r_b{}^2} + \frac{1}{2r\Delta r_b} + \frac{2}{\Delta h_b{}^2}} \left[T_{m+1,n}\left(\frac{1}{2r\Delta r_b} + \frac{1}{\Delta r_b{}^2} \right) + T_{m,n-1}\left(\frac{2}{\Delta h_b{}^2} \right) + \frac{q_b'''}{k_b} \right]$$

$$T_{m,n}{}^{6} = \frac{1}{\frac{1}{\Delta r_b{}^2} - \frac{1}{2r\Delta r_b} + \frac{2}{\Delta h_b{}^2}} \left[T_{m-1,n}\left(\frac{-1}{2r\Delta r_b} + \frac{1}{\Delta r_b{}^2} \right) + T_{m,n-1}\left(\frac{2}{\Delta h_b{}^2} \right) + \frac{q_b'''}{k_b} \right]$$

$$T_{m,n}{}^{7} = \frac{1}{\frac{1}{\Delta r_b{}^2} + \frac{1}{2r\Delta r_b} + \frac{2}{\Delta h_b{}^2}} \left[T_{m+1,n}\left(\frac{1}{2r\Delta r_b} + \frac{1}{\Delta r_b{}^2} \right) + T_{m,n+1}\left(\frac{1}{\Delta h_b{}^2} \right) + T_{m,n-1}\left(\frac{1}{\Delta h_b{}^2} \right) + \frac{q_b'''}{k_b} \right]$$

$$T_{m,n}{}^{8} = \frac{1}{\frac{1}{\Delta r_b{}^2} - \frac{1}{2r\Delta r_b} + \frac{2}{\Delta h_b{}^2}} \left[T_{m-1,n}\left(\frac{-1}{2r\Delta r_b} + \frac{1}{\Delta r_b{}^2} \right) + T_{m,n+1}\left(\frac{1}{\Delta h_b{}^2} \right) + T_{m,n-1}\left(\frac{2}{\Delta h_b{}^2} \right) + \frac{q_b'''}{k_b} \right]$$

$$T_{m,n}{}^{9} = \frac{1}{\frac{2}{\Delta r_b{}^2} + \frac{2}{\Delta h_b{}^2}} \left[T_{m+1,n}\left(\frac{2}{\Delta r_b{}^2} \right) + T_{m,n-1}\left(\frac{1}{\Delta h_b{}^2} \right) + \frac{q_b'''}{2k_b} \right]$$

$$T_{m,n}^{10} = \frac{1}{\frac{4}{\Delta r_b^2} + \frac{2}{\Delta h_b^2}} \left[T_{m+1,n}\left(\frac{4}{\Delta r_b^2}\right) + T_{m,n+1}\left(\frac{1}{\Delta h_b^2}\right) + T_{m,n-1}\left(\frac{1}{\Delta h_b^2}\right) + \frac{q_b'''}{k_b} \right]$$

$$T_{m,n}^{11} = \frac{1}{\frac{2(k_b\Delta h_b + k_m\Delta h_m)}{\Delta r_b^2} + \frac{k_b}{\Delta h_b} + \frac{k_m}{\Delta h_m} + \frac{wc_{bl}\Delta h_m}{2}} \bullet$$

$$\bullet \left[T_{m+1,n}\left(\frac{2}{\Delta r_b^2}\right) \cdot (k_b\Delta h_b + k_m\Delta h_m) + T_{m,n+1}\left(\frac{k_b}{\Delta h_b}\right) + T_{m,n-1}\left(\frac{k_m}{\Delta h_m}\right) + \frac{q_b'''\Delta h_b}{2} + \frac{wc_{bl}\Delta h_m T_i}{2} \right]$$

$$T_{m,n}^{12} = \frac{1}{k_m\Delta h_m\left(\frac{1}{\Delta r_b^2} + \frac{1}{2r\Delta r_b}\right) + (k_b\Delta h_b + k_m\Delta h_m)\left(\frac{1}{\Delta r_b^2} - \frac{1}{2r\Delta r_b}\right) + \frac{2k_b}{\Delta h_b} + \frac{2k_m}{\Delta h_m} + wc_{bl}\Delta h_m} \bullet$$

$$\bullet \left[\begin{array}{l} T_{m+1,n}(k_m\Delta h_m)\left(\frac{1}{2r\Delta r_b} + \frac{1}{\Delta r_b^2}\right) + T_{m-1,n}(k_b\Delta h_b + k_m\Delta h_m)\left(\frac{-1}{2r\Delta r_b} + \frac{1}{\Delta r_b^2}\right) + T_{m,n+1}\left(\frac{2k_b}{\Delta h_b}\right) \\ + T_{m,n-1}\left(\frac{2k_m}{\Delta h_m}\right) + q_b'''\Delta h_b + wc_{bl}\Delta h_m T_i \end{array} \right]$$

$$T_{m,n}^{13} = \frac{1}{k_m\Delta h_m\left(\frac{1}{\Delta r_b^2} - \frac{1}{2r\Delta r_b}\right) + (k_b\Delta h_b + k_m\Delta h_m)\left(\frac{1}{\Delta r_b^2} + \frac{1}{2r\Delta r_b}\right) + \frac{2k_b}{\Delta h_b} + \frac{2k_m}{\Delta h_m} + wc_{bl}\Delta h_m} \bullet$$

$$\bullet \left[\begin{array}{l} T_{m+1,n}(k_b\Delta h_b + k_m\Delta h_m)\left(\frac{1}{2r\Delta r_b} + \frac{1}{\Delta r_b^2}\right) + T_{m-1,n}(k_m\Delta h_m)\left(\frac{-1}{2r\Delta r_b} + \frac{1}{\Delta r_b^2}\right) + T_{m,n+1}\left(\frac{2k_b}{\Delta h_b}\right) \\ + T_{m,n-1}\left(\frac{2k_m}{\Delta h_m}\right) + q_b'''\Delta h_b + wc_{bl}\Delta h_m T_i \end{array} \right]$$

$$T_{m,n}^{14} = \frac{1}{\frac{2(k_b\Delta h_b + k_m\Delta h_m)}{\Delta r_b^2} + \frac{2k_b}{\Delta h_b} + \frac{2k_m}{\Delta h_m} + wc_{bl}\Delta h_m} \bullet$$

$$\bullet \left[\begin{array}{l} T_{m+1,n}\left(\frac{1}{2r\Delta r_b} + \frac{1}{\Delta r_b^2}\right) \cdot (k_b\Delta h_b + k_m\Delta h_m) + T_{m-1,n}\left(\frac{-1}{2r\Delta r_b} + \frac{1}{\Delta r_b^2}\right) \cdot (k_b\Delta h_b + k_m\Delta h_m) \\ + T_{m,n+1}\left(\frac{2k_b}{\Delta h_b}\right) + T_{m,n-1}\left(\frac{2k_m}{\Delta h_m}\right) + q_b'''\Delta h_b + wc_{bl}\Delta h_m T_i \end{array} \right]$$

$$T_{m,n}{}^{15} = \left[\begin{array}{l} 2k_m \Delta h_m \left(\frac{r}{\Delta r_m} + \frac{r}{\Delta r_b} \right) + 2k_b \Delta h_b \left(\frac{r - \frac{\Delta r_b}{2}}{\Delta r_b} \right) + 2k_b \left(r - \frac{\Delta r_b}{4} \right) \left(\frac{\Delta r_b}{\Delta h_b} \right) \\ + k_m \left(r + \frac{\Delta r_m - \Delta r_b}{4} \right) \left(\frac{\Delta r_m + \Delta r_b}{\Delta h_m} \right) \left(\frac{wc_{bl} \Delta h_m{}^2}{k_m} + 2 \right) \end{array} \right]^{-1} \bullet$$

$$\bullet \left[\begin{array}{l} T_{m+1,n} \left(2k_m \Delta h_m \right) \left(\frac{r}{\Delta r_m} + \frac{1}{2} \right) \cdot \left(k_b \Delta h_b + k_m \Delta h_m \right) + T_{m-1,n} \left(\frac{r}{\Delta r_b} - \frac{1}{2} \right) \cdot \left(2k_b \Delta h_b + 2k_m \Delta h_m \right) \\ + T_{m,n+1} \left(2k_b \right) \left(r - \frac{\Delta r_b}{4} \right) \left(\frac{\Delta r_b}{\Delta h_b} \right) \\ + k_m \left(r + \frac{\Delta r_m - \Delta r_b}{4} \right) \left(\frac{\Delta r_m + \Delta r_b}{\Delta h_m} \right) \left(2T_{m,n-1} + \frac{wc_{bl} \Delta h_m{}^2 T_i}{k_m} \right) + q_b''' \left(r - \frac{\Delta r_b}{4} \right) \Delta h_b \Delta r_b \end{array} \right]$$

$$T_{m,n}{}^{16} = \frac{1}{\frac{2\left(r + \frac{\Delta r_m}{2} \right)}{\Delta r_m} + \frac{2\left(r - \frac{\Delta r_b}{2} \right)}{\Delta r_b} + \frac{\left(r + \frac{\Delta r_m - \Delta r_b}{4} \right) \left(\Delta r_m + \Delta r_b \right) \left(\frac{wc_{bl} \Delta h_m{}^2}{k_m} + 2 \right)}{\Delta h_m{}^2}} \bullet$$

$$\bullet \left[\begin{array}{l} T_{m+1,n} \frac{2\left(r + \frac{\Delta r_m}{2} \right)}{\Delta r_m} + T_{m-1,n} \frac{2\left(r - \frac{\Delta r_b}{2} \right)}{\Delta r_b} \\ + \frac{\left(r + \frac{\Delta r_m - \Delta r_b}{4} \right) \left(\Delta r_m + \Delta r_b \right)}{\Delta h_m{}^2} \left(T_{m,n+1} + T_{m,n-1} + \frac{wc_{bl} \Delta h_m{}^2 T_i}{k_m} \right) \end{array} \right]$$

$$T_{m,n}{}^{17} = \frac{1}{\frac{2}{\Delta r_b{}^2} + \frac{2}{\Delta h_m{}^2} + \frac{wc_{bl}}{k_m}} \left[\begin{array}{l} T_{m+1,n} \left(\frac{1}{2r\Delta r_b} + \frac{1}{\Delta r_b{}^2} \right) + T_{m-1,n} \left(\frac{-1}{2r\Delta r_b} + \frac{1}{\Delta r_b{}^2} \right) \\ + T_{m,n+1} \left(\frac{1}{\Delta h_m{}^2} \right) + T_{m,n-1} \left(\frac{1}{\Delta h_m{}^2} \right) + \frac{wc_{bl} T_i}{k_m} \end{array} \right]$$

$$T_{m,n}{}^{18} = \frac{1}{\frac{4}{\Delta r_b{}^2} + \frac{2}{\Delta h_m{}^2} + \frac{wc_{bl}}{k_m}} \left[T_{m+1,n} \left(\frac{4}{\Delta r_b{}^2} \right) + T_{m,n+1} \left(\frac{1}{\Delta h_m{}^2} \right) + T_{m,n-1} \left(\frac{1}{\Delta h_m{}^2} \right) + \frac{wc_{bl} T_i}{k_m} \right]$$

$$T_{m,n}{}^{19} = \frac{1}{\frac{2}{\Delta r_m{}^2} + \frac{2}{\Delta h_m{}^2} + \frac{wc_{bl}}{k_m}} \left[\begin{array}{l} T_{m+1,n} \left(\frac{1}{2r\Delta r_m} + \frac{1}{\Delta r_m{}^2} \right) + T_{m-1,n} \left(\frac{-1}{2r\Delta r_m} + \frac{1}{\Delta r_m{}^2} \right) \\ + T_{m,n+1} \left(\frac{1}{\Delta h_m{}^2} \right) + T_{m,n-1} \left(\frac{1}{\Delta h_m{}^2} \right) + \frac{wc_{bl} T_i}{k_m} \end{array} \right]$$

$$T_{m,n}^{20} = \frac{1}{\frac{4}{\Delta r_m^{\,2}} + \frac{2}{\Delta h_m^{\,2}} + \frac{wc_{bl}}{k_m}} \left[T_{m+1,n}\left(\frac{4}{\Delta r_m^{\,2}}\right) + T_{m,n+1}\left(\frac{1}{\Delta h_m^{\,2}}\right) + T_{m,n-1}\left(\frac{1}{\Delta h_m^{\,2}}\right) + \frac{wc_{bl}T_l}{k_m} \right]$$

8 Appendix B: Error due to Finite Extent of FDM

As stated in Section 4.6.2.2, the errors in perfusion calculated from a finite-difference model are due to three sources: discretization, finite number of iterations, and finite R (R is the radius of the boundary that approximates infinity). The error due to finite R deserves more attention. In the governing equation of the temperature distribution in the tissue, the boundary condition for the lower boundary of the tissue is $T_m \rightarrow T_i$ approaching the boundary at infinity. In the FDM this lower bound was implemented by specifying $T_m = T_i$ on a semi-hemisphere of "very large radius", R.

The approximation errors due to these three sources were estimated by varying each of the sources in turn and observing the change in calculated error. Roughly,

1. refining the probe mesh from 1000 to 2000 cells produced a change in calculated perfusion on the order of 0.02 kg/m^{3}s.
2. decreasing the 'maximum change between iterations required to terminate the iterations' from 10^{-7} to 10^{-8} (i.e. increasing the number of iterations) produced a change in calculated perfusion on the order of 0.06 kg/m^{3}s.
3. increasing R from 12.7mm to 21.3mm produced a change in calculated perfusion on the order of 3 kg/m^{3}s.

This analysis demonstrates that the mesh size and number of iterations are adequate, but that the finite value of R produces a large error (3 kg/m^{3}s is often the typical level of perfusion in skin and other tissues). It is clear that it is not enough to know the error due to approximating infinity as R=12.7mm instead of R=21.3mm, but that the error from approximating infinity as R=12.7mm instead of infinity must be known in order to justify the use of the FDM.

I have used the FDM to compute ΔT_b for three different values of R, plotted in Figure 8.1 along with a second-order polynomial fit (dotted line). Because only the differences between ΔT_b-values at different R-values is important, ΔT_b at R=12.7mm is replaced by zero. Using this polynomial fit, the value of R for which $\partial \Delta T_b / \partial R = 0$ is R=21.31mm. Plugging R=21.31mm back into the polynomial fit, ΔT_b =42.61mC (mC = °C/1000) is approximately the error in ΔT_b associated with approximating infinity by 12.7mm instead of infinity. A plot from the analytical model of w vs. ΔT_b (around

ΔT_b=3°C and with typical probe and tissue thermal properties and a=1mm) shows that a change in ΔT_b of 20mC produces a change in w on the order of 1.5kg/m^{3}s. Thus, the error in w_{calc} produced by approximating infinity by R=12.7mm is on the order of 3kg/m^{3}s.

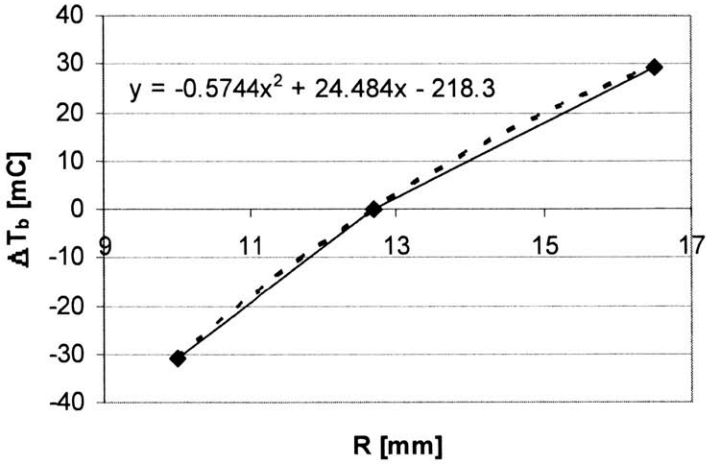

Figure 8.1 ΔT_b vs. R (slid line) with second-order polynomial fit (dashed line) and equation. Correlation=1.

9 Appendix C: FDM Isotherm Plots of Probe and Tissue

The output of the FDM is a temperature value for each of the 20'000 to 50'000 cells (depending on the mesh size and the value of R). On the following pages are plotted the isotherms of the probe and tissue at various values of perfusion, but at the same probe heat input q_b'''. Probe and tissue plots only show the left half of the probe and tissue. In the plots of the tissue isotherms, the origin marks the center of the probe-tissue interface. In the plots of the probe isotherms, the origin marks the center of the top surface of the probe, i.e. the center of the surface not in contact with tissue.

Note that as perfusion increases, more of the heat generated in the probe is carried away by convection (in addition to the heat carried away by conduction), and therefore the temperatures in the probe and the tissue decrease. In other words, as perfusion increases, the heat penetrates less deep into the tissue, which is the same as saying that the interrogated tissue volume decreases.

9.1 Disk Design

Figures 9.1-9.3 show tissue isotherms and Figure 9.4 shows probe isotherms at w=0, 5, and 15 kg/m^{3}s for the Disk design. ΔT_b=3.317183°C, 3.143704°C, 2.964222°C, respectively; a=1mm; h=0.2mm; Δr_b=0.02mm; Δr_m=0.1mm; Δh_b=0.01mm; Δh_m=0.1mm; R=12.7mm; maximum change for iteration termination=10^{-7}; q_b'''=7.5MW/m^3. Approximately 25,000 cells total. Tissue and probe thermal properties as listed in List of Values.

9.2 Disk and Ring Design

Figures 9.5-9.7 show tissue isotherms and Figure 9.8 shows probe isotherms at w=0, 5, and 15 kg/m^{3}s for the Disk and Ring design. ΔT_b=4.513792°C, 3.868039°C, 3.440828°C, respectively; a_{in}=0.4mm; a_{out}=2mm; h=0.2mm; Δr_b=0.04mm; Δr_m=0.2mm; Δh_b=0.02mm; Δh_m=0.2mm; R=42mm; maximum change for iteration termination=10^{-7}; $q_{b,in}''' = q_{b,out}'''$=5MW/m^3. Approximately 49'000 cells total. Tissue and probe thermal properties as listed in List of Values.

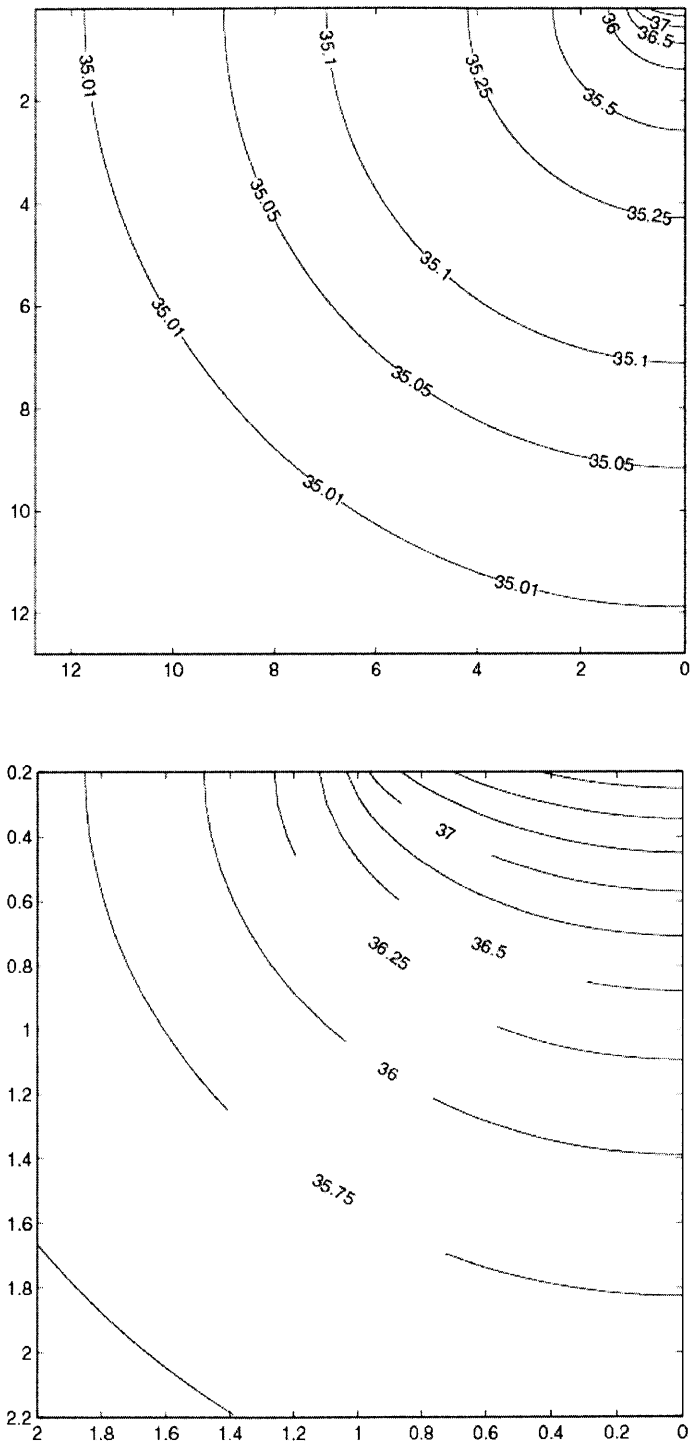

Figure 9.1 Disk design: tissue isotherms at w=0 (top: far-view, bottom: close-view). Axis dimension: mm; temperature dimension: °C. T_i=35°C.

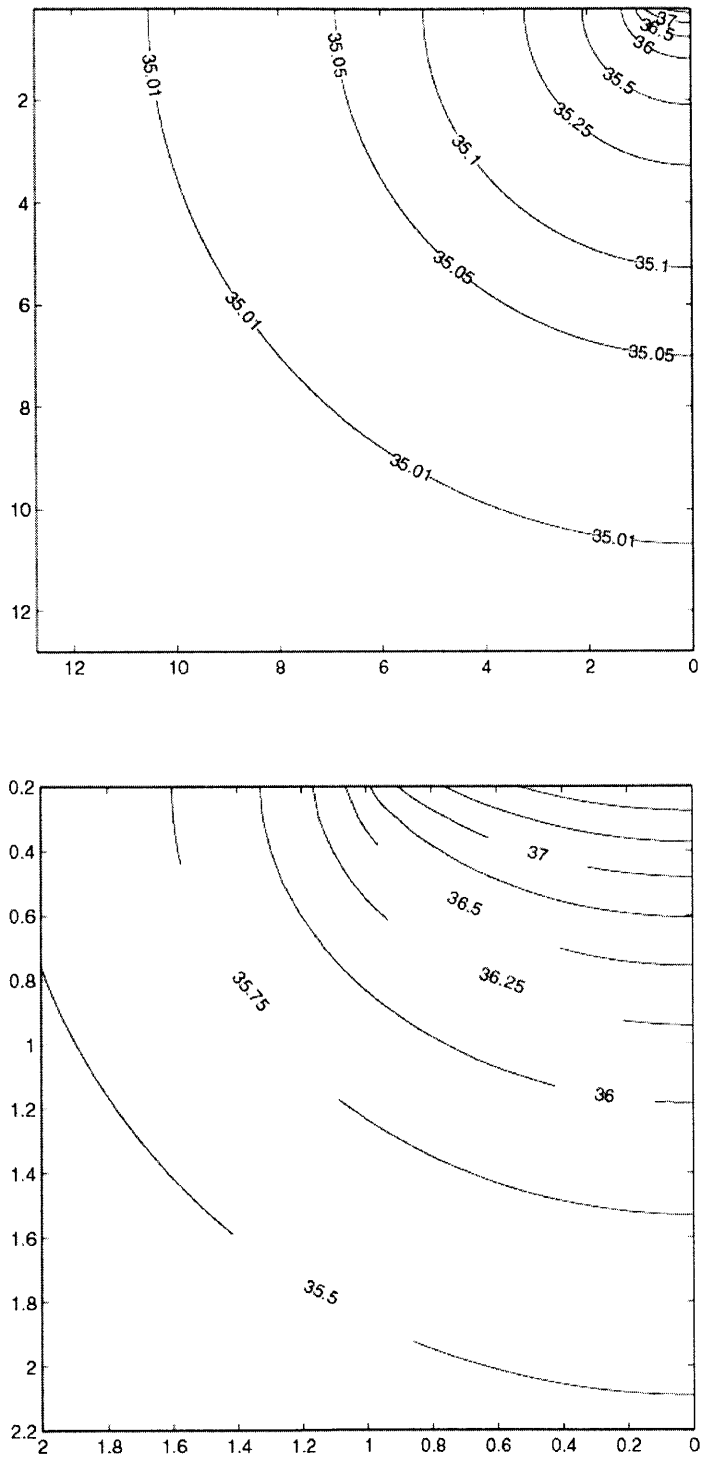

Figure 9.2 Disk design: tissue isotherms at w=5 kg/m^{3}s (top: far-view, bottom: close-view). Axis dimension: mm; temperature dimension: °C. T_i=35°C.

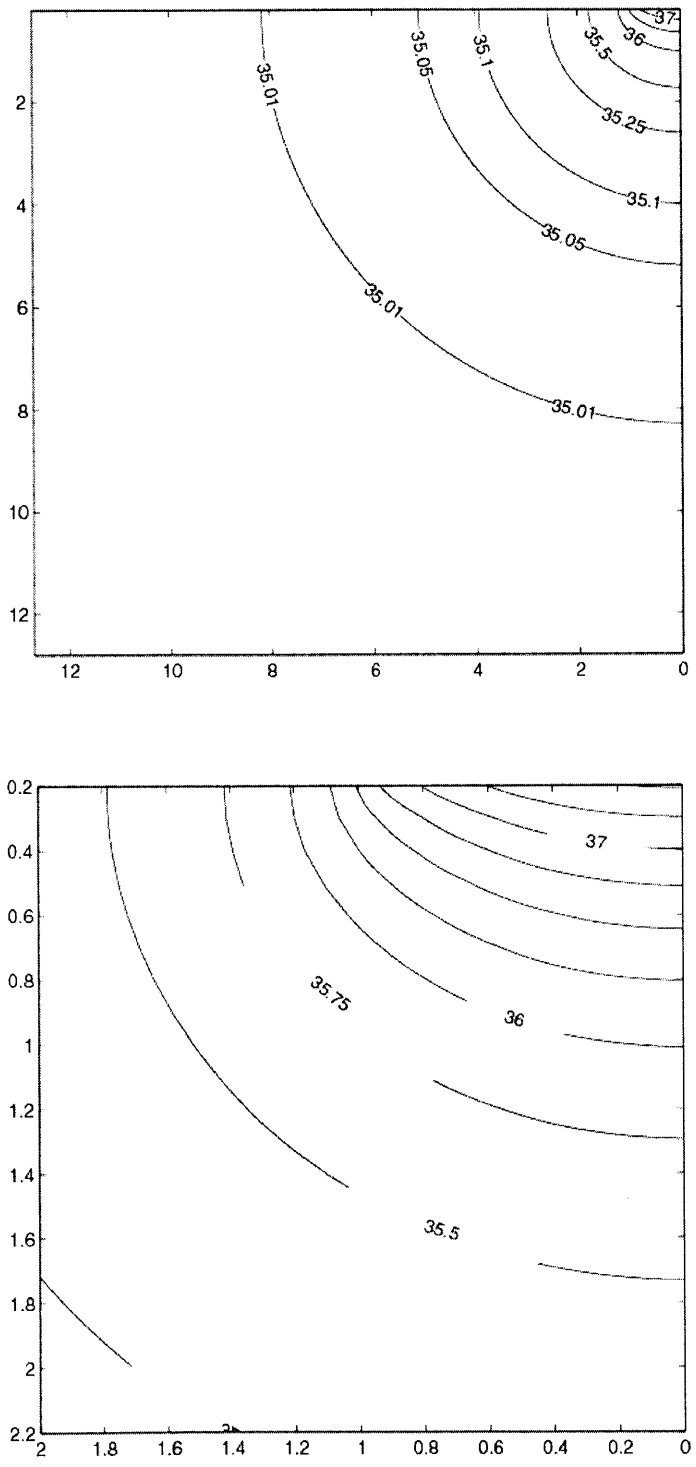

Figure 9.3 Disk design: tissue isotherms at w=15 kg/m^{3}s (top: far-view, bottom: close-view). Axis dimension: mm; temperature dimension: °C. T_i=35°C.

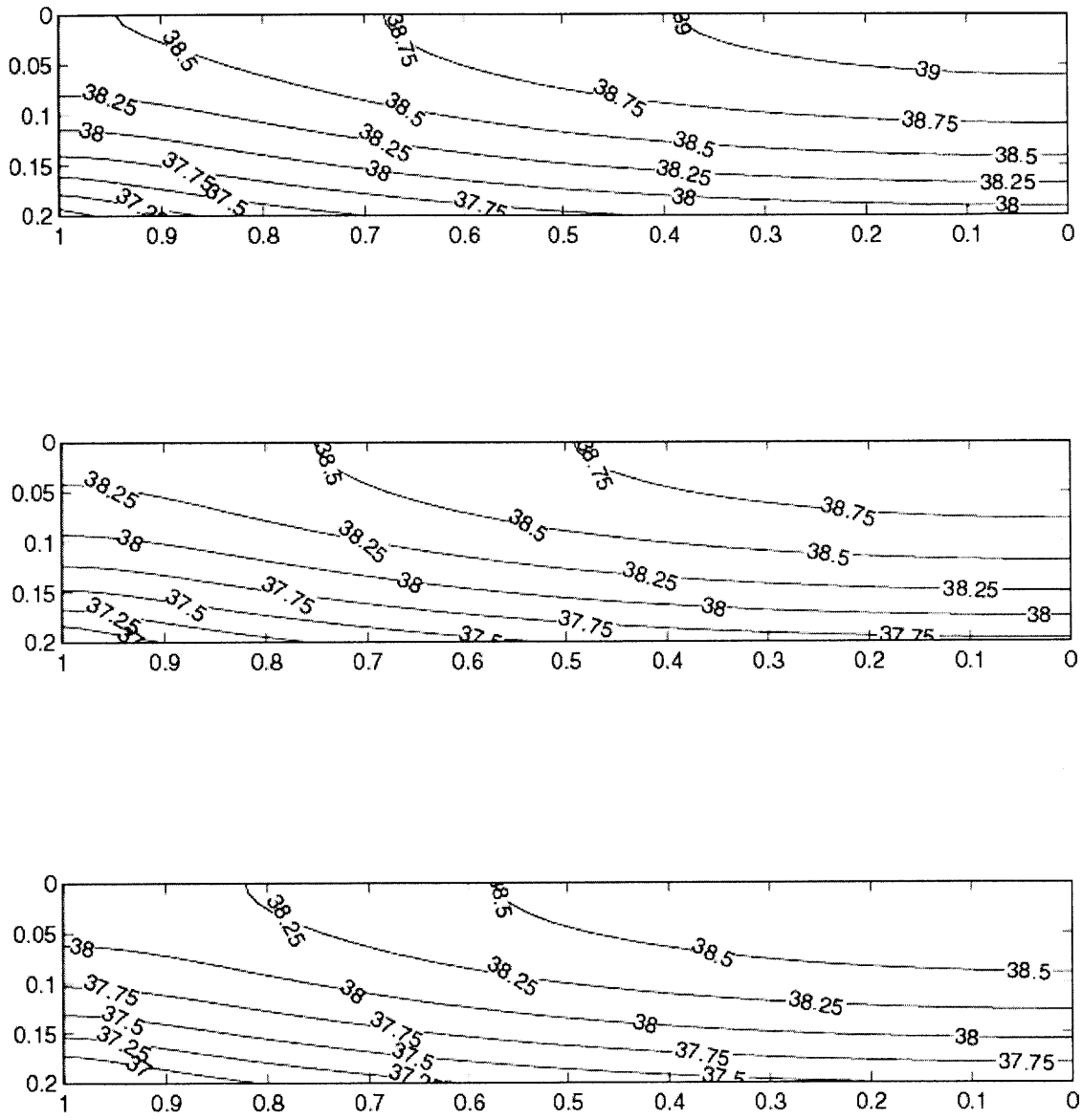

Figure 9.4 Disk design: probe isotherms at w=0 (top), w=5 kg/m^{3}s (middle), and w=15 kg/m^{3}s (bottom). Axis dimension: mm; temperature dimension: °C. T_i=35°C.

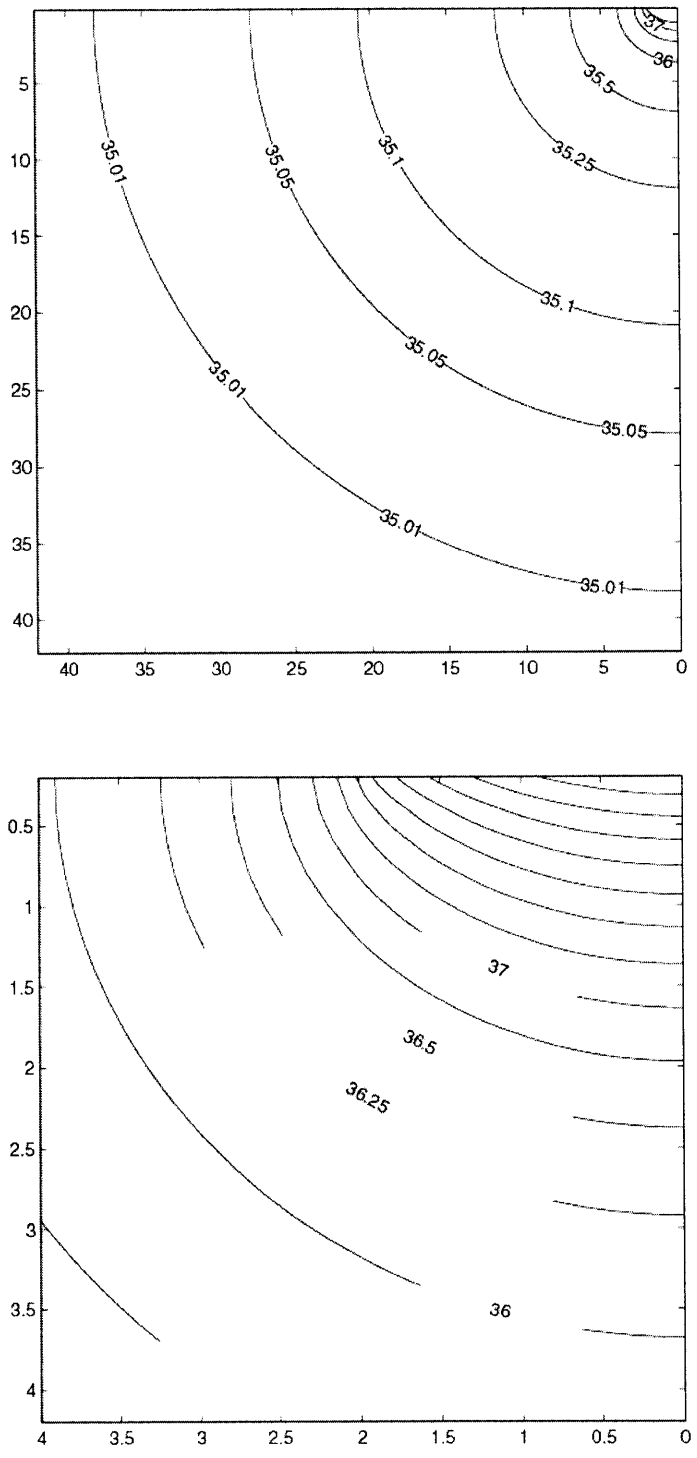

Figure 9.5 Disk and Ring design: tissue isotherms at w=0 (top: far-view, bottom: close-view). Axis dimension: mm; temperature dimension: °C. T_i=35°C.

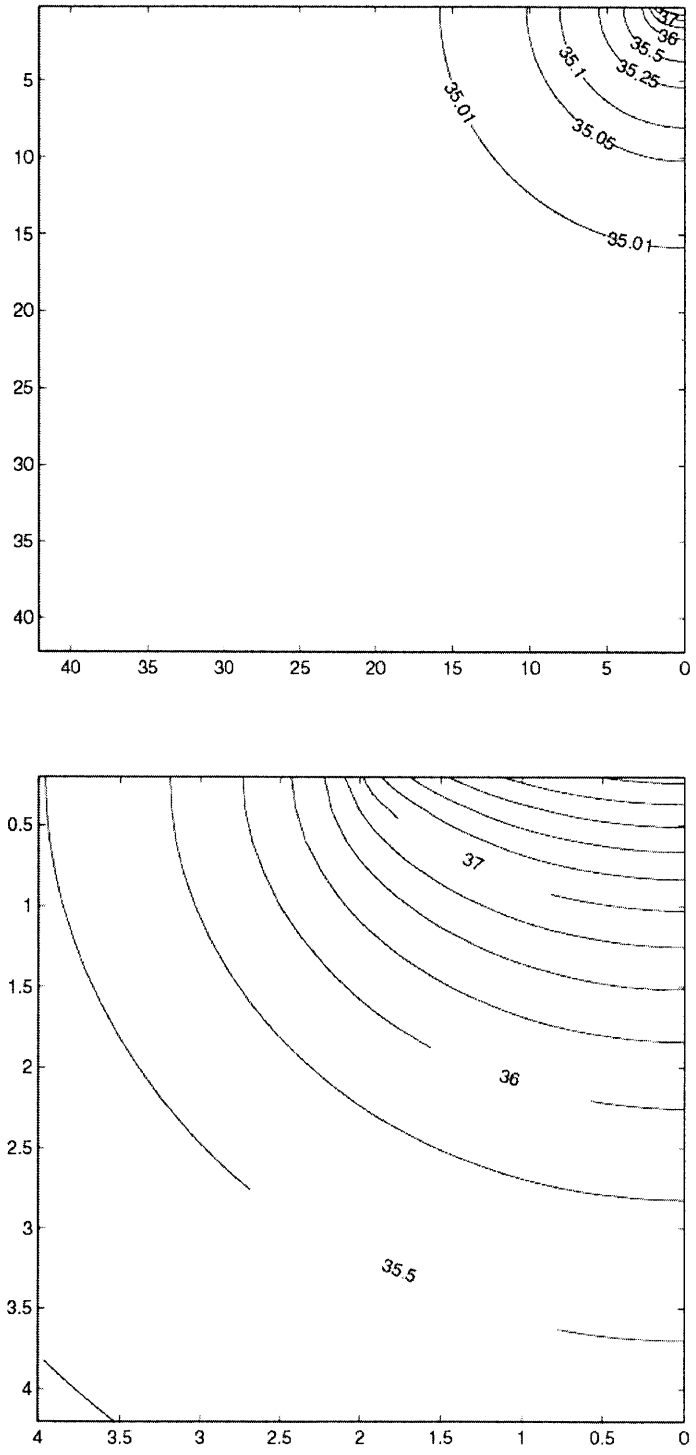

Figure 9.6 Disk and Ring design: tissue isotherms at w=5 kg/m^{3}s (top: far-view, bottom: close-view). Axis dimension: mm; temperature dimension: °C. T_i=35°C.

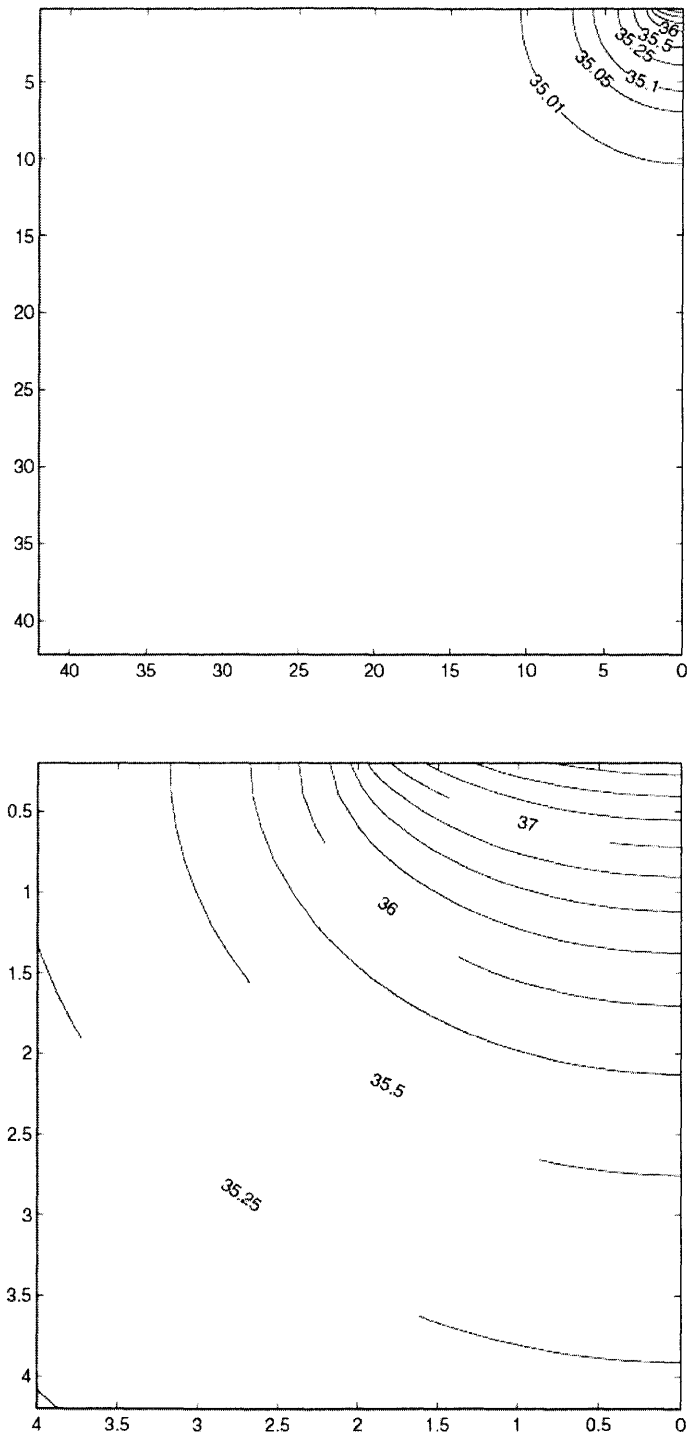

Figure 9.7 Disk and Ring design: tissue isotherms at w=5 kg/m^{3}s (top: far-view, bottom: close-view). Axis dimension: mm; temperature dimension: °C. T_f=35°C.

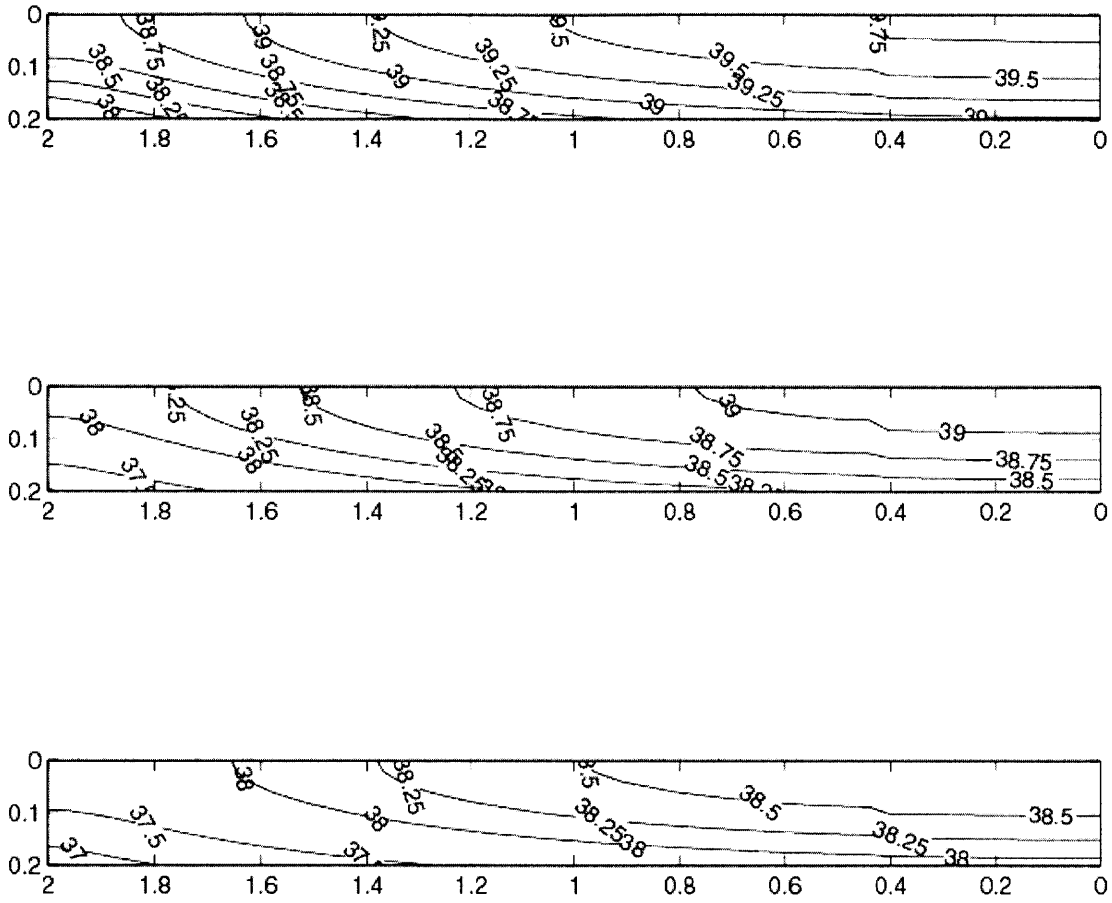

Figure 9.8 Disk and Ring design: probe isotherms at w=0 (top), w=5 kg/m3s (middle), and w=15 kg/m^{3}s (bottom). Axis dimension: mm; temperature dimension: °C. T_i=35°C.